Revisiting Aerodynamic Modifications to a Thin Transonic Wing

&

Küchemann's Critical Pressure Coefficient Rule

by

Punya Plaban

A Thesis Presented in Partial Fulfillment
of the Requirements for the Degree
Master of Science

Approved April 2021 by the
Graduate Supervisory Committee:

Prof. Timothy Takahashi, Chair
Prof. Marcus Herrmann
Prof. Ruben Perez

ARIZONA STATE UNIVERSITY

May 2021

ABSTRACT

Modern transonic aircraft have been designed and refined over the ages to achieve better and better performance. Aerodynamic refinements typically optimize a number of performance parameters: lift-to-drag ratio (*L/D*), zero-lift drag coefficient, *Cp* distribution, design Critical Mach number and design lift coefficient. This thesis explores the effects of aerodynamic refinements to a baseline thin transonic wing, namely, modifications to the leading-edge radius, camber, droop and thickness to determine their effectiveness to optimize the aerodynamic performance of the wing. Prior work has shown that these modifications can be helpful to improve the performance of a wing. In this new work, panel methods and computational fluid dynamics (CFD) have been used to show that these modifications do not necessarily help in improving the aerodynamic performance. This work also presents data to show the appropriate use of Küchemann's critical pressure coefficient equation in a 3-D flow field over a thin transonic wing integrated to a nominal fuselage. The final work of the thesis aims to provide clear definitions of the terms involved in the classical Küchemann's equation and how the design modifications depend on the correct interpretation of the Küchemann's equation. It also studies effect of winglet on design performance and throws some light on the inconsistency in the simple sweep theory.

TABLE OF CONTENTS

LIST OF TABLES

LIST OF FIGURES

Figure Page

Figure Page

Figure Page

Figure Page

Figure Page

Figure Page

Figure Page

CHAPTER 1

INTRODUCTION

Commercial aircraft play a vital role in our modern society. Design and development which contribute to improved aircraft performance are of primary importance. Modern aircraft need to fly faster and more economically than their predecessors; this is why more attention has been pushed in the direction of transonic and supersonic aircrafts. We realize that many fundamental theories and equations may be overlooked or taken as granted without further research. This thesis takes into consideration two such fundamental theories, namely, Simple Sweep Theory and Küchemann's estimation of critical pressure coefficients and explores further into application of these theories to a thin transonic wing / body. In addition to that, this work also takes a step in exploring the effects of aerodynamic design modifications on the performance of the wing-fuselage combination using computational fluid dynamics (CFD) as the tool.

Transonic wings have been traditionally designed meet the drag divergence criteria through spanwise variation of camber, incidence and thickness. However, the prime consideration in the aerodynamic design of a wing regards the control of shock waves. In the early 1960's Pearcey[10] noted that if the shock is properly handled, it can actually decrease the overall drag and through increasing leading-edge suction; conversely, improper utilisation of the shock may lead to shock induced flow separation that dramatically increases the overall drag.

One parameter which helps engineers control the formation of shock waves on the upper surface of wing is the critical pressure coefficient (C_p*). Over the years considerable work has been put forth to derive an accurate critical pressure coefficient

equation. Apart from that, a number of design modifications have been examined that help in delaying the onset of shock or help in completely eliminating the shock.

One approach in delaying the onset of shock is incorporating an increase of leading-edge radius to thin airfoils like NACA0006. The effect of leading-edge radius was studied by Fred A. Demele & Fred B. Sutton in 1951[22] on a wing with 35-degree sweepback but they hand waved their explanations and never applied the concept to NACA0006 airfoil i.e., they did not study the effects the modification has for a thin blunt airfoil and how the flow around such an airfoil behaves. This work presents evidence and test data to show the effects of increasing leading edge radius and explores the nature of the flow field around such a wing.

An alternative approach to deal with the shock is to utilize drooping. The effect of drooping applied to the leading-edge was studied by E.W.E Rogers, C.J. Berry & J.E.G. Townsend[21] in 1960 in the Aerodynamic Division of National Physics Laboratory of the UK. They studied the effects of drooping on an untapered wing in a of 50-degree leading-edge sweep at stream Mach numbers ranging from 0.6 to 1.2 in a wind tunnel.

This research work begins with an initial designed wing-fuselage combination using the potential flow VORLAX[2] code and analyses it using the SU2[3] computational fluid dynamics suite. Then, it applies the modifications and compares the results to the works done previously to explore the loopholes in the presented theories. It presents the challenges that we faced during the design process of a thin transonic wing. The end goal of this research is to determine why these modifications do not work properly in the improvement of the performance of the wing and to provide detailed

explanations to the misleading character of Küchemann's critical pressure coefficient rule.

In order to explain why the effects of aerodynamic modifications are minimal and to explore the Küchemann's equation of critical pressure coefficient, this work employed an open-source CFD tool named SU2 (developed in the Stanford University), Pointwise, a 3-D vortex lattice (VORLAX), PARAVIEW and TECPLOT. This thesis will explore the fundamental works done by Küchemann, Boyd (Conical Camber), Bowed airfoil theory and the Prandtl-Glauert rule from a 3-D perspective. This new work explains ideas developed by these early authors and explains the equations and concepts for applications to real world.

This thesis overviews the Küchemann's predicted critical pressure coefficient rule and explains the missing link between the equation and its application to the design of a real 3-D wing. Then it sets forth the idea about how the Küchemann's equation can be used for the estimation of critical pressure coefficient for a low Mach number case from the solution obtained at a high subsonic Mach number using the terms in its general sense.

CHAPTER 2

PRIOR ART

Effect of Increasing Leading Edge Radius

In 1947, Eggers[18] performed a high-speed wind tunnel investigation to compare the aerodynamic properties of a 12-percent-chord thick, single-wedge airfoil section and a reverse NACA 0012 profile. This investigation was interesting because it compared the two extreme cases of sharp and blunt airfoils. He compared the lift, drag and quarter chord pitching moment for the two test cases for small angles of attack and

Mach numbers ranging from 0.3 to 0.9. According to Eggers[18], at small constant angles of attack, lift coefficient of the wedge section increases continuously with Mach Number to the highest Mach number whereas the corresponding property of the reversed airfoil does not significantly increase or decrease at Mach numbers above the critical. However, the most important conclusion from his research was that at higher lift coefficients in the supercritical Mach Number range, the drag characteristics of the reversed NACA 0012 profile are superior to those of the normal NACA 0012 section.

From previous wind tunnel investigations at subsonic velocities, they found that the Mach numbers associated with unfavourable changes in section properties corresponded to the Mach numbers at which the shock waves became evident because one of the principal effects of shock is thickening of boundary layer due to the adverse pressure gradient. Consequently, the region behind the shock can be thought to have an altered geometry and characteristics compared to the case of no shock. So, to minimize the shock-induced distortions in order to experience less severe changes in aerodynamic properties at supercritical speeds, one alternative is to push the shock extreme rearward of the chord position. The only penalty that has to be incurred is that the subcritical drag characteristics will be adversely affected.

From the drag characteristics results (see Figure 1 and 2), the reversed NACA 0012 airfoil (sharp leading edge to the incoming flow) displayed superior results compared to the conventional blunt airfoil.

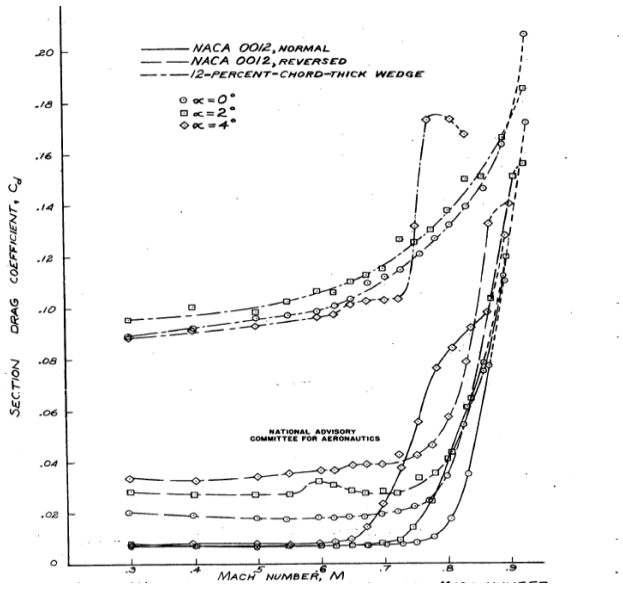

Figure 1: Variation of Section Drag Coefficient with Mach number for the Reversed and Normal NACA 0012 Airfoils 12-percent-chord-thick Wedge Airfoil, Reproduced from Aerodynamic Characteristics at Subcritical and Supercritical Mach numbers of Two Airfoil Sections having Sharp Leading Edges and Extreme Rearward Position of Maximum Thickness, A.J. Eggers, Jr.

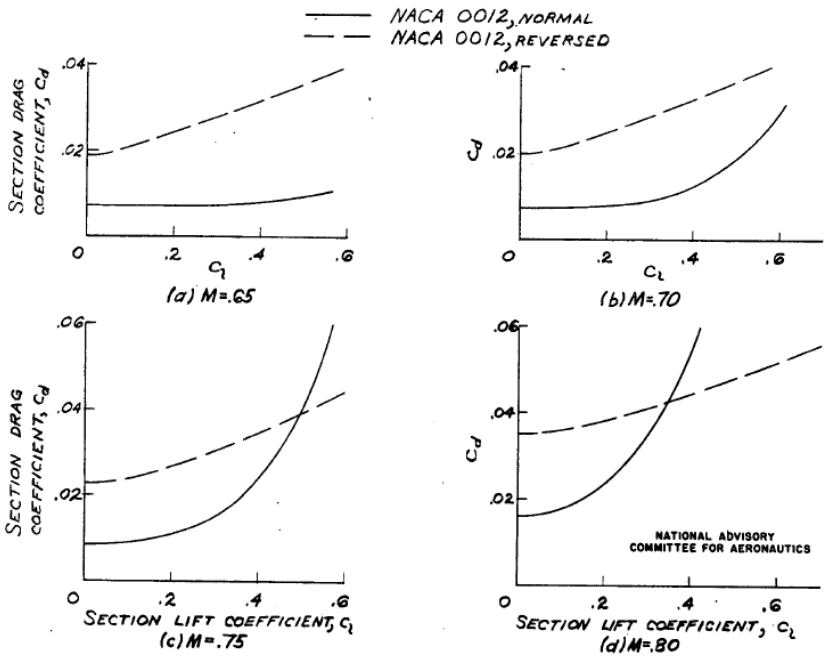

Figure 2: Comparison at Several Mach Numbers of the Variation in Section Drag Coefficient with Section Lift Coefficients for the Reversed and Normal NACA 0012 Airfoils, Reproduced from Aerodynamic Characteristics at Subcritical and Supercritical Mach numbers of Two Airfoil Sections having Sharp Leading Edges and Extreme Rearward Position of Maximum Thickness, A.J. Eggers, Jr.

Eggers argued that by employing boat tailing on a section with sharp leading edge and an extreme rearward maximum thickness, supercritical lift characteristics superior to those of conventional profiles can be established but he handwaved explanations to the effect of a sharp leading edge to the formation of shock. This thesis does not question the results that has been obtained, instead it is motivated from this work to explore the possibilities and challenges in the design of a thin transonic wing with a rear shock/ no shock because of its additional benefits in reducing the cost and weight of the aircraft. This work further explores the importance of leading-edge radius, camber and droop keeping the thickness profile constant for a sharp edged airfoil that was ignored by Eggers and most importantly presents data regarding when these modifications does not work as expected. This thesis also aims to show the importance of critical pressure coefficient and the importance of its accurate estimation which was completely removed from attention in Eggers paper.

In 1951, Fred A. Demele & Fred B. Sutton[22] studied the aerodynamic effect of increasing the leading-edge radius and adding forward camber on the aerodynamic characteristics of a wing with 35 degree of sweepback. They increased the leading-edge radius of the original NACA 64010 section and introduced a small amount of camber over the forward portion of the chord. They claimed that the aerodynamic characteristics of the modified wing were much more sensitive to the changes in Reynolds Number than the original wing. At higher Reynolds Number, the modified wing was able to delay the separation effects to much higher lift coefficients. They mentioned that “swept-back wings without twist or camber and having small leading-edge radii undergo serious changes in aerodynamic characteristics at relatively low lift coefficients” and this is because of the use of sections like NACA 6-series sections but they never really considered the NACA 0006 section. They took a model wing

which had 35-degree sweepback and increased the leading-edge radius of the NACA 64A010 section and simultaneously added a small amount of camber on the forward portion of the chord see Figure 3).

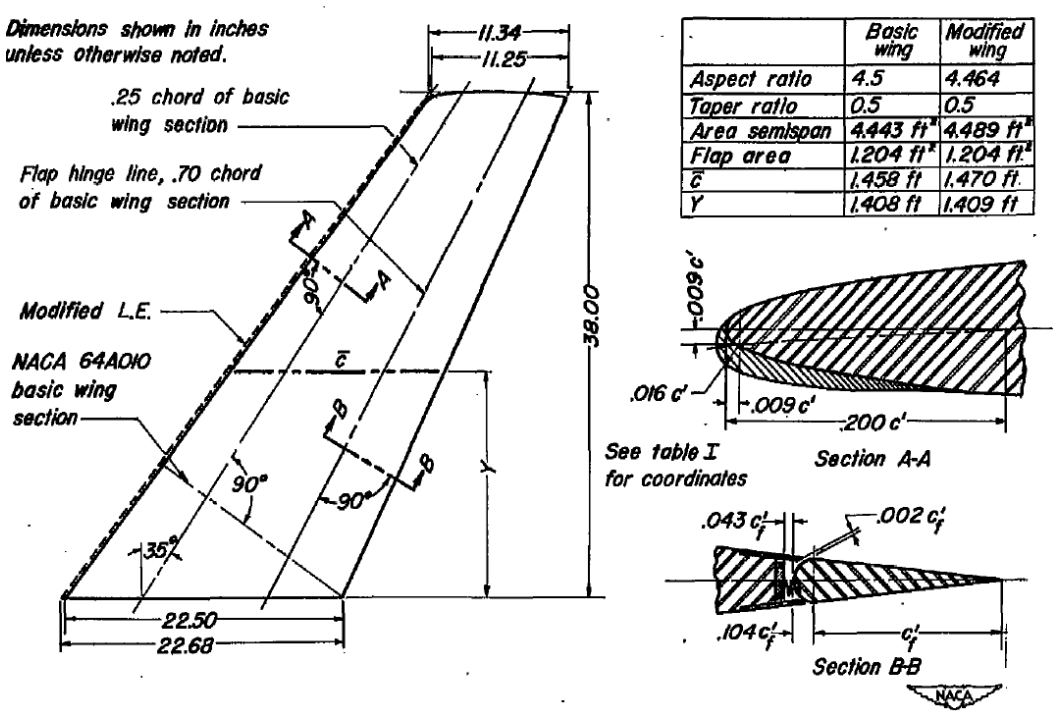

	Basic wing	Modified wing
Aspect ratio	4.5	4.464
Taper ratio	0.5	0.5
Area semispan	4.443 ft²	4.489 ft²
Flap area	1.204 ft²	1.204 ft²
$\bar{c}$	1.458 ft	1.470 ft.
Y	1.408 ft	1.409 ft

Figure 3: Co-ordinates for NACA 64A010 Airfoil Section and the Modified NACA 64A010 Airfoil Section, Reproduced from "The effects of increasing the leading-edge radius and adding forward camber on the aerodynamic characteristics of a wing with 35-degree of sweepback" by Fred A. Demele & Fred B. Sutton

So, they never really tried to investigate the individual effects of these modifications. Finally, they compared the aerodynamic characteristics of the original wing and the modified wing (see Figure 4 and 5).

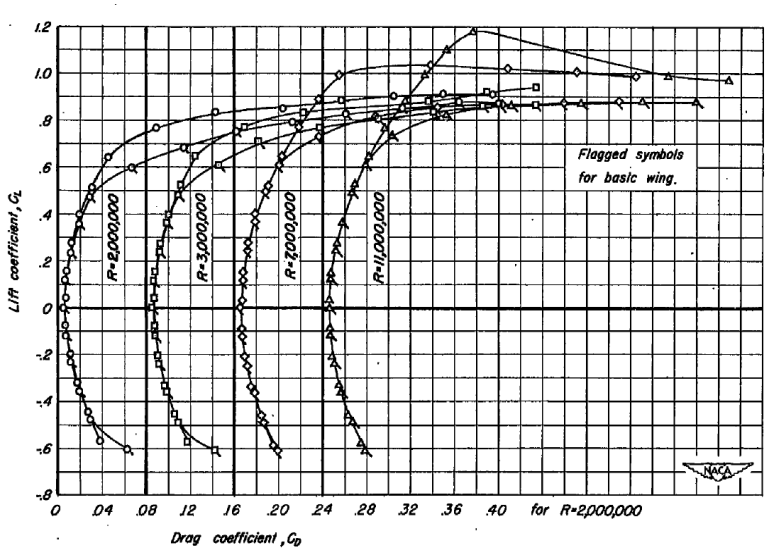

Figure 4: The effect of Reynolds number on the low-speed aerodynamic characteristics, Reproduced from "The effects of increasing the leading-edge radius and adding forward camber on the aerodynamic characteristics of a wing with 35-degree of sweepback" by Fred A. Demele & Fred B. Sutton

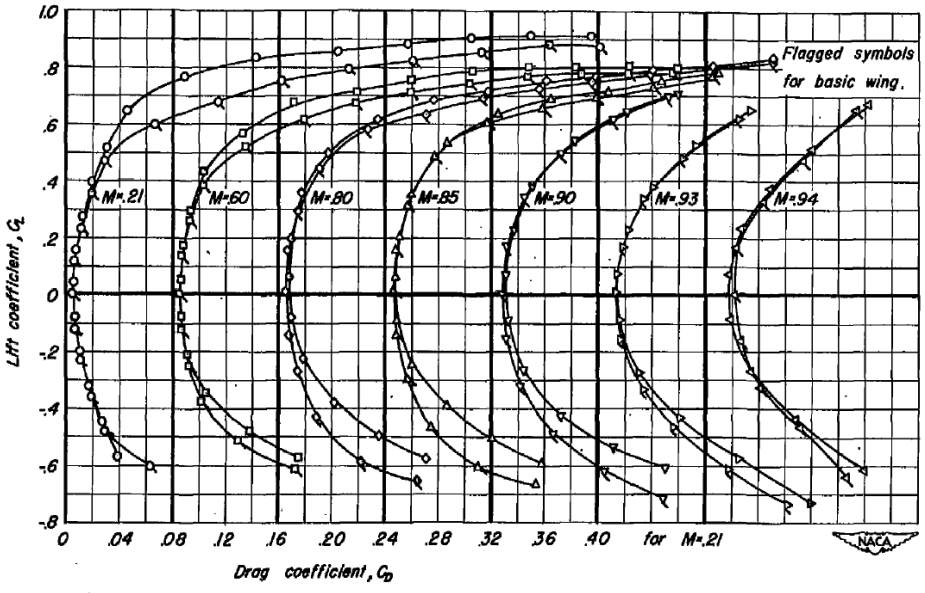

Figure 5: The effect of Mach number on aerodynamic characteristics. Re = 2,000,000, Reproduced from "The effects of increasing the leading-edge radius and adding forward camber on the aerodynamic characteristics of a wing with 35-degree of sweepback" by Fred A. Demele & Fred B. Sutton

They argued that at lower Reynolds Number, the modifications resulted in slight improvements in aerodynamic characteristics at low speed, however, the increase in Reynolds Number resulted in the increase in lift coefficient to the order of 50 percent

and delayed separation. It is also evident from the above results that the drag decreases above a lift coefficient of about 0.50 at Reynolds numbers of 2,000,000 whereas large reductions in drag are observed at Reynolds numbers of 7,000,000 and 11,000,000 above a lift coefficient of 0.65. It is inferred from these statements that there is no effect of modification below the lift coefficient of 0.5. This thesis does not question the results and conclusions but merely explores the missing links of the findings i.e., the consideration of testing a similarly modified wing both at high Reynolds number and high Mach number simultaneously to see the effect of modification on the aerodynamic characteristics.

Droopy Leading Edge

In 1960, E.W.E. Rogers, C.J. Berry & J.E.G. Townsend[21] studied the effects of leading-edge modifications on the flow over a 50-degree sweptback wing at transonic speeds. They incorporated leading-edge droop to an untapered swept wing in seven stages ranging from a fairly extensive droop to an undrooped section with a large leading-edge radius (see Figure 6). We predict that this test case is an exaggeration in predicting the aerodynamic characteristics as the effect of sweep dominates the effect of drooped leading-edge by admitting a higher negative critical pressure coefficient (C_p*) on the upper surface of the wing and perhaps, that's why they handwaved the explanation regarding measurement of surface pressures. Moreover, wing sweep helps in delaying the onset of shock formation and therefore the separation effects. This thesis work is more inclined to see the effects of leading-edge droop at a smaller wing sweep.

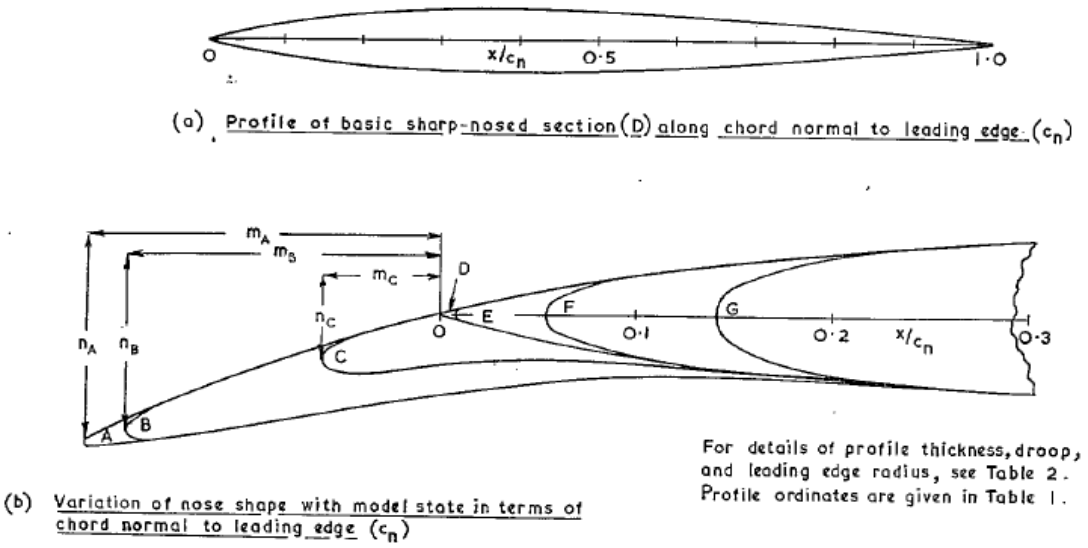

Figure 6: Details of seven model states, Reproduced from "A Study of the Effect of Leading-Edge Modifications on the Flow over a 50-deg Sweptback Wing at Transonic Speeds" by E.W.E. Rogers, C.J. Berry & J.E.G. Townsend of the Aerodynamics Division, N.P.L.

They argued that leading-edge droop increased the wing near drag near zero lift but reduced the lift depended drag component excluding the highest test Mach Numbers. Droop also increased the lift coefficient at which leading-edge separation occurred on the upper surface at moderate subsonic speeds but reduced the Mach number for transonic flow attachment. In addition to that, the appearance of forward shock was delayed with leading-edge droop. This paper points out an important thing that the undrooped sections with an increase in leading-edge radius accompanies an earlier appearance of forward shock which contradicted the research done by Demele & Sutton that has been described earlier. Typically, the most difficult task is to get rid of the rear shock. This thesis does not explore methods to remove the rear shock rather uses the idea of Pearcey[10] (that is described in a later section) to place the shock at the crest to have maximum benefits of leading-edge suction.

Another interesting outcome of their work is that with increase in stream Mach number, supersonic flow occurs first near the tip and subsequently spreads inboard

and this effect is accentuated by placing the wing at incidence due to higher local loading over the outboard part of the wing. This phenomenon opposes the simple sweep theory which predicts that the shock does not spread all over the wing if it is generated at one specific location. This thesis work, as a part of its discussion, presents data and simulation results to prove this phenomenon.

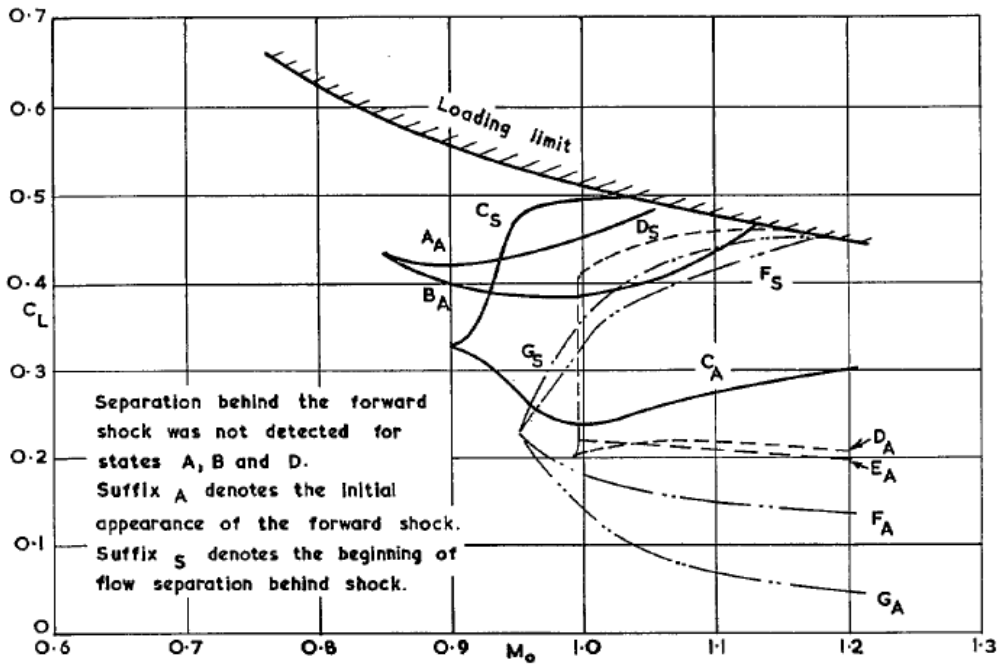

Figure 7: Forward Shock Characteristics Deduced from Oil Patterns, Reproduced from "A Study of the Effect of Leading-Edge Modifications on the Flow over a 50-deg Sweptback Wing at Transonic Speeds" by E.W.E. Rogers, C.J. Berry & J.E.G. Townsend of the Aerodynamics Division, N.P.L.

Further, they stated that when the flow is locally supersonic, small pressure disturbances in the leading-edge region are propagated at local Mach angle relative to local flow direction and with increase in freestream Mach Number, the local Mach Number over the outboard portion can become sufficiently high so that the disturbances will propagate at a greater sweep angle than the leading-edge. Hence, the first appearance of forward shock is dependent on local Mach Number distribution in the leading-edge region and is sensitive to modifications in leading-edge (see Figure

7). However, the test cases in this thesis work show that the disturbances can also propagate at a sweep angle less than the leading-edge. So, the statement provided by the authors is not universally true for all cases.

Pearcey's Peaky Leading-Edge

H.H Pearcey[10], H.H., in his paper "The Aerodynamic Design of Section Shapes for Swept Wings" developed a systematic method of section design and improved shapes taking the work of Küchemann[6] on yawed wing and the swept-wing fuselage combination in terms of aircraft design. To estimate the shock, he relied on empirical methods to replace the mathy soup from early 1950's but these methods are good until the shock causes separation reaching the trailing edge or the angle of attack becomes high which is evident in Figure 8 as M_0* decreases as we move towards the trailing edge.

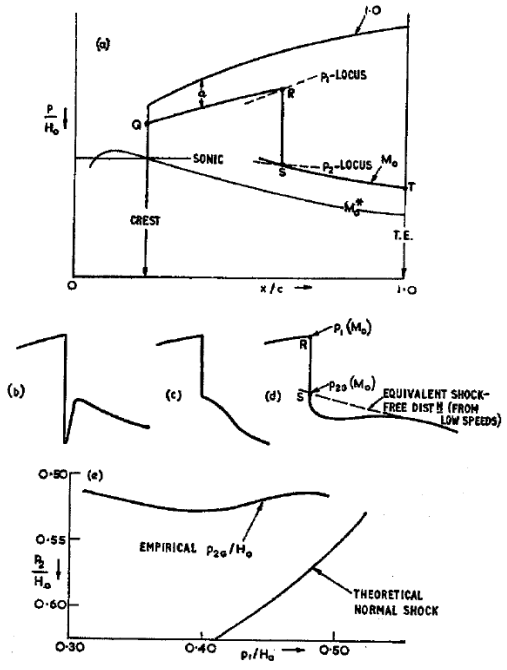

Figure 8: Derivation of Pressure Distribution with Shock Wave, Reproduced from "The Aerodynamic Design of Section Shapes for Swept Wings" by H.H. Pearcey, Aerodynamics Division, N.P.L., Teddington, United Kingdom

He further argued that the appearance of a Mach number appreciably greater than unity is not essentially an indication of a significant wave drag as some isentropic compression ahead of shock is possible and because the losses at the shock can fall rapidly to zero above the surface if the shock is short. So, the idea is to keep the shock weak as it passes the crest to prevent premature drag rise. Further, to seek a correlation with types of section shape and low-speed pressure distribution, he coined the terms “suction loop” and “drag loop”. With this idea, he came up with three types of pressure distributions, namely roof-top, peaky and triangular (see figure 9).

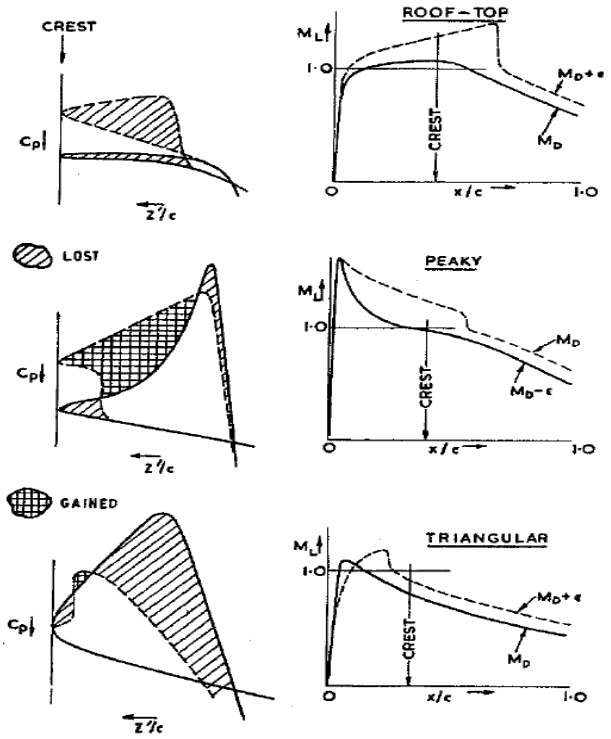

Figure 9: Types of Upper Surface Pressure Distribution and Corresponding Suction Loops, Reproduced from "The Aerodynamic Design of Section Shapes for Swept Wings" by H.H. Pearcey, Aerodynamics Division, N.P.L., Teddington, United Kingdom

Pearcey argued that the roof-top distribution, shock is formed behind the crest due to which we lose leading-edge suction whereas in the peaky pressure distribution, the shock is formed ahead of the crest providing the opportunity of exploiting the

maximum benefits of leading-edge suction i.e., “peaky” sections have most of the suction near leading-edge where the combination of thickness, incidence and camber means this suction generates lift and opposes drag. Further, peaky distributions spring from the favourable manner in which supersonic flow is able to keep the shock weak and to delay the onset of wave drag and shock induced separation. However, the important link Pearcey missed is the correlation of exploiting this benefit with the prediction of accurate critical pressure coefficient. In the present work, we exploited the idea of peaky pressure distribution from the initial optimized design in VORLAX citing this paper as a prior art but one of the interesting outcomes of this thesis work is to show that a low-speed peaky pressure distribution may trigger a shock at higher subsonic speeds if the estimation of critical pressure coefficient goes wrong i.e., there exists an interlink between the critical pressure coefficient and the type of pressure distribution on the upper surface of the wing which was ignored by Pearcey.

Further, in 1970, H.H. Pearcey & J. Osborne[24] studied the problems and features of transonic aerodynamics in which he addressed that it is not always possible to delay separation in the design with NACA profiles. As it can be seen from figure 10, thickness does not have a significant role in location of the crest as they seem to be nearly identical. We conclude that thickness adds pressure to both upper and lower surfaces. Also, two airfoils with the same upper surface shapes but different underlying camber and thickness forms develop identical upper surface pressures. This is an important idea in the consideration of the interplay between thickness, camber and incidence for a design process.

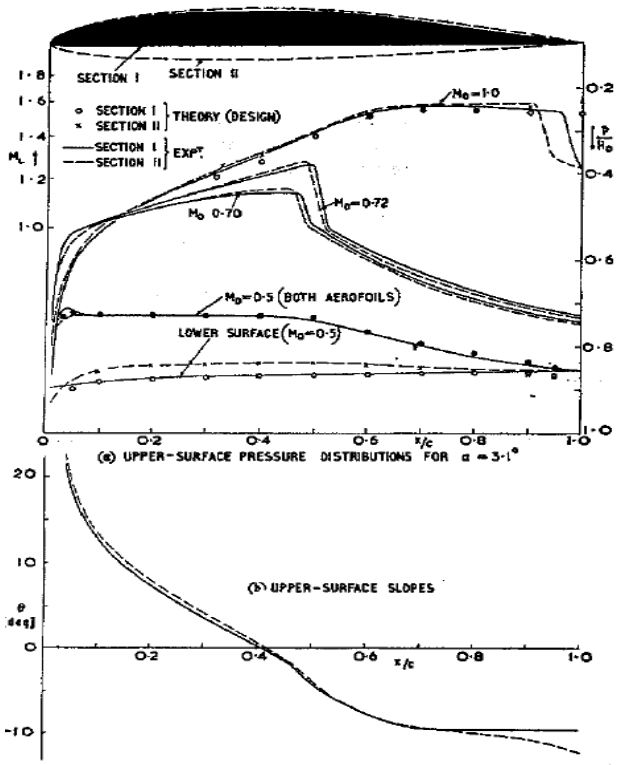

Figure 10: Comparison of design and results for two aerofoils with the same upper-surface shape and flow, Reproduced from "The Aerodynamic Design of Section Shapes for Swept Wings" by H.H. Pearcey, Aerodynamics Division, N.P.L., Teddington, United Kingdom

Moreover, as lift coefficient is a function of thickness, camber and angle of attack, it can be said that crest is a function of lift coefficient as a whole. Pearcey sees that most of the drag rise is caused by pressure drag effects on the airfoil. We infer from Figure 11 that the total pressure drag increase at higher subsonic speeds first comes from the loss of leading-edge suction and later on, the increase in drag comes through the increase in pressure drag due to trailing edge separation. This thesis work presents results in support of the argument.

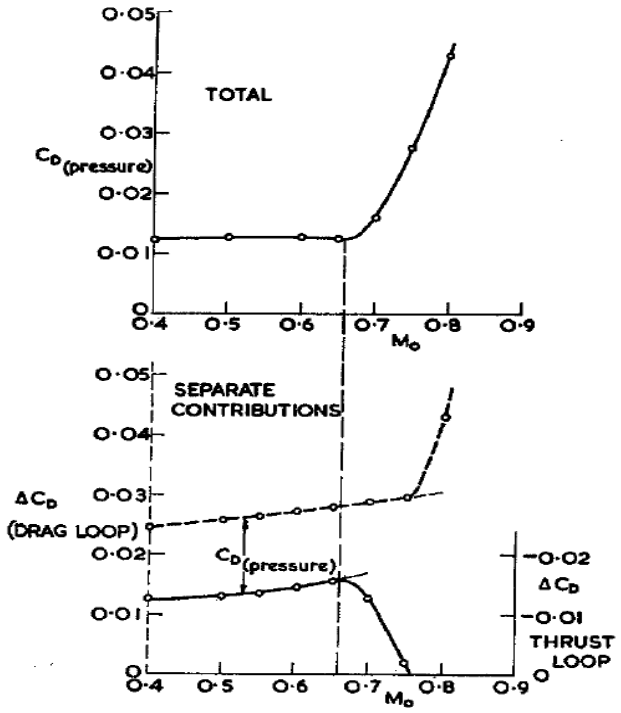

Figure 11: Results for NACA 0009 1/2 at AOA = 4-deg, Reproduced from "The Aerodynamic Design of Section Shapes for Swept Wings" by H.H. Pearcey, Aerodynamics Division, N.P.L., Teddington, United Kingdom

Boyd Conical Camber

A milestone in the design of sweptback wings was the study of conical camber for triangular and sweptback wings done by John W. Boyd, Eugene Migotsky & Benton E. Wetzel[20] in 1955. They did a theoretical and experimental study to determine the effectiveness of camber in reducing drag due to lift resulting from the pressure forces acting on low aspect ratio sweptback wings. A part of this thesis work is motivated by this paper as this paper considers sweptback wings and the aspect ratio of the VORLAX generated initial optimized wing was lower. At high subsonic speeds, the use of a moderate amount of camber results in significant reductions in drag coefficients above a lift coefficient of around 0.1 and the penalties in the drag coefficient at zero lift are small at supersonic speeds.

They also argued that the experimental drag polars for the moderately cambered wings predict the drag coefficients at the lift coefficient for which the camber was

designed closely but above the design lift coefficient, the experimental drag coefficients were those predicted from a theory where no leading-edge-suction was taken into account. Below the design lift coefficient, the experimental values were between the full suction and no suction. At subsonic speeds for swept wings, the camber helped in delaying the reduction of longitudinal stability to higher lift coefficients. Figure 12 shows that an increase in leading-edge radius for a cambered wing at high lift coefficients near a Mach Number of 0.60 reduced the drag coefficients. However, they did not consider the test cases at transonic Mach Numbers and a modified leading-edge to see the effect of conical camber on sweptback wings. This thesis fills the gap by considering the effect of conical camber on a wing with 35-degree sweep and at a higher subsonic Mach Number.

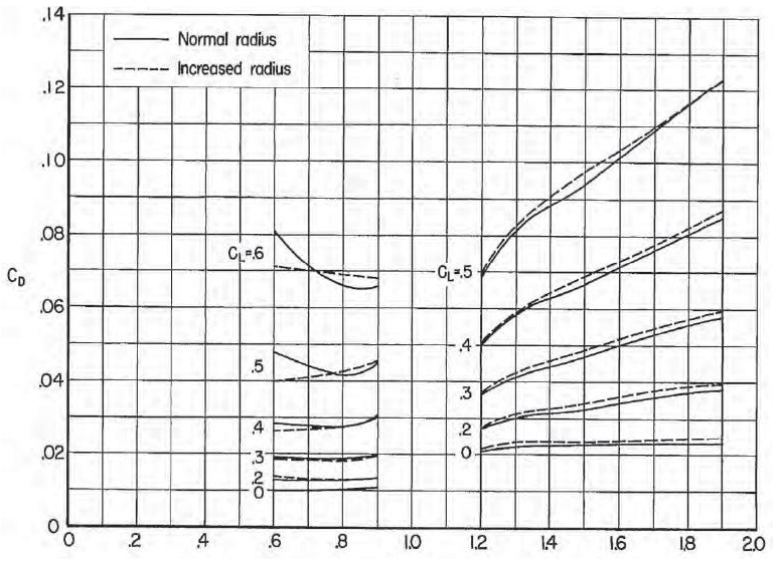

Figure 12: Cambered wing for a design lift coefficient of 0.292, Reproduced from "A Study of Conical Camber for Triangular and Sweptback Wings" by John W. Boyd, Eugene Migotsky & Benton E. Wetzel, Ames Aeronautical Laboratory, Moffett Field, Calif.

An interesting idea of the research is that a very thin blunt leading-edge airfoil with no camber and droop looks like a sharp leading-edge airfoil. This is exactly the case

for a thin transonic wing e.g., a tapered wing having wing profiles like NACA 0006 at its tip.

Leading-edge camber can make a thin/sharp airfoil look blunt by distributing the suction pressure over a large area of the wing. It is impossible to reach pressures required for full leading-edge suction which makes the leading-edge to appear blunt. Comparing the effectiveness of design methods with linear theory calculations (see Figure 12), it seems that conical camber restores the leading-edge suction at reasonable lift coefficients and modified no suction shows significantly higher drag coefficient at zero lift. Also, there is no noticeable improvements of drag due to lift but the data matches with full suction case (see Figure 14). This thesis work uses the concept of conical camber with drooped leading edge (see Figure 13) and modified nose radius on a thin transonic wing and presents data that correlates these design variables with the importance of estimating an accurate critical pressure coefficient.

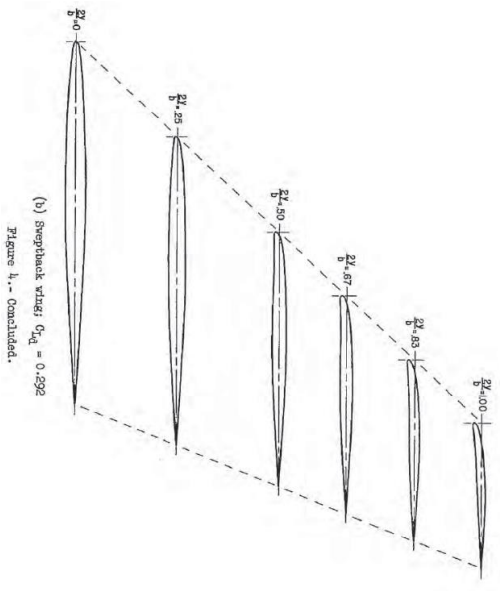

Figure 13: Representative airfoil sections for conically cambered wing (Sweptback Wing, CLd = 0.292), Reproduced from "A Study of Conical Camber for Triangular and Sweptback Wings" by John W. Boyd, Eugene Migotsky & Benton E. Wetzel, Ames Aeronautical Laboratory, Moffett Field, Calif.

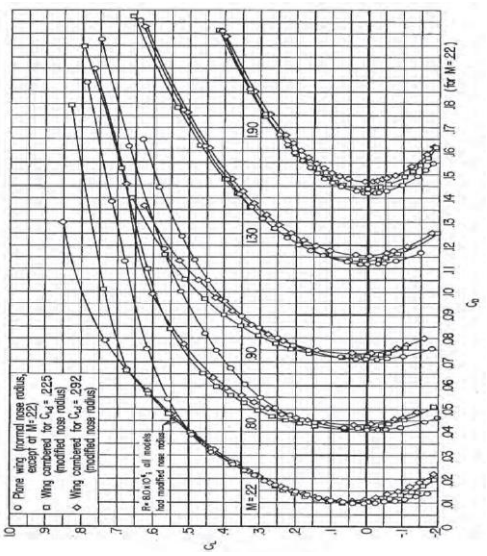

Figure 14: Effect of Conical Camber on the Variation of Drag Coefficient with Lift Coefficient for a 5-percent-thick Sweptback Wing with Fixed Transition; Re = 290000000, Reproduced from "A Study of Conical Camber for Triangular and Sweptback Wings" by John W. Boyd, Eugene Migotsky & Benton E. Wetzel, Ames Aeronautical Laboratory, Moffett Field, Calif.

It is also evident that aerodynamic centre and lift curve slope near zero are primarily functions of wing planform and are uninfluenced by provision of camber but a slight positive shift in the angle of zero lift occurs due to washout from camber. The summary of their work was to vary the position of the droop along with the amount of droop to restore the leading-edge suction by spreading the suction area over a large area of the wing upper surface. However, they did not consider the importance of critical pressure coefficient and thickness in analysing these effects. The present work gathers all the ideas of the various authors to study the effect on aerodynamic characteristics as a whole, the final aim being the study of Küchemann's critical pressure coefficient rule and eliminate the misleading character of the sweep term.

Critical Pressure Coefficient

In the design process of a thin transonic wing, which is the primary consideration in this thesis work, it is important to know the flight conditions where incipient shock

wave occurs because a shock wave can induce flow separation which further worsens the performance of an aircraft due to a large drag impact.

To deal with the shock, it becomes important to know the conditions that generate shock. Where a shock wave starts to form is the critical Mach Number of the wing i.e., the Mach Number at which sonic flow is first accomplished some place on the wing. Apparently, this phenomenon is also related to the critical pressure coefficient i.e., shock develops at the speed when the peak underpressure of the local airflow falls below critical pressure coefficient. The overall design process demands accurate prediction of the speed and lift and lift coefficient at which the sonic conditions lead to formation of a shock wave because the wing performance depends on optimization of lift, drag, pitching moment as well as its suitability to be integrated to a fuselage and sufficient room for other components.

Due to the importance of critical pressure coefficient, numerous authors have tried to predict the critical pressure coefficient as accurately as possible using different assumptions and approximations. Theodore Von Karman[14] used Glauert's[16] approximation that allows linearization of perturbation velocities neglecting the higher order perturbation terms. This leads to the derivation of the following equation.

$$C_p^* = \frac{2\left[(1-M_\infty^2)^{\frac{3}{2}}.(1+M_\infty^2)^{\frac{1}{2}}\right]}{M_\infty}$$

where, M_∞ is the freestream Mach number. The issue with this equation is that Glauert's approximation does not hold good at higher subsonic Mach numbers[16]. Theodore Von Karman also points out this fact that the above equation is not exact due to linearization and suggests the Eastman Jacobs' equation[25] to be a good starting point towards an accurate prediction of critical pressure coefficient.

Eastman Jacobs considers thermodynamic relationships. He included some necessary corrections to the errors present in the approximation of linear theory. Jacobs' equation considers the specific heat ratio which was ignored by Theodore Von Karman[14].

$$C_p^* = \frac{2\left\{1 - \left[\frac{2 + (\gamma - 1)M_\infty^2}{\gamma + 1}\right]^{\frac{\gamma}{\gamma - 1}}\right\}}{\gamma M_\infty^2}$$

However, Eastman Jacobs never really explained his rationale in any of his authored papers. The loophole in this equation is that there is no term including sweep which says that sweep has no effect on critical pressure coefficient. Also, it is interesting to note that the critical Mach number lines in NACA TR-824[5] follow the Von Karman's equation to predict the critical Mach number from the peak underpressure in a low-speed testing. This suggests that although Jacobs' equation is a good starting point, a lot of work is still needed to predict an accurate equation of critical pressure coefficient.

Further, attempts were made to improve the prediction of critical pressure coefficient. John D. Anderson[7] published an equation for the prediction of C_p^* considering isentropic relationships between the static and total pressure.

$$C_p^* = -\frac{2}{\gamma M_\infty^2}\left\{\left[\frac{2 + (\gamma - 1)M_\infty^2}{\gamma + 1}\right]^{\frac{\gamma}{\gamma - 1}} - 1\right\}$$

He argues that this relation is valid for every freestream Mach number as the critical pressure coefficient goes to zero when Mach number reaches 1. However, this equation falls apart for a sweptback wing as there is no term considering the effect of sweep.

It was Schlichting[12] who first introduced a sweep term into the critical pressure coefficient equation for a sweptback wing of constant chord and infinite span. He claimed that by knowing the critical Mach Number beforehand, the critical pressure coefficient can be found easily from the minimum pressure coefficient and the critical conditions are dependent on flow normal to the leading-edge of the wing. His equation has been reproduced here to compare it with the other derived equations.

In 3-D: $$C_p^* = -\frac{2}{\gamma+1}\frac{1-Ma_{\infty_{cr}}^2(cos\Phi)^2}{Ma_{\infty_{cr}}^2}$$

In 2-D: $$C_p^* = -\frac{2}{\gamma+1}\frac{1-Ma_{\infty_{cr}}^2}{Ma_{\infty_{cr}}^2}$$

The most widely used and accepted equation for the prediction of critical pressure coefficient till date is that derived by Küchemann[6]. He derived the equation through the use of isobars on the upper surface of a swept wing and the thermodynamic relationship between pressure, velocity and total head. According to him, critical conditions occur when the flow normal to isobars i.e., in the direction of local pressure gradient reaches the local speed of sound.

$$C_p^* = \frac{2}{\gamma M_\infty^2}\left\{\left(\frac{2}{\gamma+1}\right)^{\frac{\gamma}{\gamma-1}}\left(1+\frac{\gamma-1}{2}M_\infty^2(cos\Phi)^2\right)^{\frac{\gamma}{\gamma-1}}-1\right\} \quad (1)$$

where, Φ is the angle of sweep.

In 1949, Neumark[9] presented his work on the derivation of critical Mach Number for sweptback wings considering straight untapered wings and adding a $cos\Phi$ term. Therefore, he argues that the critical conditions depend only on Mach Number normal to the leading-edge which is different from the ideas of Küchemann[6] and Schlichting[12]

who argued that critical conditions not only depend on the Mach number normal to the leading-edge but also the freestream Mach number.

From the discussion, it is evident that many authors have tried to reach at final equations estimating C_p^* through different basic governing physics. It can be easily proved that these equations give different values of C_p^* at the same freestream Mach number. So, it becomes important to resolve the inconsistencies between the derivations as it inspires no hope in the design process for accurate prediction of shock wave. This thesis takes into consideration the equation derived for a three-dimensional flow field by Küchemann as the starting point in the design process and goes on to show that the initial optimized wing using VORLAX does contain a shock wave and a maximum negative underpressure exceeding that predicted using the Küchemann's equation. Then, it applies a number of modifications to further optimize the wing-fuselage combination and corrects the sweep term present in the Küchemann's equation.

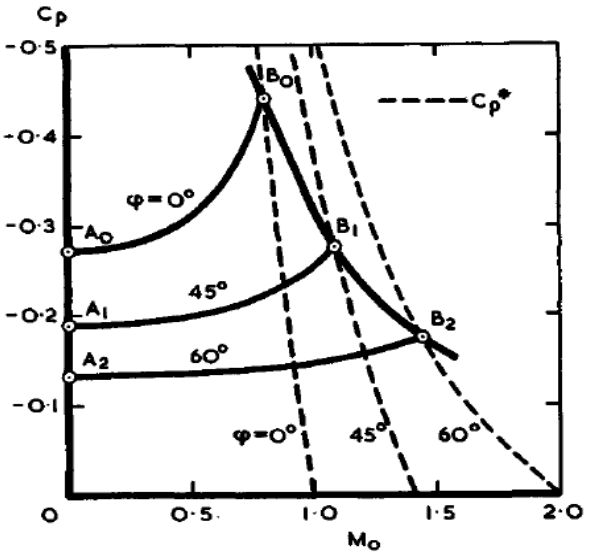

Figure 15: Pressure Changes with Mach number on infinite sheared wings. Biconvex section, t/c = 0.1, AOA = 0, Reproduced from "The Aerodynamic Design of Aircraft" by Dietrich Küchemann

It is evident from Figure 15 that an increase in angle of sweep reduces the supervelocities at M_0 (points A) and the pressure rise with M_0 gets flatter until it reaches the critical pressure at point B. This proves that sweep plays an important role in extending the speed range of aircrafts above and below the sonic flight speed. However, Küchemann never really specified which sweep angle has to be considered when one uses his equation to determine C_p^*. This thesis work attempts to resolve this famous Küchemann's equation of critical pressure coefficient, specifically the misleading character of sweep angle and presents results in support of the argument.

Simple Sweep Theory

In order to deal with a classical sweptback wing aircraft, it is essential to look through the simple sweep theory. A swept wing of infinite aspect ratio behaves like an unswept wing with equivalent flow conditions normal to the leading edge. Wing sweep delays shock formation by reducing the Mach number normal to the leading-edge, reduces the dynamic pressure normal to the leading-edge and reduces the overall lift.

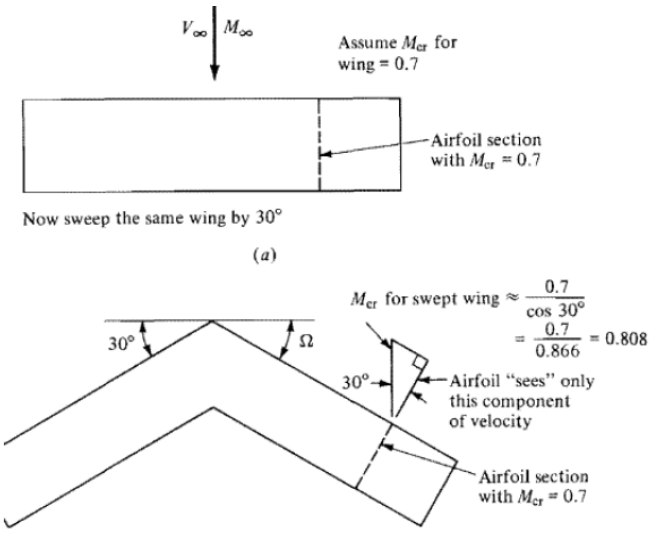

Figure 16: Effect of swept wing on critical Mach number, Reproduced from Anderson[15]

The equivalent wing when swept, functions as if it only sees the component of flow normal to the leading-edge. Therefore, sweep increases the critical Mach number but simple sweep theory overlooks the compressibility effects of leading-edge as opposed to freestream reference frame pressure changes. Unlike the geometric analogies postulated by simple sweep theory, Küchemann estimated the local speed of sound based upon pressure changes imposed by all of the perturbation velocities, both in leading-edge reference frame and cross flow reference frame and this C_p^* matters the most in the design process. Further, simple sweep theory states that if a shock is created at some point on the upper surface of the wing, it stays there and does not spread all over the wing. A part of the thesis work shows that this is not necessarily true for all design cases which suggests the oversimplification of the simple sweep theory and its inadequacy to be applied in the design process.

CHAPTER 3

COMPUTATIONAL METHODS

This thesis uses essential computational methods to prove the arguments that has been stated in the prior art section. Specifically, this work includes the use of an open-source computational fluid dynamics (CFD) code as well as a subsonic/ supersonic potential flow solver named VORLAX. The computations performed involve test cases with different wing-fuselage geometries at various Mach numbers at a constant angle of attack. The final aim of the computations was to determine the effect of leading-edge radius, forward camber, droop, conical camber and the validity of Küchemann's critical pressure coefficient equation for a three-dimensional flow configuration with a sweptback wing.

VORLAX

VORLAX is an old FORTRAN program full-featured vortex lattice potential flow code which is a compressibility corrected potential flow solver developed by Luis Miranda in Lockheed-California under contract from NASA[2]. It is a pressure-based solver known for its capability to predict accurately the inviscid aerodynamics for geometric configurations with fully attached, shock free flows. VORLAX takes input in three forms namely, simple, thin flat panels, a thickness simulating sandwich panel and thin, cambered panels. It can also simulate cases with twist and full leading-edge suction. For transonic wing-body configurations, computations from VORLAX agree well enough with experimental results provided the inviscid, attached flow assumptions are still in place. However, above the critical Mach number, which is the Mach number at which critical pressure coefficient reaches its threshold and causes the onset of separation, VORLAX underpredicts drag. VORLAX produces a number of flow solution data including Oswald efficiency as a function of Mach number and angle of attack, the overall force and moment coefficients (lift, drag, pitching moment, rolling moment, yawing moment and side force), net differential pressure coefficients for thin, flat and cambered panels and actual pressure coefficients for thickness simulating cambered panels. Useful in number of applications, VORLAX has some disadvantages. It does not produce thickness dependent forces and moments or viscous dependent forces and moments. This code is only applicable to cases where thin airfoil theory applies.

In this thesis, VORLAX has been mostly used to find an initial optimised design for a sandwich panel case (subcritical allowable pressure distributions and an elliptical load distribution in the spanwise direction) as VORLAX is incapable to simulate cases with a shock wave rather it can only identify regions of incipient sonic flow where

VORLAX solutions can no longer be relied upon because of its nature of divergence from a real solution. With the iterative design process throughout the work, solutions from the open source CFD code were reproduced using VORLAX to ensure that the spanwise elliptical load distribution is not altered.

SU2

SU2 is an open-source CFD code that uses volume grid method to make multidisciplinary design optimization including the free form deformation available for free around the world[26]. The source code has been written in C++ and python to analyse the governing equations of computational fluid dynamics and PDE-constrained optimisation on structured and unstructured grids using numerical methods. The reason SU2 being widely used is because of its capability of solving numerous partial differential equations with different numerical methods appropriate for both low-speed and high-speed solutions.

SU2 was originally developed at Stanford for computational fluid dynamics calculations for a wide range of problems including compressible and incompressible flow solvers (Reynolds Averaged Navier-Stokes (RANS), Euler and Navier-Stokes). It can also be automated using a python script which is beneficial in a generative design process. Apart from solving the simple problems in fluid mechanics, SU2 also deals with adaptive meshes for dynamic optimisation and unsteady problems. It is also beneficial for convergence acceleration by employing multigrid (V-cycle/W-cycle) solver and can be used for an inverse design problem to have a target pressure distribution.

SU2 is a volume grid method whereas VORLAX is a surface panel method. Unlike the polygon meshes that represent the surface as polygons, the interior surface is also

discretized in volumetric generation in SU2. Though SU2 is currently gaining attraction, there are still some challenges that need to be resolved. It employs density-based solver which makes it difficult to analyse flows at lower Mach numbers. In contrast, VORLAX uses a potential flow solver with Prandtl-Glauert corrections to model shock-free subsonic and transonic flows which allows it to produce excellent predictions at lower Mach number range ($M < 0.4$)[16]. Another challenge that has to be noted is the computational time. For a very fine mesh with local refinements on the geometry as needed, the input mesh becomes quite heavy for SU2 to handle it. Due to this factor, this thesis work uses a coarser mesh with local refinement and grid convergence study as well as GCI analysis have been performed to prove the accuracy of the computational results.

The input mesh to SU2 can be generated through various online meshing tools like GMSH and Pointwise. This thesis uses Pointwise[27] to generate meshes because of its easier use and diversified options. Local refinement was created by placing sources at appropriate locations and using voxel meshing (hex-core meshing) which is a unique feature in Pointwise. The average delta s specified in Pointwise acts as a starting point to get the surface mesh initialized. It has also the options to set transition layers which tells Pointwise how many isotropic hexahedral layers are to be used per level of mesh in the final volume. A higher number of transition layers ensures that the volume mesh grows at a slower rate as the volume near resolved features is kept small for a larger distance from the surface.

The final step in preparing the surface mesh has options to set the boundary decay value which changes the number of connectors having an influence on the interior surface mesh. Increasing this value from 0 to 1 tends to increase the number of

surface cells on a domain and refine the surface mesh according to its connector refinement. So, voxel meshing longer than tetrahedral meshing but it creates flow aligned cells for traditional external aerodynamics simulations.

TECPLOT is a post-processing tool that can produce a wide range of data from the CFD simulations including line plotting, 2-D and 3-D surface plots and 3-D volumetric visualisation[28]. This thesis work uses TECPLOT to post process the solutions obtained from SU2 simulations. We are particularly interested in the nature of isobars and the pressure distribution curves as the initial solution from VORLAX does not address the incipient shock wave formation.

We used the wing-fuselage combination with a symmetry plane at the centre of the fuselage cutting the fuselage into half along the direction of flow. This was done to create a coarser mesh as well as to reduce the computational time. To implement this, the input file to SU2 contained a symmetry boundary condition on the symmetry plane. All other surfaces were included in Euler wall boundary condition and three far-field markers were created to include far-field in the simulation.

CHAPTER 4

MOTIVATION AND INITIAL DESIGN

The motivation for this thesis work is study of performance of a very large/medium range aircraft. The wing-fuselage combination developed and studied represents a custom-designed B777x fuselage class but medium range airliner. The principal design variables taken for the study are as follows:

- Design Cruise Speed: Mach ~ 0.84
- Design Critical Mach number: Mach ~ 0.79

- Design Lift: 950,000-lbm with an elliptical load distribution
- Design Altitude: FL350 (35,000 ft pressure altitude)
- Wing-span (tip-to-tip): 225 ft
- Fuselage Length: 240-ft
- Fuselage Diameter: 21 ft

The initial design was done in VORLAX. To start with the design, first we estimated the wing surface area and the mean chord. The second step was to determine the ideal transverse lift distribution from the mean chord, lift and the reference area to compare the lift distribution at every iteration of the design process with the ideal lift. We used the following equation from T.Takahashi's performance book (volume 2)[1] to calculate the ideal lift.

$$L'(y) = 1.226 \times \sqrt{\left\{1 - \left[\frac{y}{\frac{b}{2}}\right]^2\right\}} \left(\frac{W}{S}\right) \bar{c}$$

where, b is the wing-span, y is the semi-span length varying from zero to semi-span, $\bar{c}$ is the mean chord, W is the design lift and S is the wing reference area. The ideal lift distribution plot for this case is shown below.

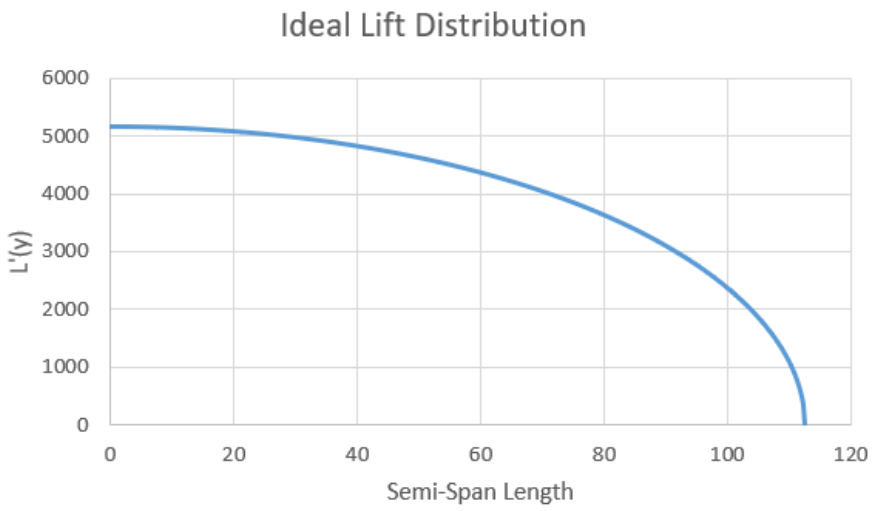

Figure 17: Ideal Semi-Span Lift Distribution for the design process

The next crucial step in the design process is the prediction of critical pressure coefficient which sets the threshold to have a shock-free flow. We used Küchemann's famous critical pressure coefficient equation to calculate C_p^* for a 35-degree sweptback wing. The angle of sweep was predicted based on the available data of Boeing 777 as the flight conditions and design variables closely match with this existing "well-designed" flight. The VORLAX model uses five wing panels for design. Fuselage and the wing panels are modelled as sandwich panels with full leading-edge suction. The final model from VORLAX i.e., the optimized initial design has the following:

- Wing Trapezoidal Planform Area (*Sref*): ~8715 sq. ft
- Wing Loading (*W/Sref*): ~ 110 lbf/ft^2
- Leading-Edge Sweep (Λ_{LE}): 35-deg
- Quarter Chord Sweep ($\Lambda_{c/4}$): 31-deg
- Aspect Ratio (*AR*): 5.8
- Taper Ratio (*TR*): 0.31
- *t/c* at side-of-body: 15%

- *t/c* at wing-tip: 6%
- VORLAX Computed Inviscid Drag Coefficient: 0.02532
- VORLAX Computed Lift Coefficient: 0.48617
- Mach number normal to Leading-Edge: 0.647
- Design C_p* = − 0.686

The other parameters from the initial design have been plotted and produced here.

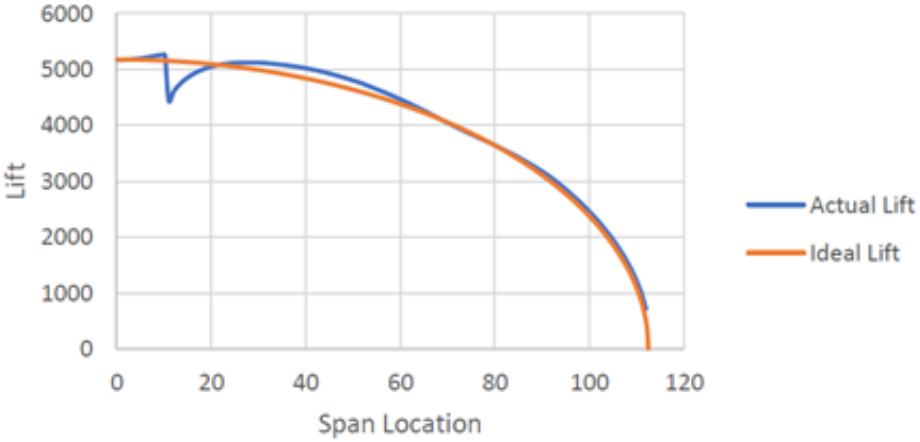

Figure 18: Final Lift Distribution from the Initial Design

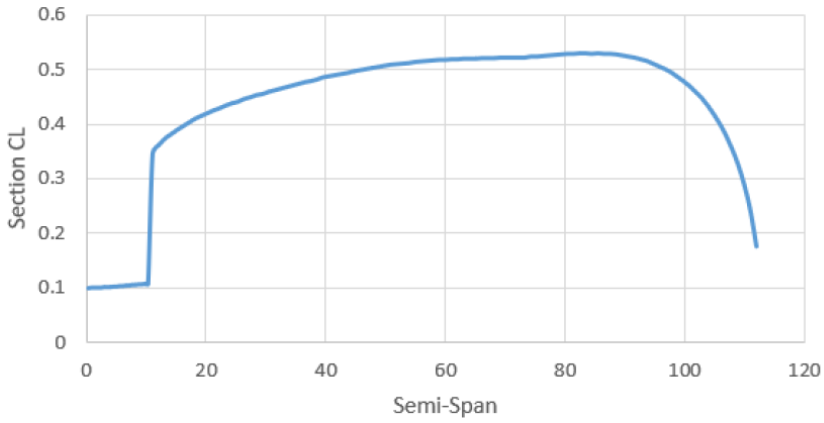

Figure 19: Transverse CL distribution @CL ~ 0.5

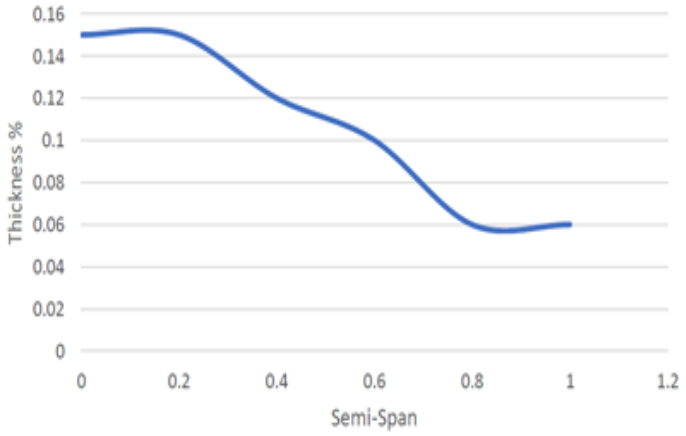

Figure 20: Wing (t/c) as a function of semi-span (%)

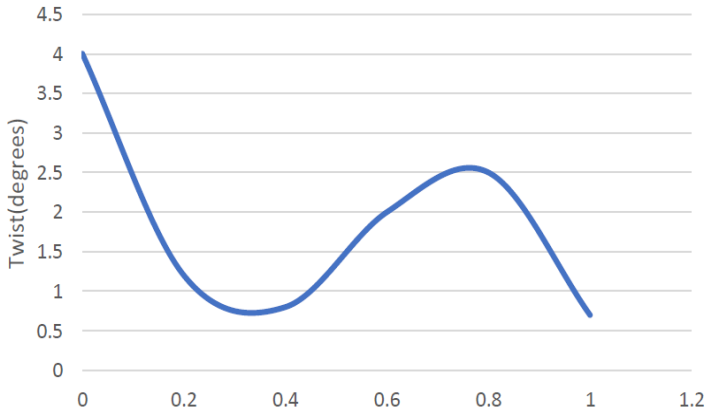

Figure 21: Wing Twist (+ incidence is LE up)

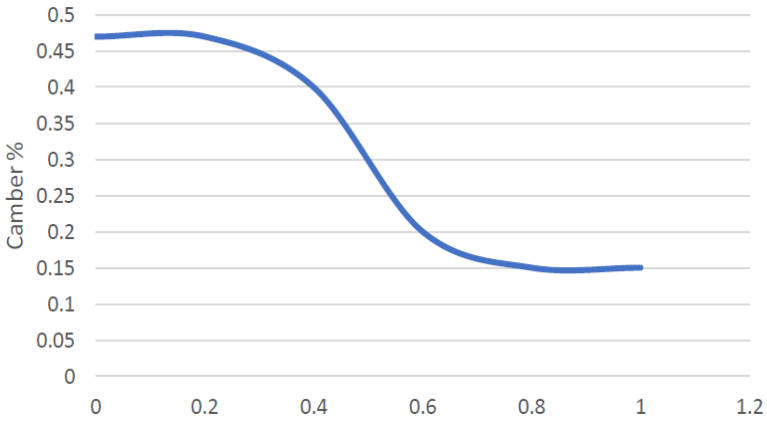

Figure 22: Camber Scale Factor

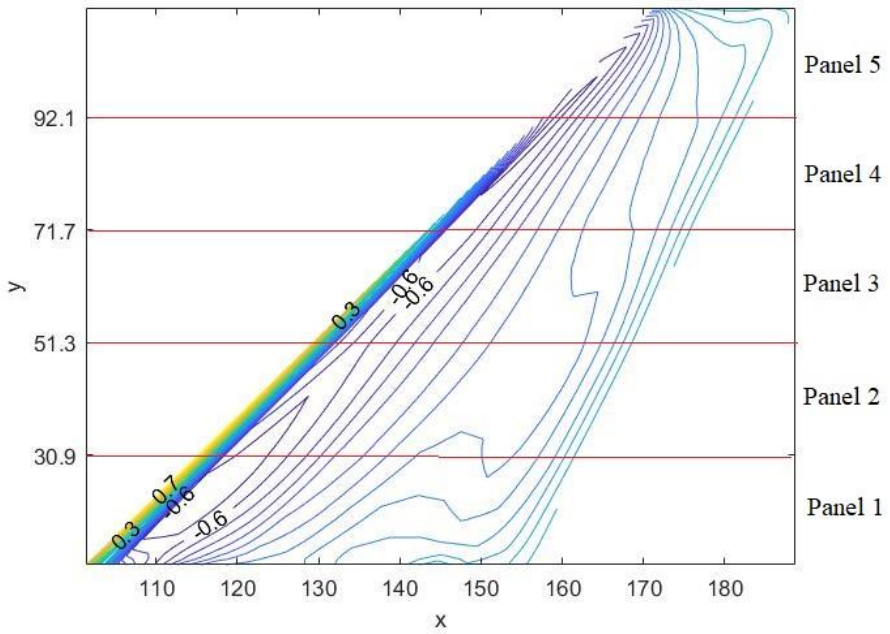

Figure 23: Cp isobars from VORLAX @ M=0.79, CL ~ 0.5 and AOA=1-deg

It is evident from Figure 23 that the isobars are smooth except near the trailing edge which is a concern to be addressed. To obtain these smooth isobars where Cp_{min} across the span was pushed as much as possible to the critical pressure coefficient near the leading-edge resulted in the thickness distribution shown in figure 20; the wing is 15% thick at the side-of-body and tapers to 6% at the tip. During the design process, we realized that increasing the incidence on wing panels makes the Cp_{min} on the upper panels of each wing panel more negative than increasing camber does. So, it is possible to achieve an elliptical lift distribution and allowable pressure distributions at the same time by decreasing incidence and increasing the percentage of camber. Another take away from VORLAX solutions is that thickness does not contribute to lift; it just changes the pressure distribution. Moreover, thickness helps in elevating Cp_{min} making it more negative which gives Cp_{min} values closer to the Cp_{crit} calculated from Küchemann's equation. We used superposition principle which is based on the fact that airfoil lift is the sum of pressures due to camber, incidence and thickness

respectively. The sharp decrease in lift is due to the boundary layer ingestion at the wing-fuselage junction and the wing-body interactions. The additional *t/c* near the side of the body helps in elevating the critical *Cp* near the leading-edge of the wing which helps it in utilizing leading-edge suction and keeping the sweep of the pressure isobars relatively uniform (see Figure 23).

To have an elliptical lift distribution over the fuselage, the angle of attack of the whole model had to be other than zero because we modelled the fuselage as a flat panel that can't generate lift at zero angle of attack. The VORLAX model indicated that the ideal transverse lift distribution was attained when the wing/body configuration was designed for the fuselage to fly at α = 1-deg i.e., 1-degree of deck angle on the fuselage.

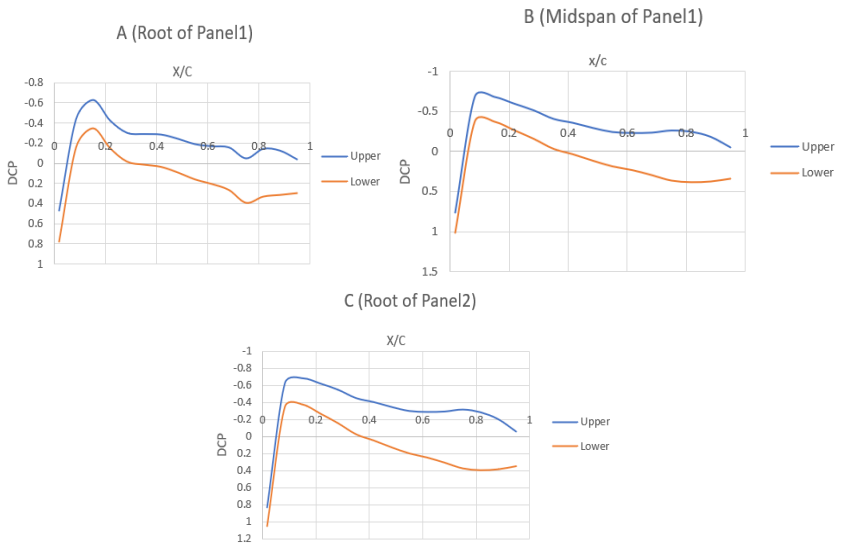

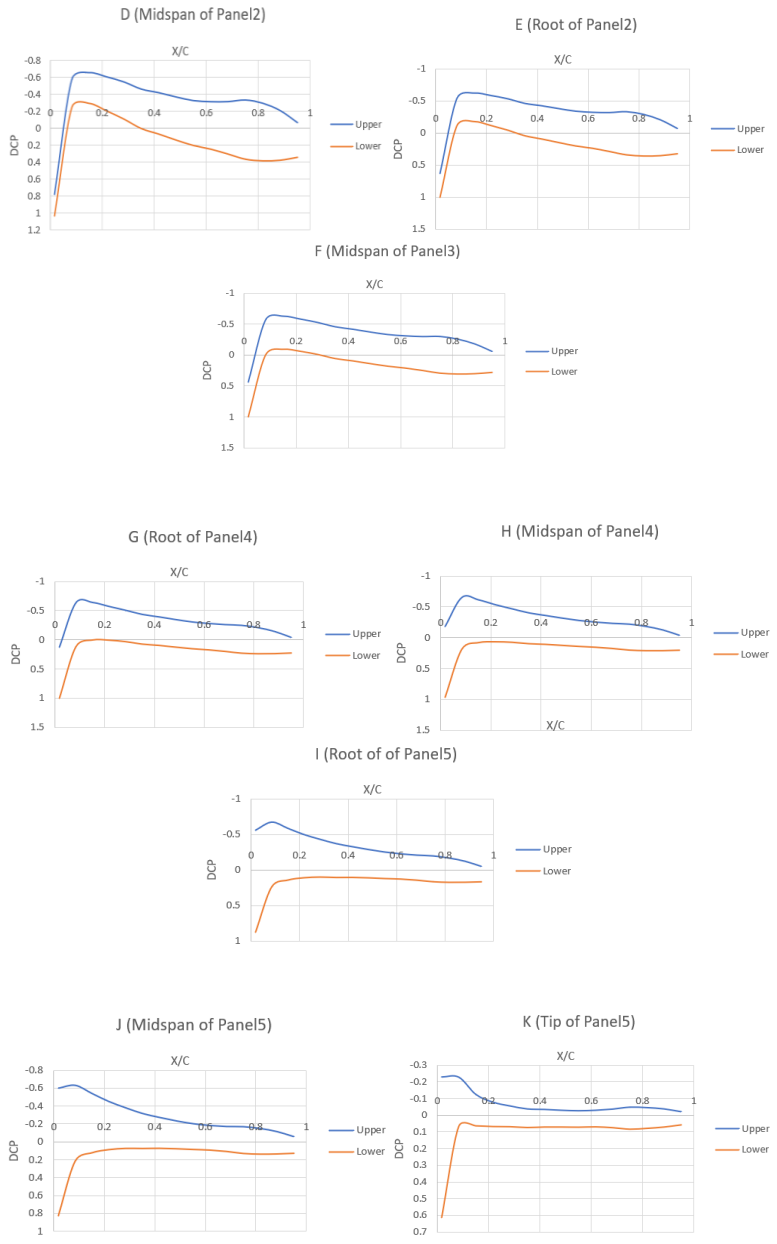

Figure 24: Cp distributions from VORLAX along various cuts – Mach 0.79 – CL~0.50; AOA=1, Cp*swept = -0.686

Here, in Figure 24, we present the pressure distributions obtained from initial wing-fuselage combination design in VORLAX. This design was inspired by Pearcey's peaky leading-edge pressure profiles from the pressure distribution plots along the various cuts of the wing because the peak suction of the initial design wing is far forward on the wing (about 10% *x/c*) across the whole span. At the coarse panelling level of VORLAX mode, target near-critical pressure distributions (*Cp* ~ *Cp**) across

most of the span simultaneously with the desired quantity (C_L ~ 0.5) and quality (elliptical loading) of lift. These solutions are obtained assuming full leading-edge suction (SPC = 1 in VORLAX). Also, these solutions are known to be accurate at low Mach numbers because generally, low Mach number flows are shock-free. So, the solutions obtained for low Mach number flows from the computational fluid dynamics tool, SU2, were first validated with the solutions of VORLAX to check the accuracy of design process.

The initial design that was made in VORLAX provided a lot of preliminary insights. However, it gives only 40% of the actual result as it is not capable to simulate test cases involving shocks. Hence, this preliminary optimized design needs additional attention if it has to be used in practical applications. The further work in this thesis determines the associated problems involved in the solution obtained from VORLAX and studies the effect of design modifications on the performance of aircraft using a computational fluid dynamics tool, SU2. Indeed, the computed and so-called optimized design from VORLAX produced a shock when modelled using a 3-D CAD tool (CATIA) and simulated in SU2 using a symmetry boundary condition at the centre of fuselage. This work does not take into account the stability and control of the aircraft i.e., the role of horizontal and vertical tails on the performance of flight but a couple of test cases have been studied including winglets. The initial design is also produced in CATIA (figure 25).

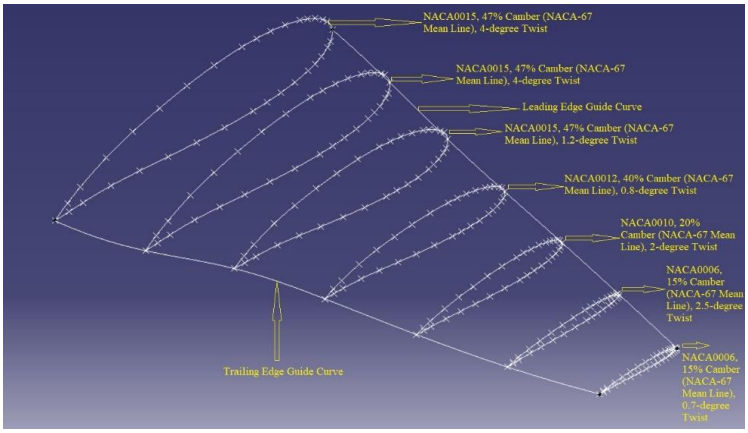

Figure 25: Basic Wing Geometry in CATIA

The initial design included airfoils from the NACA 4-digit blunt leading-edge thickness form[5] and appropriate percentages of NACA-67 moderately aft-loaded camber form. The model is designed in such a way that camber, thickness and incidence were allowed to vary at each control point. Thus, the basic wing geometry (see Figure 25) is parameterized in terms of 18 independent design variables to define a complex shape governed by a constant reference area, aspect ratio, taper ratio and leading-edge sweep angle.

This VORLAX model on a coarser level was reproduced using a 3-D CAD tool (CATIA) surface design where each of the six-control point airfoils is further defined by 35 coordinates per section. However, there are some discrepancies during the transition of control points from VORLAX to CATIA. These are as follows.

- VORLAX allows open airfoils i.e., the trailing edge need not be closed. So, a trailing-edge radius can be incorporated that exactly match with the airfoil data taken from the NACA-824 Abbott & Doenhoff paper[5], however, CATIA does not allow to create surface loft using open trailing-edge airfoils. So, all the designs in this thesis work include a sharp trailing edge.

- Secondly, as the fuselage design in VORLAX was done using a flat panel, there was no concern regarding the creation of a watertight wing-fuselage junction whereas using the multi-section surface tool in CATIA, the actual wing co-ordinates imported from VORLAX resulted in the creation of a wing-fuselage junction that had a gap between wing and the fuselage due to which mesh generation failed. To resolve this issue, a so-called dummy airfoil was created that extended to the centre of fuselage keeping the sweep and trapezoidal planform intact. This resulted in a watertight wing/body configuration.
- Moreover, VORLAX creates the wing geometry as a sandwich panel, thus there is no need of a guide curve joining the leading-edges and trailing-edges of the all the airfoils but in a real 3-D design, there must be a smooth transition between adjacent airfoils to avoid any sharpness or separation point on the wing upper surface. To ensure this, we employed splined guide curves in CATIA.
- Finally, in VORLAX, the area at which the wing connects the "flat panel" fuselage does not comes to place but in a real 3-D design (as in CATIA in thesis), the area at which the wing connects the fuselage can be varied. To see the effect of this, we designed three different models with different points of connections of the wing to fuselage. However, the results show that slight variation in the area of connection does not affect much the pressure distribution or the elliptical spanwise load distribution. Thus, the "original" z co-ordinates from VORLAX were used in the initial CAD design.

All together, we have 245 coordinates to define the high-fidelity loft that directly trace camber, thickness and incidence variables used in the potential flow design.

Further, the fuselage was designed as a cylinder that has a hemisphere in the front (with the same radius of cockpit dimensions in VORLAX) and conically tapers at the back.

Pointwise was used as the meshing tool for SU2. Initially, meshing was done in regular procedure and refining the leading and trailing edges of the wing to resolve the curvature. Subsequently, voxel meshing was implemented wherever necessary as it has the option to include transition layers and sources that is beneficial for external aerodynamics. To examine the presence of shock waves over the wing EULER solver has been chosen for all the simulations. EULER wall boundary condition was set all over the model and far-field markers were used to represent far-field. Figures 26 and 27 show the isobar pattern and *Cp* distribution over the wing surface for the initial design at the design Mach number (M = 0.79). Figure 28 shows the local Mach number contour at the same conditions.

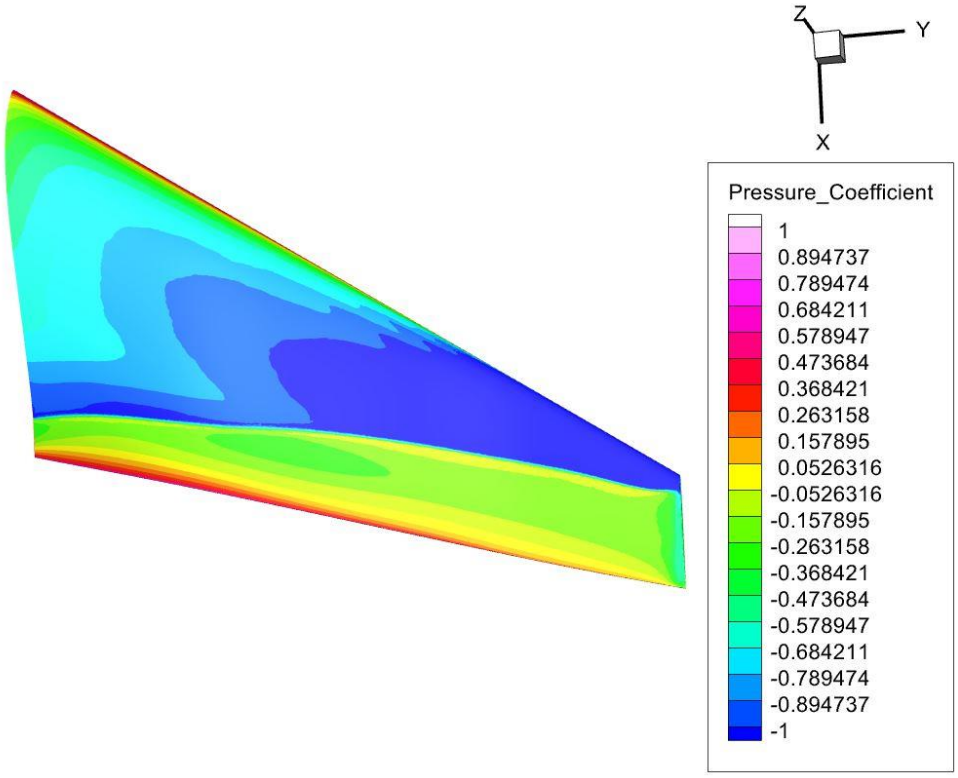

Figure 26: Upper Surface Isobars for Initial Design (M = 0.79, AOA = 1)

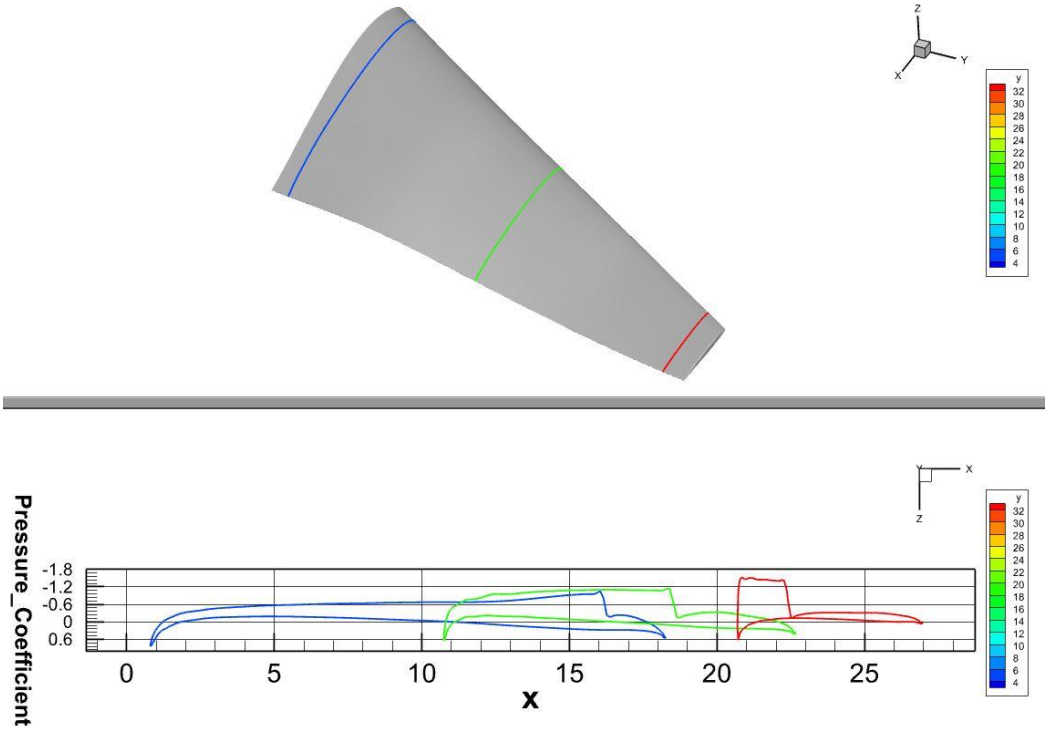

Figure 27: Variation of Pressure Coefficient on the Initial Designed Wing (M = 0.79, AOA = 1)

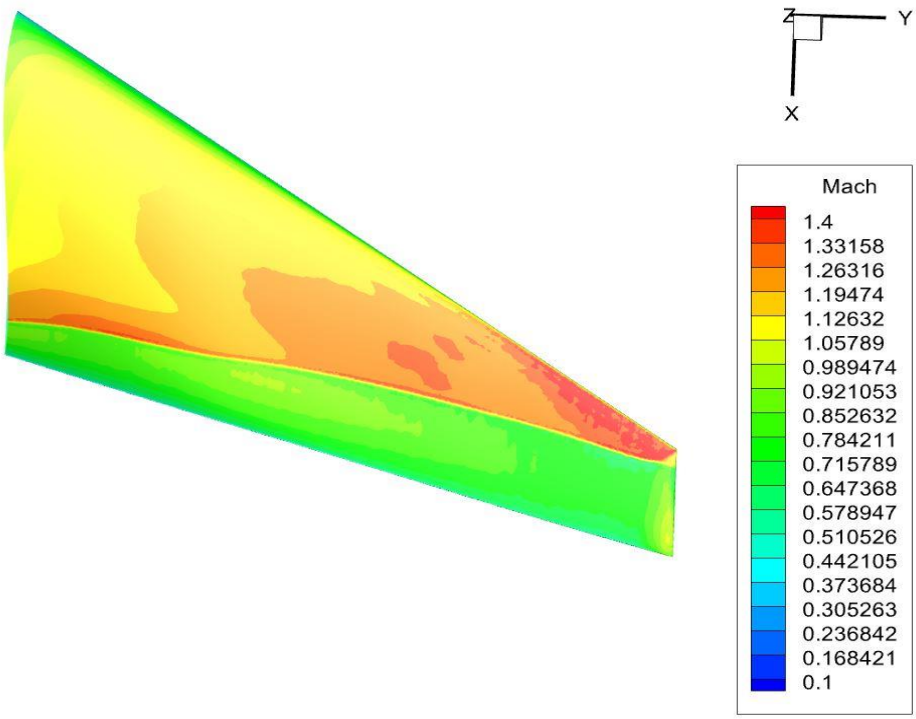

Figure 28: Variation of Local Mach Number on the Initial Designed Wing (M = 0.79, AOA = 1)

Analysing Figures 26 and 27, it is evident that the VORLAX designed wing contains an aft shock. In addition, the pressure coefficients over a large portion of the upper surface of the wing goes beyond -1 which suggests that the pressure coefficient at the wing-fuselage junction exceeds the estimated critical pressure coefficient from Küchemann's equation (Equation 1) by a large margin at about 94% *x/c*. Similar is the case for midspan *Cp* distribution but the strong shock moves forward to around 70% *x/c*. At the wing-tip, there is a strong shock at about 8% *x/c*.

From these initial design results, we conclude that there is a shock generated at wing-fuselage junction and the wing-tip which spread and induce shocks over a large area of the wing and the shock moves forward as we move from root to tip. This is certainly not predicted by simple sweep theory that we assumed to hold true during

the design process in VORLAX. Again, looking at the local Mach number contour plot, we observed that though the design Mach number for the wing-fuselage combination is 0.79, there are regions on the wing that experience supersonic Mach numbers and there is a string shock when Mach number changes from supersonic to subsonic.

If we strictly follow Küchemann's critical pressure coefficient rule, it is the Mach number normal to leading edge that matters. Equating $M_\infty \cos(\Lambda) = 1$, M_∞ is nearly equal to 1.22. So, there are supersonic regions at several places of wing upper surface starting at the tip and the junction. Another interesting point to note here is that even if the initial optimized design was done using the Küchemann's critical pressure coefficient equation, there is an aft shock all the way from root to tip and the shock seems to be unswept.

We suspect that this is perhaps due to the thin tip airfoil as a thin blunt airfoil acts like a sharp airfoil[20] in a three-dimensional flow-field or due to wing-fuselage interference effect that causes a sharp decrease in lift seen as a kink in the lift distribution plot and triggers a shock. So, first we need to check the solutions at a lower Mach number. As SU2 is still in developing stage for the low Mach number cases, the lower Mach number simulations (M < 0.4) did not converge to a particular solution. So, we restricted the lower Mach simulations to M = 0.4. The *Cp* curves and the surface isobars are presented in Figures 28 and 29.

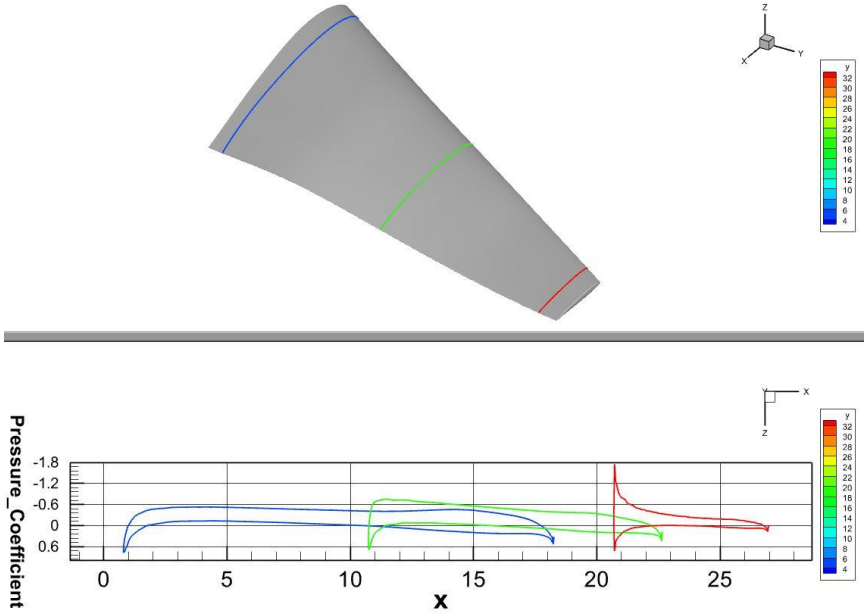

Figure 29: Variation of Pressure Coefficient on the Initial Designed Wing (M = 0.4, AOA = 1)

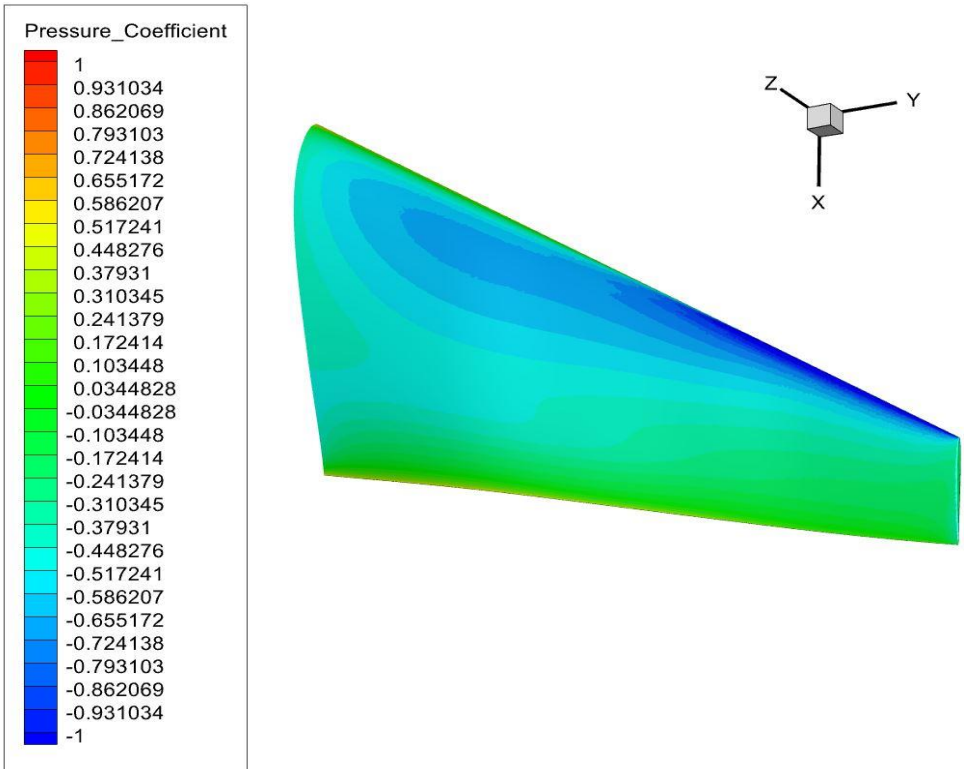

Figure 30: Upper Surface Isobars for Initial Design (M = 0.4, AOA = 1)

The pressure distribution curves (see Figure 28) are smooth at the root and half of the midspan. However, there is a strong leading-edge suction towards the tip due to the

peaky type pressure distribution[10]. In addition to that, the drop in pressure coefficient at the tip is huge which may be the cause of a premature shock. Despite the difference in grids and solver used by VORLAX and SU2, the results obtained for this particular case by both methods agree well with a few exceptions. In general, the isobar patterns obtained from VORLAX and SU2 match very well with the following differences.

- SU2 estimates the minimum pressure coefficient near the wing tip as a value considerably more negative than that predicted by VORLAX on a coarser grid (~ −1.8 as opposed to −0.686). This pressure coefficient is sufficiently negative than the swept wing estimation by Küchemann's critical pressure coefficient. This low-speed computation indeed points that an unintended shock formation when analysing the wing-fuselage combination near its predicted critical Mach (M ~ 0.79)
- With both SU2 and VORLAX, the isobar contours unsweep as we cross the fuselage. Due to the simplified flat panel fuselage in VORLAX as opposed to the cylindrical fuselage in SU2, there exists some differences in solutions at the wing-body junction and the tip regions. These specifically impact the sweep of isobar lines in these regions. If the unswept isobar pressure coefficients are less than the unswept critical pressure coefficient target (C_p^* = −0.464), unintended premature shock formation may take place when we analyse the model near its predicted critical Mach (M ~ 0.79). A visual inspection of the SU2 solution shows a few suction "hot-spots" at the wing-fuselage junction that may trigger a shock.

The takeaway from these results is that the actual critical Mach number is lower than the predicted critical Mach number by VORLAX. The solutions suggest that the root

and midspan of the wing are shock-free and have a smooth pressure distribution but a prominent shock is likely to form at the leading-edge near the tip and a possible shock may form at wing/body junction around the mid-chord.

CHAPTER 5

TRADE STUDIES

In this thesis work, we have used calculations to run various trade studies to verify the effects of aerodynamic design modifications as well as the misleading character of Küchemann's critical pressure coefficient relation.

Thickening the Outboard Section

The first trade studies were run to determine the effect of thickening the outboard section because prior works in this field show that thickness does not alter the lift distribution helping keep the elliptical spanwise load distribution intact but it affects the pressure distribution. We changed all the NACA0010 and NACA0006 airfoils in the initial design to NACA0012 (see Figure 31) keeping the percentage of camber constant (The initial design had NACA 0006 with a small percentage of NACA-67 mean line aft camber). According to theory, from a drag divergence perspective, a thinner wing is always more preferred compared to a thicker wing because it reduces the net suction over both the upper and lower surfaces. If the pressure coefficients due to increasing thickness are less negative, for a given critical pressure coefficient, they will be capable of generating greater lift without developing any shock. As Boyd conical camber theory shows that a thin blunt airfoil behaves like a sharp airfoil in a 3-D flow-field, so adding thickness to outboard sections is expected to help reduce separation. This section of the thesis shows the limitation of thin airfoil theory

because sharp leading-edge profiles accentuate the incidence dependent suction profile of the wing.

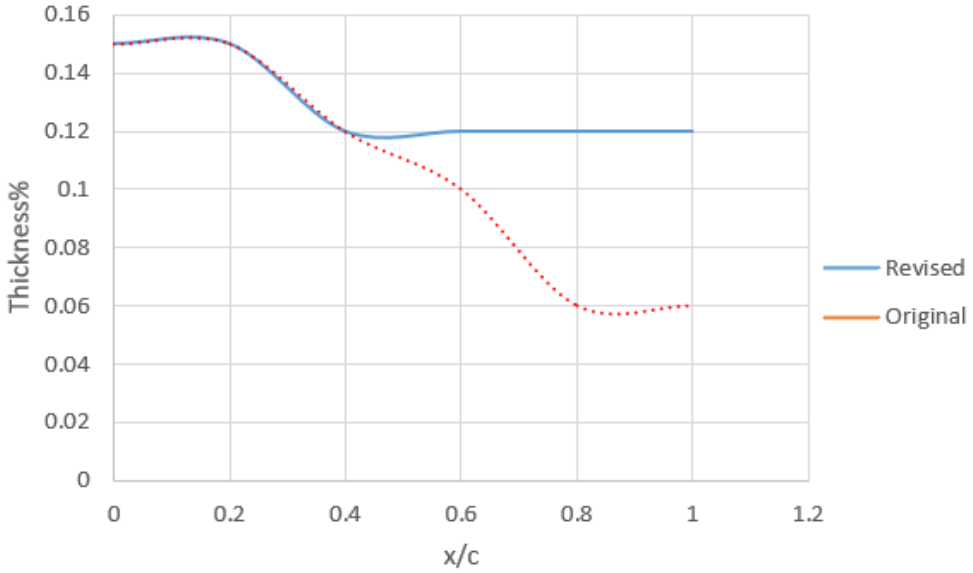

Figure 31: Initial and Revised t/c Spanwise Distribution

Since leading-edge radius and thickness distribution are closely related, this thesis work first explores the changes in transonic aerodynamic characteristics by increasing the thickness of the outboard section. However, we first need to ensure that the low-speed solutions are shock free and it does not imply a premature shock at higher subsonic Mach numbers. Figures 32 and 33 show the upper surface isobars and the pressure distribution over the wing for a Mach number of 0.4.

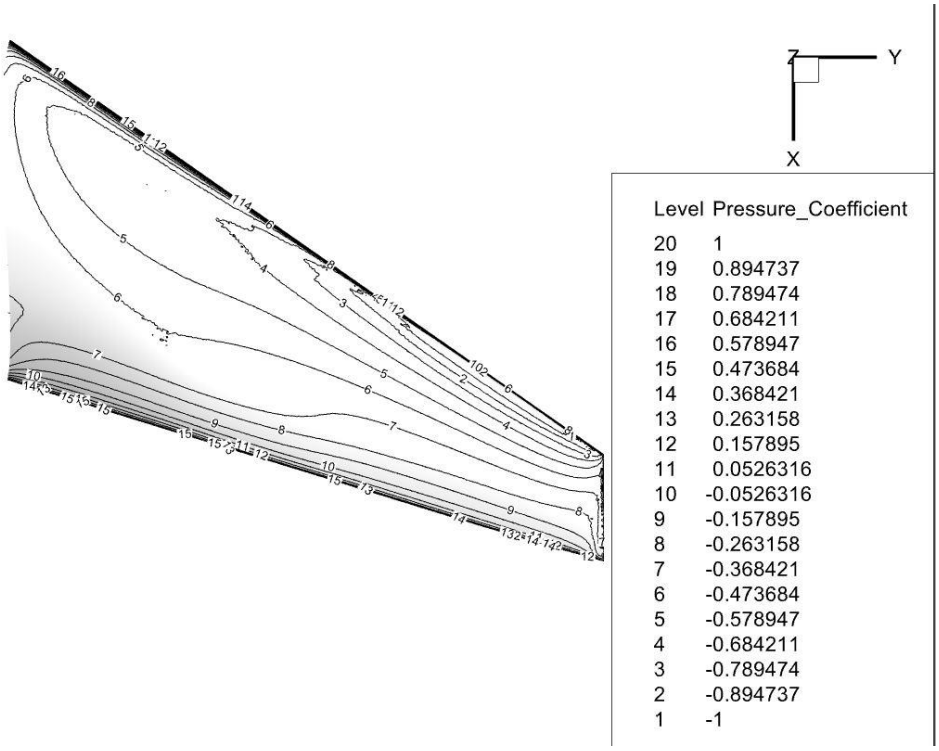

Figure 32: Upper Surface Isobars for the Thickened wing (M = 0.4, AOA = 1)

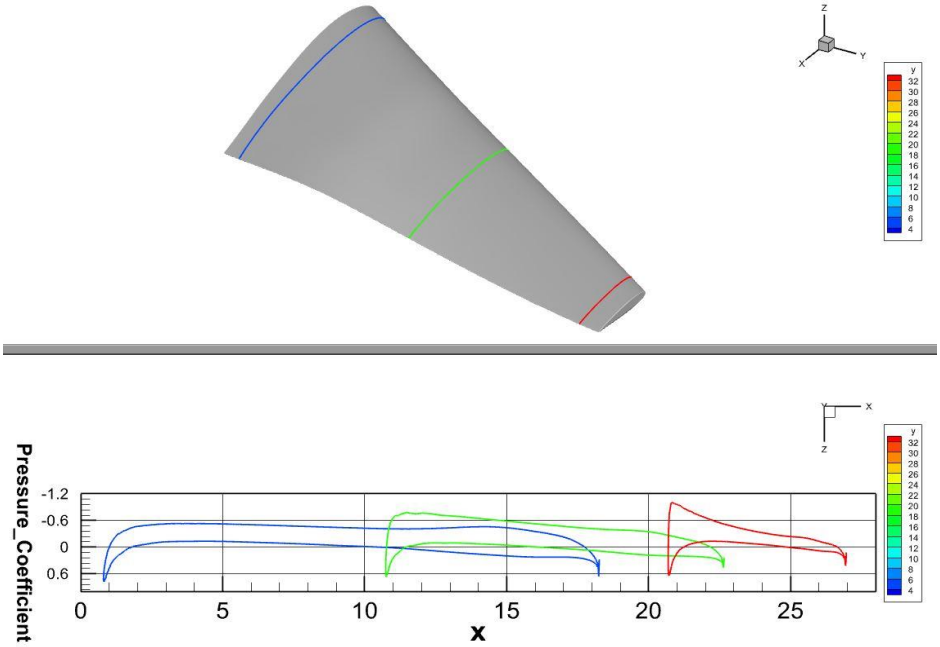

Figure 33: Cp cuts over the wing at three spanwise locations (M = 0.4, AOA = 1)

From the upper surface isobars, it is evident that the wing is shock-free and the isobars are smooth and represent straight shocks which are good for leading-edge suction. The significant effect of thickening the outboard sections is that the pressure

coefficients dropped from ~ −1.8 to ~ −1 and the tip pressure distribution has been smoothened eliminating unnecessarily large leading-edge suction which immediately hints about appearance of a strong shock at the predicted critical Mach number. So, leading-edge radius and thickness details that were neglected in coarse-grid VORLAX turns out to be important for solving the premature shock problem.

With this insight, analysing the solutions at the design critical Mach number (M = 0.79), the upper surface isobars (see Figure 34) show that there still exists a prominent shock aft of the wing.

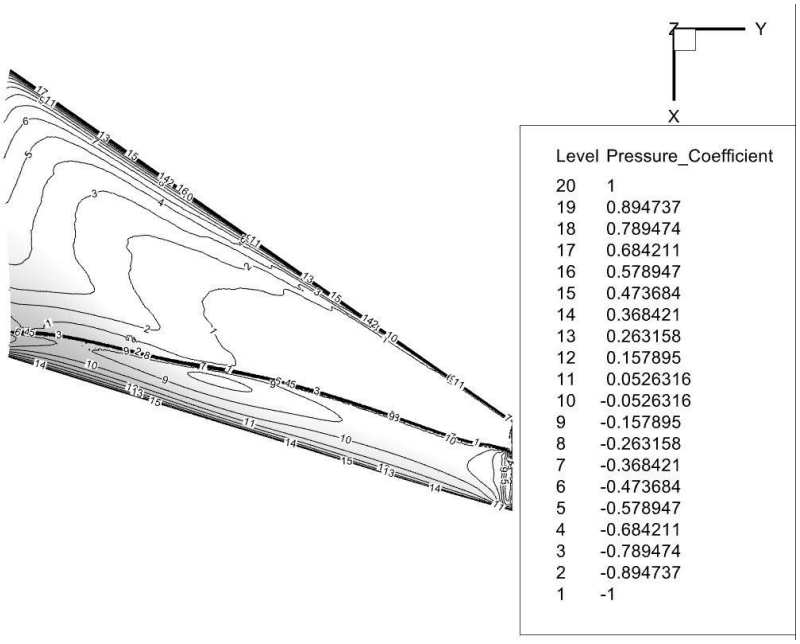

Figure 34: Upper Surface Isobars for the Thickened wing (M = 0.79, AOA = 1)

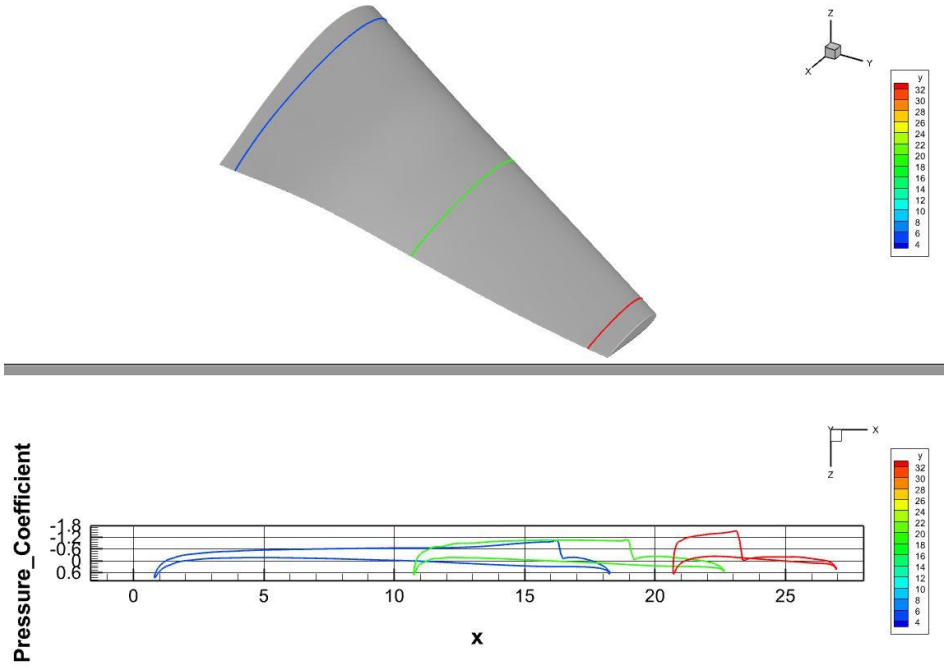

Figure 35: Cp cuts over the wing at three spanwise locations (M = 0.79, AOA = 1)

Another interesting point to note is that though the shock moves forward as we move from root to tip, the tip shock is pushed aft to about 20% *x/c* which suggests that the crest has been pushed aft of the chord due to the thickening but the area enclosed by the pressure curves stay the same. Analysing the results, we conclude that there is no significant effect on wing performance due to the thickening of outboard sections at transonic Mach numbers whereas this design modification affects the upper surface isobars and pressure distribution at a lower Mach number. This may be due to some other serious mistake done during the design process that dominates this design modification. This thesis work finally aims to resolve this blunder due to which this design modification does not produce satisfactory results.

Increasing Leading-Edge Radius and Forward Camber

The second set of trade studies were performed by increasing the leading-edge radius of the thin blunt airfoils, specifically the two NACA0006 airfoils towards the tip section and simultaneously adding a small amount of forward camber.

Prior arts have shown that increasing the leading-edge radius helps in delaying the separation to a higher lift coefficient and the aerodynamic characteristics are more dependent on Reynolds number as compared to the Mach number. We increased the leading-edge radius of the last two airfoils (towards the tip) from 0.4% of the chord to 1.1% of the chord in succession and simulated some intermediate leading-edge radii to compare the modified aerodynamic design with the initial design. Addition of proper camber line and percentage were motivated from the Boyd conical camber[20] theory which resulted in choices of 220, 240 and 250 mean lines to be added to the last three airfoils. This helped in pushing the crest aft as we moved from root to tip.

Also, in the prior art, the cases tested have Mach numbers ranging from 0.21 to 0.94 and Reynolds number ranging from 2,000,000 to 11,000,000 but no cases have been tested at both higher Reynolds number and higher Mach number at the same time. The following show the variation of pressure coefficient and the upper surface isobars for a case with a leading-edge radius of 1.1% *x/c* and the aforementioned forward cambers added to the last three airfoils of the tapered wing respectively.

We also present a schematic of CAD model (see Figure 36) which was created for this simulation run. It is clearly visible that the leading edge is blunt and smooth. We first considered simulations run at lower Mach numbers (M = 0.4) to see if any change in aerodynamic characteristics occur. After analysing the results at low Mach number, we will simulate high Mach number cases if needed.

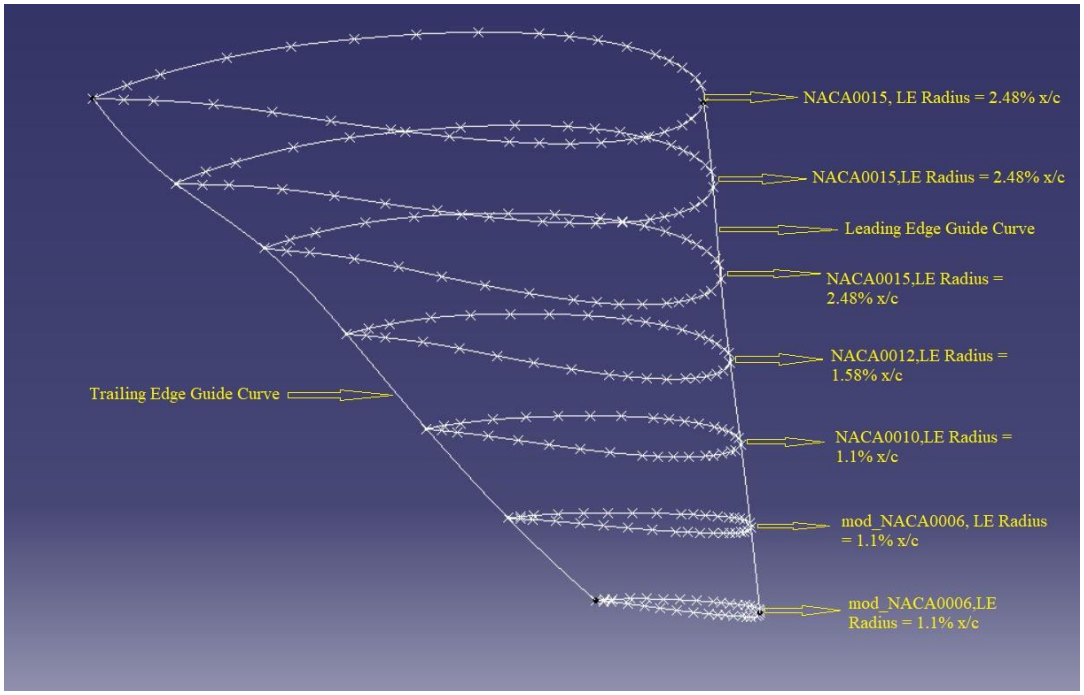

Figure 36: Schematic and CAD Model of last two profiles replaced with mod_NACA0006 (LE Radius = 1.1% x/c)

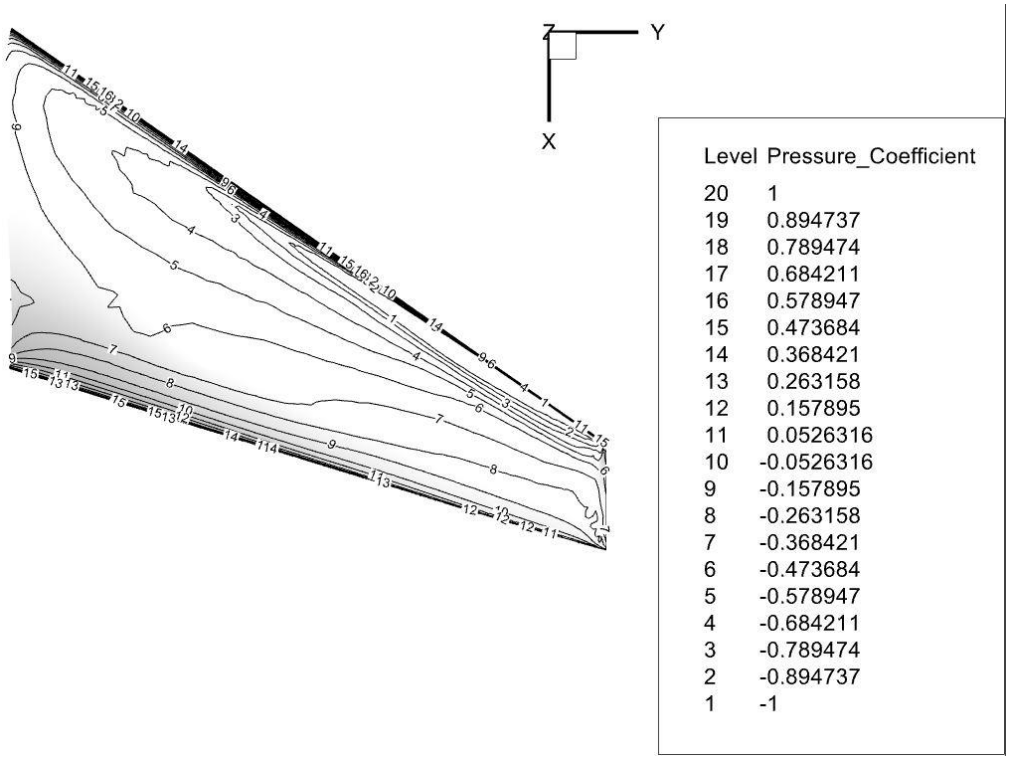

Figure 37: Upper Surface Isobars on the wing with increased LE Radius and Added Forward Camber (M = 0.4, AOA = 1)

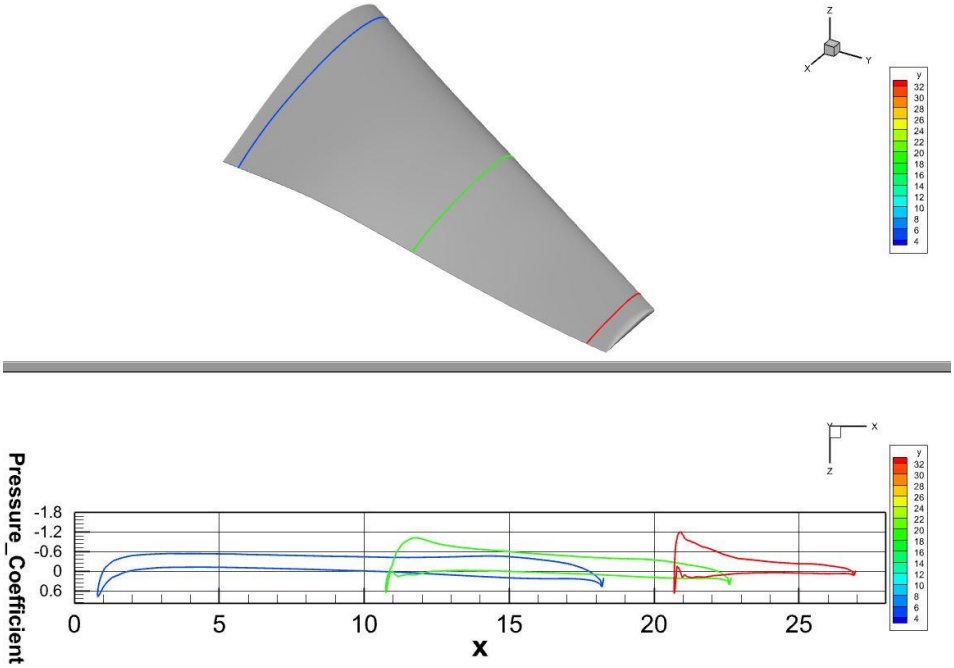

Figure 38: Cp cuts over the wing at three spanwise locations (M = 0.4, AOA = 1)

The upper surface isobars (see Figure 37) are smooth and the local sweep of the isobars are approximately equal to the leading-edge sweep angle of the wing up until the mid-chord. After that, the isobars start to unsweep all the way to the trailing edge. Comparing this with the initial design, there is no significant change in aerodynamic characteristics but the leading-edge suction spike at the tip (see Figure 38) has been reduced from ~ −1.8 to ~ −1. Simultaneously, the leading-edge suction at the mid-span has been increased a bit which is good in creating more lift and opposing drag. This does not necessarily hint at the formation of an unintended shock at the predicted design critical Mach number. As the simulation resulted in a less negative pressure coefficient over the region of modification which, for a given critical pressure coefficient, enable greater lift generating capability.

With the benefits realised, we further simulated the testcase at the design critical Mach number keeping the elliptical load distribution in place. However, there is still a prominent aft shock from the root to tip of the wing. The shock is again

approximately unswept at the wing-fuselage junction and the shock sweep increases as we move from root to tip. So, the argument made by Demele & Sutton in their research paper[22] regarding the delay of separation up to a higher lift coefficient does not hold in this case. This may be due to two reasons.

- The modification may not be good for cases at both a transonic Mach number and a higher Reynolds number (> 11,000,000) due to which they did not perform any test with both these conditions in place.
- There may be a design parameter that dominates this design modification and the mistake undertaken in choosing that design parameter prevent this design modification to work well.

This thesis work shows the importance of that design parameter (discussed later) over the design modifications and resolves the issue satisfactorily.

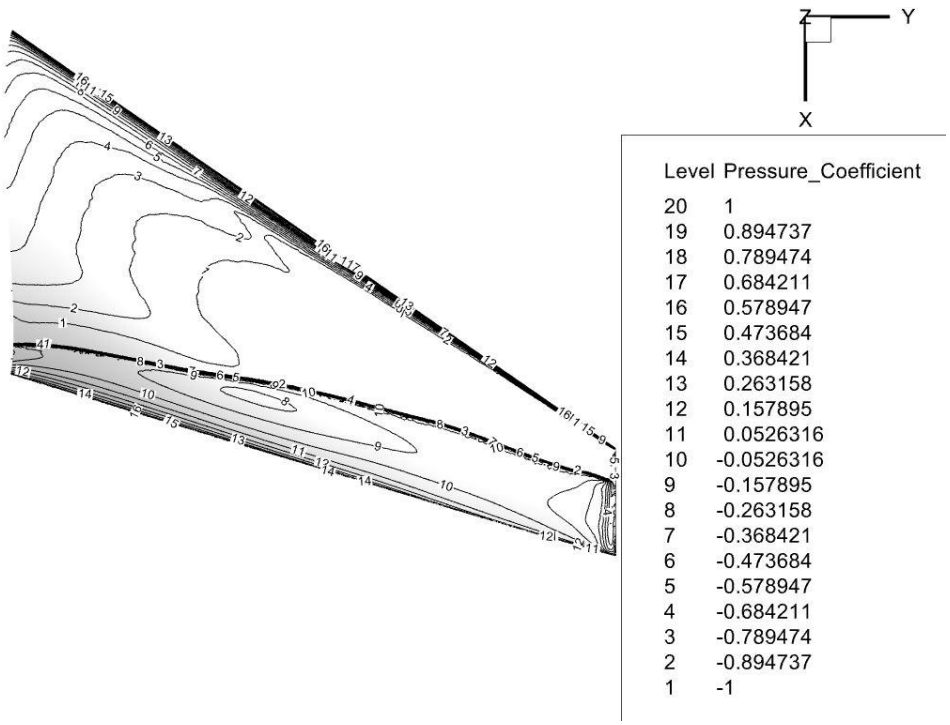

Figure 39: Upper Surface Isobars on the wing with increased LE Radius and Added Forward Camber (M = 0.79, AOA = 1)

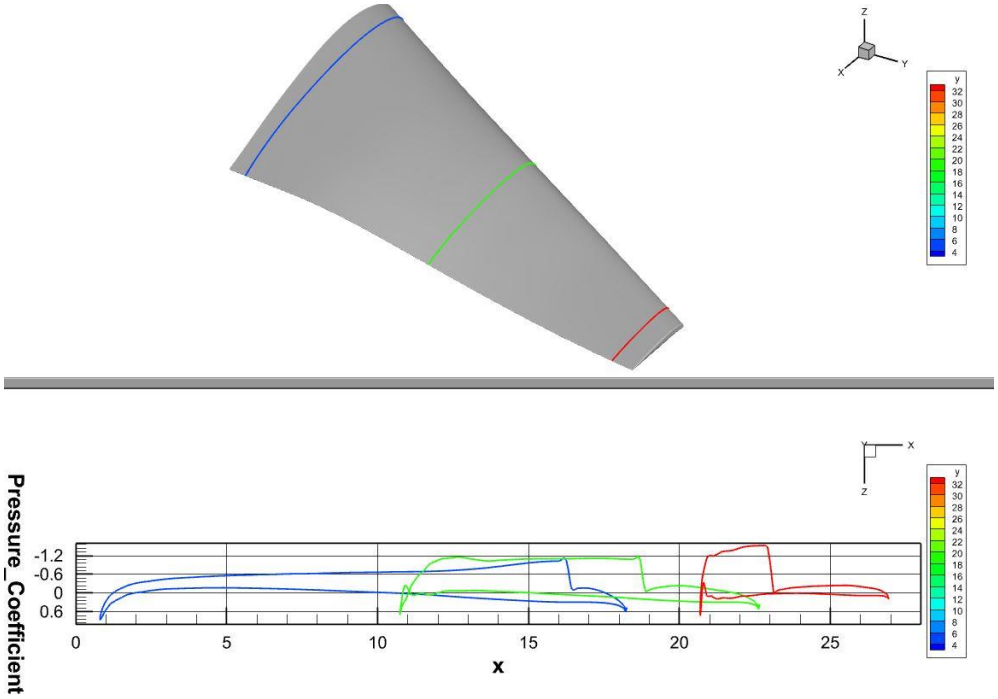

Figure 40: Cp cuts at three spanwise locations on the wing with increased LE Radius and Added Forward Camber (M = 0.79, AOA = 1)

Drooping the Leading-Edge

The third trade studies were performed for a drooped leading-edge wing. As the shock places itself aft of the wing at the root and moves forward with the spanwise direction, there was no droop applied to the root airfoil and also the airfoil adjacent to that. Droop has been used in prior works to delay the onset of shock and to use the shock pretty well by placing it at the crest that maximizes leading-edge suction, thereby creating more lift and opposing drag. In this respect, both the position of droop and the amount of droop matter.

We present here effects of droop coupled with the increase in leading-edge radius and forward camber in a successive manner with five stages of drooping applied to the initially designed wing. Figures 41 and 42 show the test cases with drooping applied once to the specific airfoils at the design critical Mach number (M = 0.79)

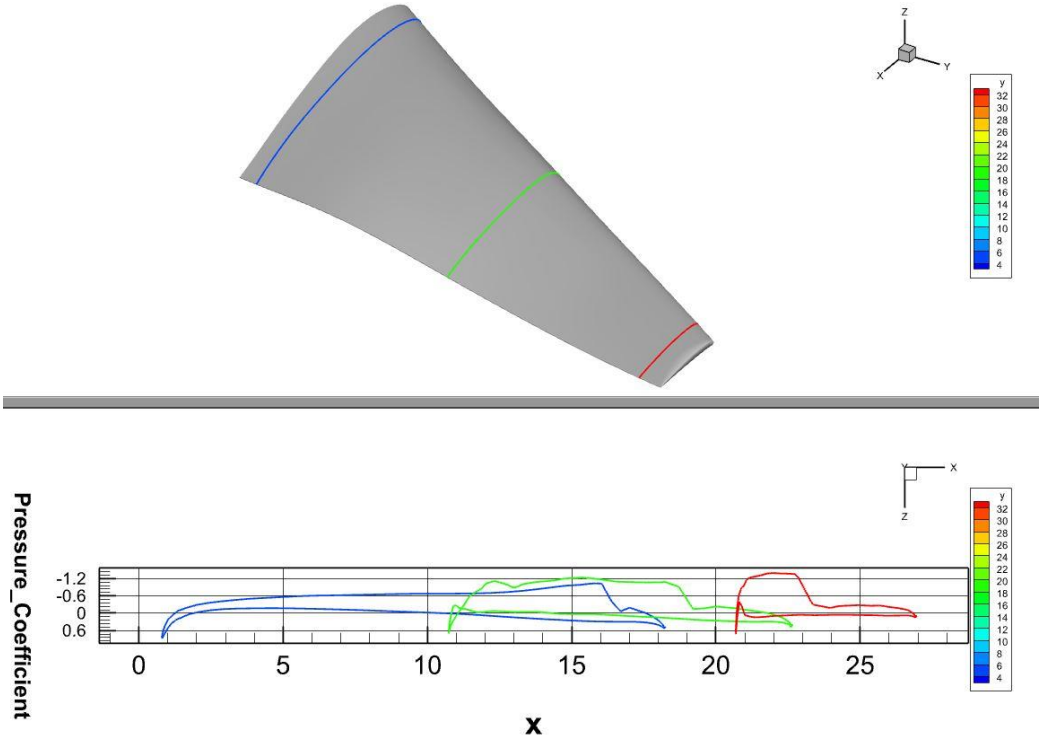

Figure 41: Cp cuts over the wing at three spanwise locations (M = 0.79, AOA = 1)

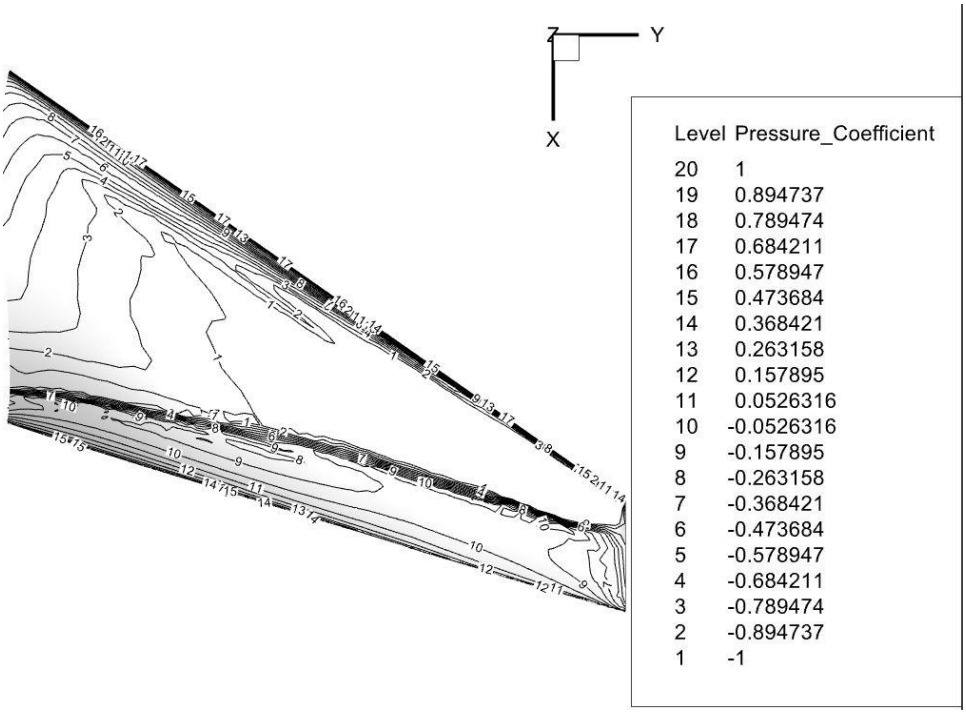

Figure 42: Upper Surface Isobars @ M = 0.79, AOA = 1 (Wing with modNACA0006, added forward camber and droop)

The pressure distribution curves (see Figure 41) show the aft shock at three spanwise locations. It is to be noted that the shock has been weakened due to the application of droop and the shock position has been changed. Additionally, spanwise lift distribution remains the same compared to the VORLAX designed wing. An important thing to note that the aerodynamic design modifications performed do not drastically change the spanwise load distribution, hence help maximize the performance. However, the aft shock is still present all the way from root to tip and looks similar to the initial design.

We observe that the minimum pressure coefficient over the wing as a function of span decreases whereas the region over which the minimum pressure coefficient exceeds the estimated critical pressure coefficient approximately stays the same with the addition of droop. We suspect that an optimization of the degree of droop and the position of droop are required for better results in pressure distribution and shock elimination. Apart from that, another remarkable observation was that the strong leading-edge suction has been marginally reduced for Mach number = 0.4 which means that this modification has worked well for lower Mach numbers (see Figures 42 and 43)

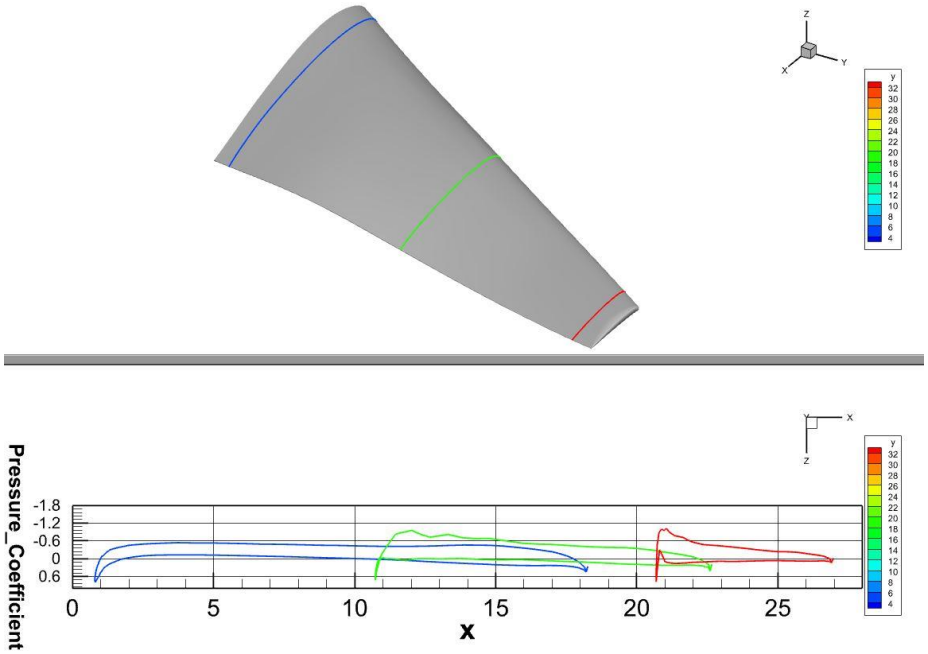

Figure 43: Cp cuts over the wing at three spanwise locations @M = 0.4, AOA = 1 (Wing incorporating mod_NACA0006 with 1.1% x/c and drooped leading edge)

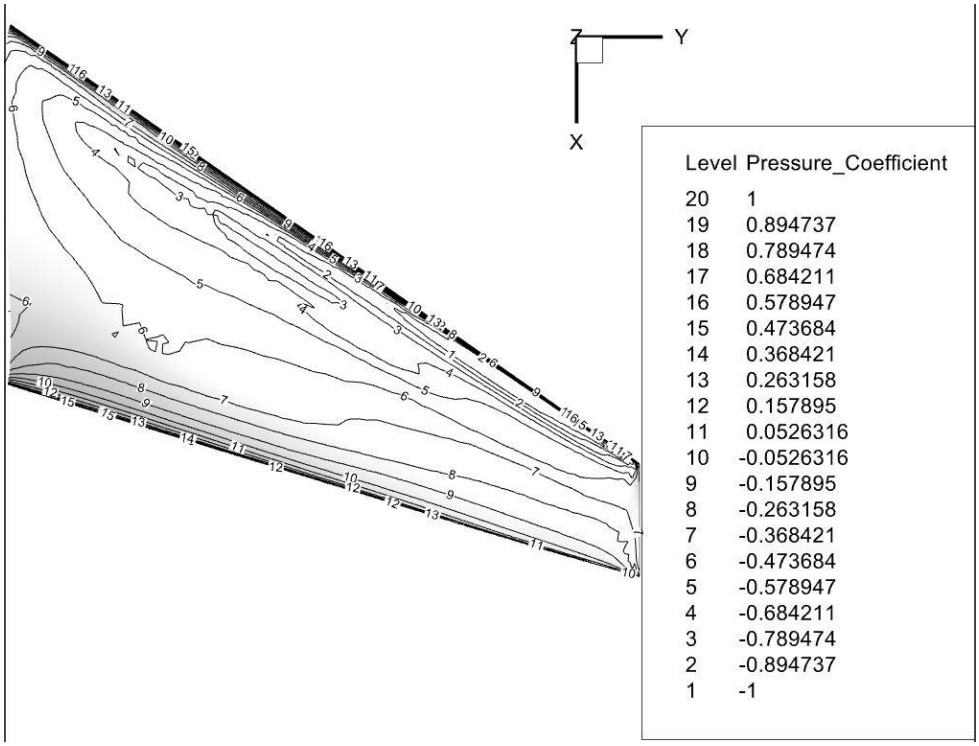

Figure 44: Upper Surface Isobars @M = 0.4, AOA = 1 (Wing incorporating mod_NACA0006 with 1.1% x/c and drooped leading edge)

The next trade studies were run with more drooping applied to the NACA0012, NACA0010 and NACA0006 airfoils following the Boyd conical camber theory with

220, 240 and 250 mean lines added to the last four airfoils. In addition to that, the leading-edge radii of NACA0006 airfoils was increased to 1.83% of their respective chords. This is done to exploit more benefits as we observed when we increased the leading-edge radius to 1.1 % of their respective chords with NACA0006 airfoils, the pressure distributions became smoother.

The following figures show the results we obtained from the simulations using this design modification.

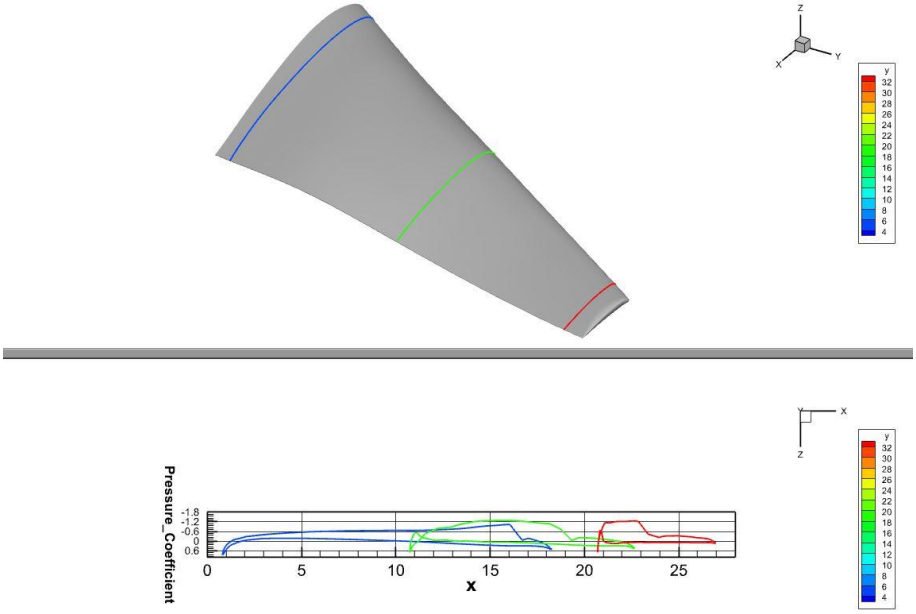

Figure 45: Cp cuts over the wing at three spanwise locations @M = 0.79, AOA = 1 (Wing incorporating mod_NACA0006 with 1.83% x/c and drooped leading edge)

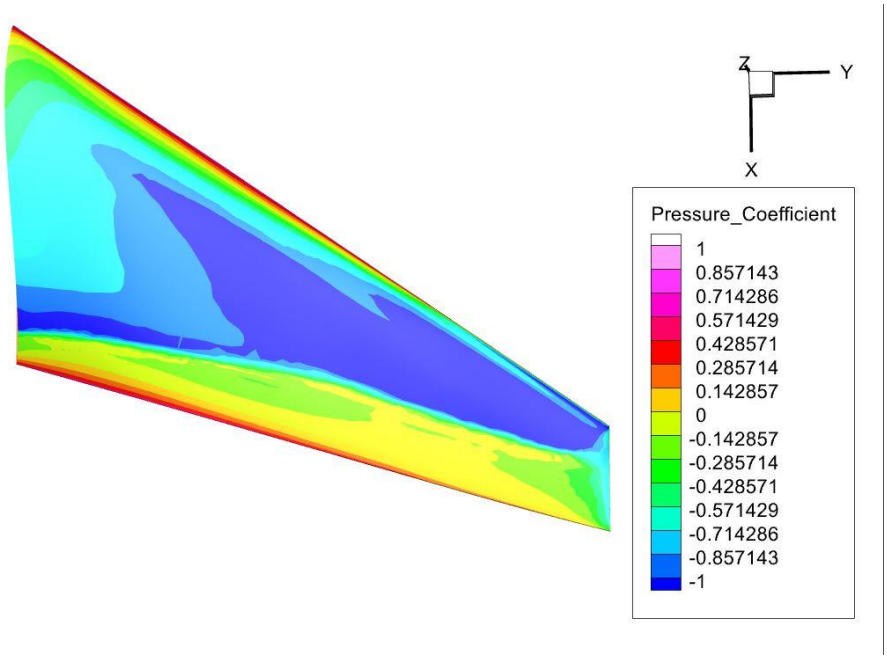

Figure 46: Upper Surface Isobars @M = 0.79, AOA = 1 (Wing incorporating mod_NACA0006 with 1.83% x/c and drooped leading edge)

The drooping was applied to the last five airfoils in the following way:

- 12 control points (6 on the upper surface and 6 on the lower surface) for the airfoil with a chord of 50.8 ft, 16 control points (8 on the upper surface and 8 on the lower surface) were chosen near the leading-edge for the airfoil with a chord of 42.8 ft
- 18 control points for the airfoil with a chord of 34.8 ft, 20 control points for the airfoil with a chord of 26.8 ft, and
- 22 control points for the airfoil with a chord of 18.38 ft.

This helped in changing both the degree of drooping and position of drooping exploiting the concept of Boyd conical camber. Though the pressure distributions (see figure 45) show that the shock is further weakened due to smoothening of *Cp* curves, there is clearly a typical lambda shock clearly visible in figure 46. As we increased

the leading-edge radius to 1.83% *x/c* for the NACA0006 airfoils which is higher than the leading-edge radius percentage of a basic NACA0012 airfoil, we conclude that the tip airfoils do not get benefitted by making them blunter. So, we kept the leading-edge radius constant and increased the degree of drooping utilising the same number of control points as mentioned at the top of this page. Only, the degree of drooping was changed to restore the leading-edge suction that was mentioned in Boyd conical camber theory[20]. However, that did not work in this case. This change in geometry to the initial design indeed helped move around the shock and optimization of this has the potential to place the shock perfectly at the crest to utilize maximum leading-edge suction but it just did not help increase the critical Mach number on the wing.

The next trade study considered drooping applied to only the tip airfoil to make it more drooped compared to other airfoils but no significant changes in aerodynamic characteristics was observed. Again, the last three airfoils were drooped in the next run and finally, all the five airfoils were drooped except the root airfoil. Figures 47, 48, 49, 50 and 51 shows the successive drooping modifications applied to the airfoils during the design process. Figures 52 and 53 show the simulation results of the last modification.

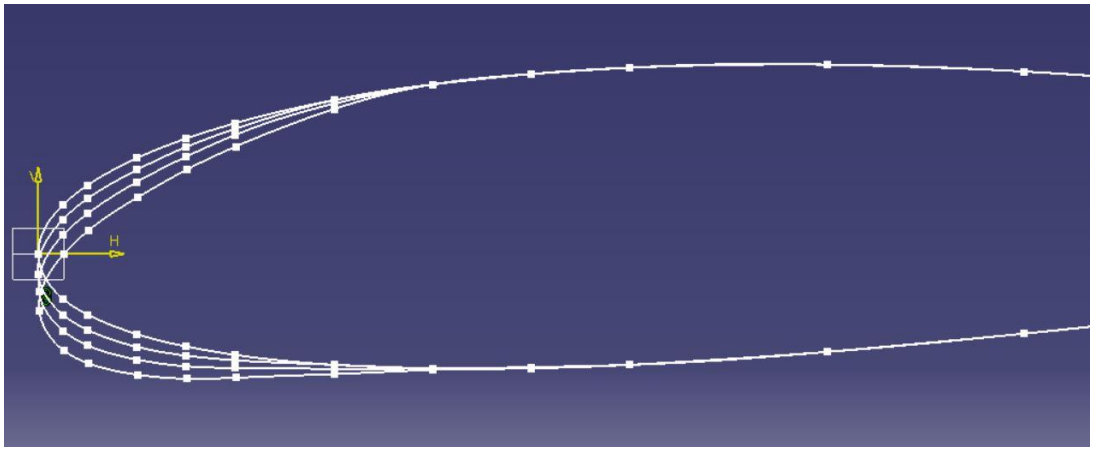

Figure 47: Drooping Developments for the chord with chord-length 50.8 ft

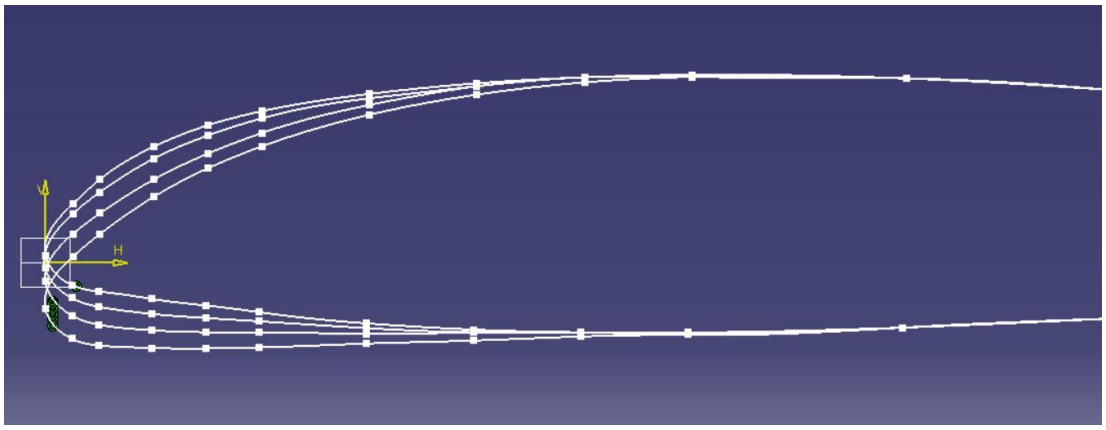

Figure 48: Drooping Developments for the chord with chord-length 42.8 ft

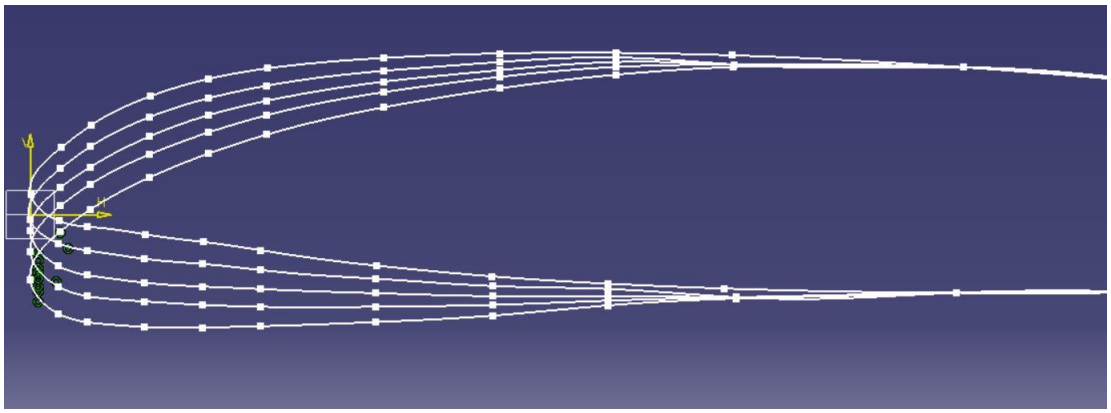

Figure 49: Drooping Developments for the chord with chord-length 34.8 ft

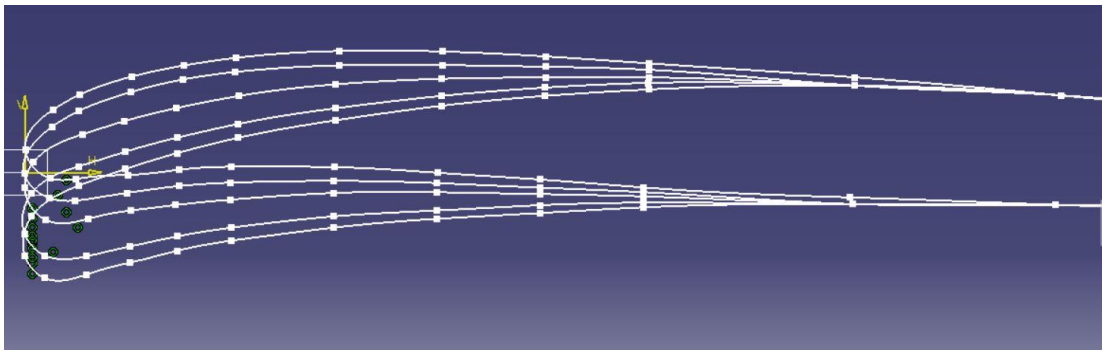

Figure 50: Drooping Developments for the chord with chord-length 26.8 ft

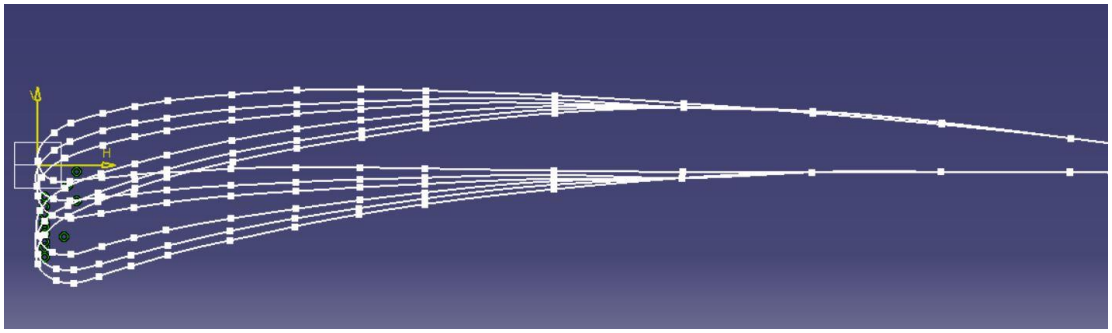

Figure 51: Drooping Developments for the chord with chord-length 18.38 ft

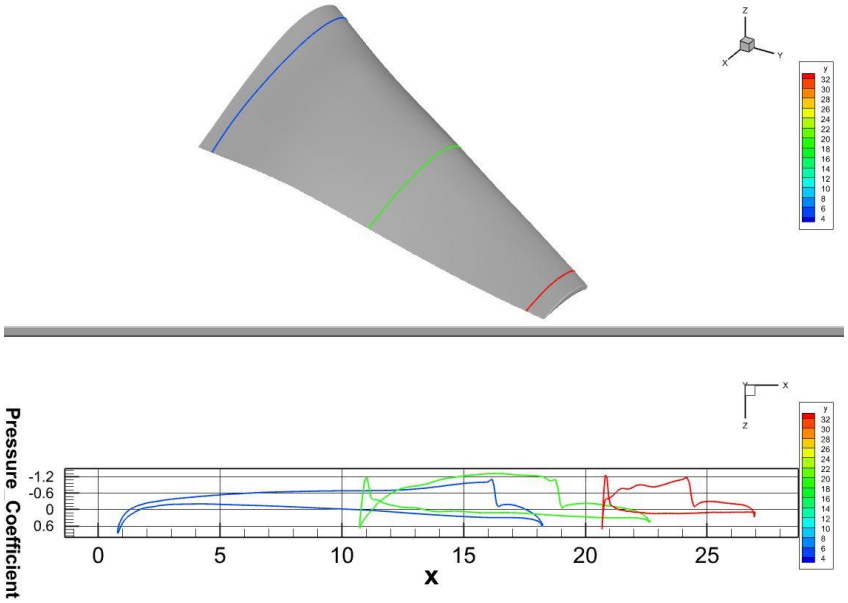

Figure 52: Cp cuts over the wing at three spanwise locations @M = 0.79, AOA = 1 (Wing incorporating mod_NACA0006 with 1.83% x/c and drooped leading edge)

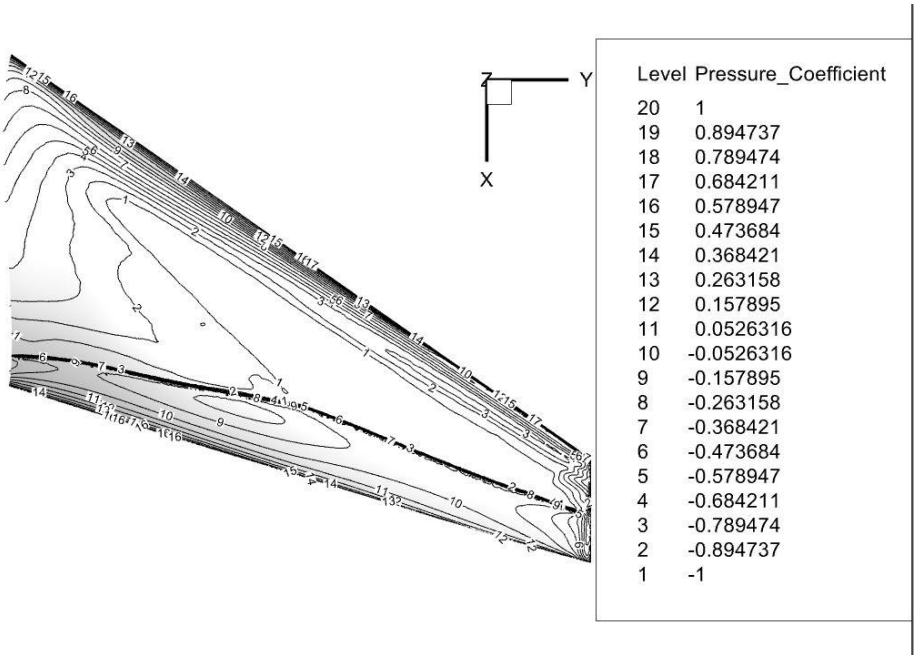

Figure 53: Upper Surface Isobars @M = 0.79, AOA = 1 (Wing incorporating mod_NACA0006 with 1.83% x/c and drooped leading edge)

Analysing the pressure distribution curves and the upper surface isobars, it is evident that after all the design modifications, we are unable to remove the shock. Comparing the final design with the initial design, it can only be said that the shock has been pushed aft of the wing due to the design modifications. All the design modifications were motivated by utilising the maximum out from the shock by placing it at the crest. So, we have the maximum benefits of leading-edge suction, thereby creating more lift. After all these design modifications, we compared the spanwise load distribution with that of VORLAX to ensure that the design modifications have not altered or drastically affected the lift distribution. Figure 49 proves this fact.

Figure 54: Comparison of Spanwise Lift Distribution for the initial and final design

It is evident now that there is some critical design parameter that has been misunderstood or wrongly calculated due to which all the design modifications that have been proved to work well in many cases have not performed satisfactorily well in this case. The next section will address the importance of this critical design parameter that dominates these design modifications.

Critical Pressure Coefficient

As discussed in the prior art section in the thesis, many authors have derived different numerical equations to calculate the critical pressure coefficient. This parameter plays an extremely important role in the design process as flow separation occurs beyond this critical point accompanied by a lot of undesirable phenomena. Because the equations derived diverge from one another at low Mach numbers where they predict higher underpressures i.e., more negative values of critical pressure coefficient, this thesis work intends to determine the misleading character of one of the most popular equations and its impact on the whole design process.

For the transonic 3-D wing design problem, wing sweep is often applied to reduce the Mach number normal to leading-edge. It is precisely in this region that the traditional

equations differentiate from one another. As the real wings carry lift as well as they have a specific structure to meet the design conditions, primary importance is given to the interplay between underpressures created by generation of lift by incidence, camber and thickness. If an initial design depends upon an overly optimistic value of critical pressure coefficient, drag divergence onsets early. So, we have two options, either to adjust with reduced performance or we can accept a schedule slip to redesign a thinner wing.

To start with, we analysed the wind tunnel pressure test data of a symmetrical NACA0012 section. C.D. Harris tested a 2-D flow over a NACA0012 section at NASA 8-foot transonic pressure tunnel. He performed these tests considering the flow velocity constant and varying the Mach number by lowering the static temperature, thereby lowering the speed of sound of the flow. The two-dimensional airfoil section was placed in the wind tunnel at different angles of attack and the upper and lower surface pressure distributions were noted. Tests were conducted at lift coefficients starting from zero to maximum values with Mach numbers ranging from 0.30 to 0.86 for Reynolds numbers of 3,000,000 and 9,000,000. The transition was fixed at 5-percent chord. Additionally, transition free data were also obtained through Mach numbers ranging from 0.30 to 0.86 for zero lift and Reynolds number of 3,000,000. Studying this two-dimensional experimental result is necessary as they can predict the nature of three-dimensional flow up to a reasonable extent. Top notch distributed test information affirms the wide utility of all the logical assessment recipes yet can’t separate between them.

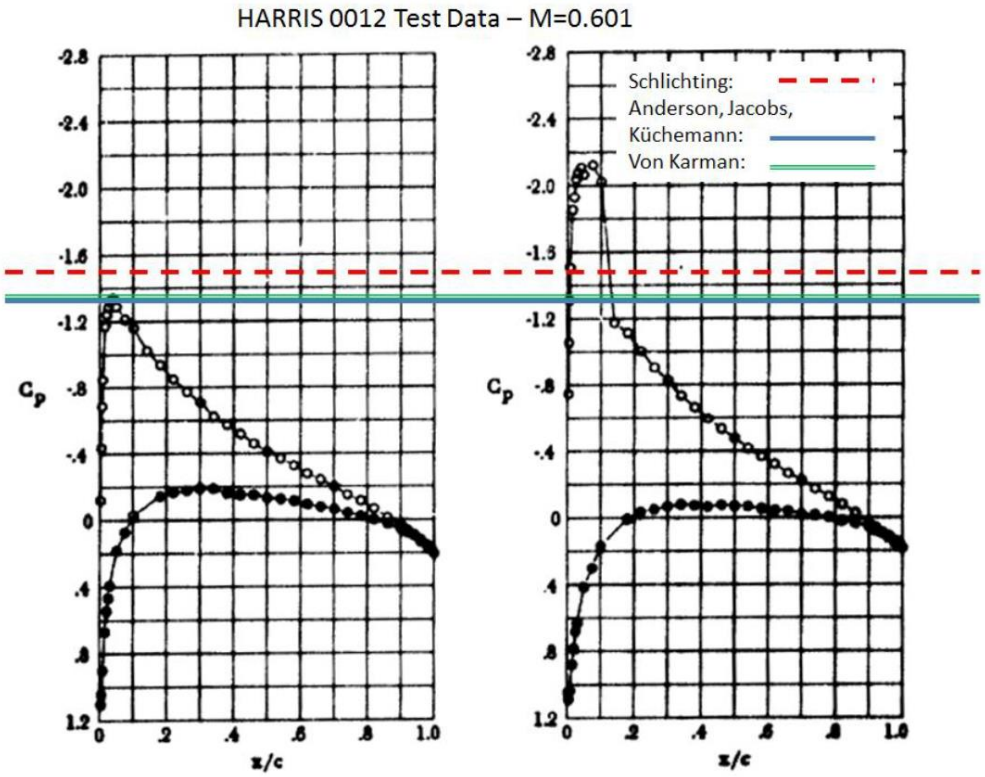

Figure 55: Wind Tunnel Test Data of a 2-D NACA0012 airfoil at freestream Mach = 0.601, Reproduced from Harris, C.D. (1981). Two-Dimensional Aerodynamic Characteristics of the NACA0012 airfoil in the Langley 8-foot Transonic Pressure Tunnel. (National Aeronautics and Space Administration TM 81927)

Initially, we studied the experimental data collected at a freestream Mach number of 0.601 at two different angles of attack (AOA = 3.86-deg and AOA = 5.86-deg) (see figure 53). For this test case, the critical pressure coefficient calculated according to Küchemann is -1.288. It differs from Schlichting's predicted critical pressure coefficient of -1.474 but the experimental data does not find any major shock wave at AOA = 3.86-deg and a noticeable shock at AOA = 5.86-deg. It has to be noted that Schlichting's equation predicts a subcritical flow at the AOA of 3.86-deg while Küchemann predicts supercritical flow at that condition.

This thesis work sets forth the platform to determine how accurate is Küchemann's critical pressure coefficient equation and how the misleading character of this equation dominates the design modifications that have been used in this thesis.

Revisiting the classical Küchemann's critical pressure coefficient equation[6]

$$C_p^* = \frac{2}{\gamma M_\infty^2}\left\{\left(\frac{2}{\gamma+1}\right)^{\frac{\gamma}{\gamma-1}}\left(1+\frac{\gamma-1}{2}M_\infty^2(cos\Phi)^2\right)^{\frac{\gamma}{\gamma-1}}-1\right\}$$

where, Küchemann claims that the sweep angle involved in this equation is the leading-edge sweep angle associated with the wing. We analysed a number of cases with each design modification applied separately to see the effect this critical pressure coefficient calculation has on the design and whether the argument made by Küchemann works well in a three-dimensional flow field. So, before moving further, we present the following table showcasing the critical pressure coefficients at different Mach numbers and sweep angles (see Table 1).

Table 1: Cp* Associated with Shock Wave for different Mach numbers and Sweep Angles (0.6 < M < 0.8)

Mach No.	Cp* (No sweep)	Cp*(5-deg sweep)	Cp*(10-deg sweep)	Cp*(15-deg sweep)	Cp*(20-deg sweep)	Cp*(25-deg sweep)	Cp*(30-deg sweep)	Cp*(35-deg sweep)	Cp*(40-deg sweep)	Cp*(45-deg sweep)
0.6	-1.29	-1.30	-1.31	-1.34	-1.37	-1.40	-1.45	-1.50	-1.55	-1.60
0.61	-1.23	-1.24	-1.25	-1.27	-1.30	-1.34	-1.39	-1.43	-1.48	-1.53
0.62	-1.17	-1.18	-1.19	-1.21	-1.25	-1.28	-1.33	-1.38	-1.43	-1.48
0.63	-1.12	-1.12	-1.13	-1.16	-1.19	-1.23	-1.27	-1.32	-1.37	-1.42
0.64	-1.06	-1.07	-1.08	-1.10	-1.14	-1.17	-1.22	-1.27	-1.32	-1.37
0.65	-1.01	-1.01	-1.03	-1.05	-1.08	-1.12	-1.17	-1.21	-1.27	-1.32
0.66	-0.96	-0.96	-0.98	-1.00	-1.03	-1.07	-1.12	-1.17	-1.22	-1.27
0.67	-0.91	-0.92	-0.93	-0.95	-0.99	-1.03	-1.07	-1.12	-1.17	-1.22
0.68	-0.87	-0.87	-0.88	-0.91	-0.94	-0.98	-1.03	-1.07	-1.13	-1.18
0.69	-0.82	-0.83	-0.84	-0.87	-0.90	-0.94	-0.98	-1.03	-1.08	-1.14
0.7	-0.78	-0.78	-0.80	-0.82	-0.86	-0.90	-0.94	-0.99	-1.04	-1.09
0.71	-0.74	-0.74	-0.76	-0.78	-0.82	-0.86	-0.90	-0.95	-1.00	-1.06
0.72	-0.70	-0.70	-0.72	-0.74	-0.78	-0.82	-0.86	-0.91	-0.97	-1.02
0.73	-0.66	-0.67	-0.68	-0.71	-0.74	-0.78	-0.83	-0.88	-0.93	-0.98
0.74	-0.63	-0.63	-0.65	-0.67	-0.70	-0.75	-0.79	-0.84	-0.89	-0.95
0.75	-0.59	-0.60	-0.61	-0.64	-0.67	-0.71	-0.76	-0.81	-0.86	-0.91
0.76	-0.56	-0.56	-0.58	-0.60	-0.64	-0.68	-0.73	-0.78	-0.83	-0.88
0.77	-0.53	-0.53	-0.55	-0.57	-0.61	-0.65	-0.69	-0.75	-0.80	-0.85
0.78	-0.49	-0.50	-0.52	-0.54	-0.58	-0.62	-0.66	-0.72	-0.77	-0.82
0.79	-0.46	-0.47	-0.49	-0.51	-0.55	-0.59	-0.63	-0.69	-0.74	-0.79
0.8	-0.43	-0.44	-0.46	-0.48	-0.52	-0.56	-0.61	-0.66	-0.71	-0.77

The above table shows C_{pmin} values on the upper surface of the wing for Mach numbers ranging from 0.6 to 0.8 which is the domain of analysis in this thesis work.

Table 2: Cp* Associated with Shock Wave for different Mach numbers and Sweep Angles (0.8 < M < 0.1)

Mach No.	Cp* (No sweep)	Cp*(5-deg sweep)	Cp*(10-deg sweep)	Cp*(15-deg sweep)	Cp*(20-deg sweep)	Cp*(25-deg sweep)	Cp*(30-deg sweep)	Cp*(35-deg sweep)	Cp*(40-deg sweep)	Cp*(45-deg sweep)
0.81	-0.41	-0.41	-0.43	-0.45	-0.49	-0.53	-0.58	-0.63	-0.69	-0.74
0.82	-0.38	-0.38	-0.40	-0.43	-0.46	-0.51	-0.55	-0.61	-0.66	-0.72
0.83	-0.35	-0.36	-0.37	-0.40	-0.44	-0.48	-0.53	-0.58	-0.64	-0.69
0.84	-0.33	-0.33	-0.35	-0.38	-0.41	-0.45	-0.50	-0.56	-0.61	-0.67
0.85	-0.30	-0.31	-0.32	-0.35	-0.39	-0.43	-0.48	-0.53	-0.59	-0.64
0.86	-0.28	-0.28	-0.30	-0.33	-0.36	-0.41	-0.46	-0.51	-0.57	-0.62
0.87	-0.25	-0.26	-0.28	-0.30	-0.34	-0.38	-0.43	-0.49	-0.54	-0.60
0.88	-0.23	-0.24	-0.25	-0.28	-0.32	-0.36	-0.41	-0.47	-0.52	-0.58
0.89	-0.21	-0.22	-0.23	-0.26	-0.30	-0.34	-0.39	-0.45	-0.50	-0.56
0.9	-0.19	-0.19	-0.21	-0.24	-0.28	-0.32	-0.37	-0.43	-0.48	-0.54
0.91	-0.17	-0.17	-0.19	-0.22	-0.26	-0.30	-0.35	-0.41	-0.46	-0.52
0.92	-0.15	-0.15	-0.17	-0.20	-0.24	-0.28	-0.33	-0.39	-0.45	-0.50
0.93	-0.13	-0.13	-0.15	-0.18	-0.22	-0.26	-0.31	-0.37	-0.43	-0.49
0.94	-0.11	-0.11	-0.13	-0.16	-0.20	-0.24	-0.30	-0.35	-0.41	-0.47
0.95	-0.09	-0.09	-0.11	-0.14	-0.18	-0.23	-0.28	-0.34	-0.39	-0.45
0.96	-0.07	-0.08	-0.09	-0.12	-0.16	-0.21	-0.26	-0.32	-0.38	-0.44
0.97	-0.05	-0.06	-0.08	-0.11	-0.14	-0.19	-0.25	-0.30	-0.36	-0.42
0.98	-0.03	-0.04	-0.06	-0.09	-0.13	-0.18	-0.23	-0.29	-0.35	-0.40
0.99	-0.02	-0.02	-0.04	-0.07	-0.11	-0.16	-0.21	-0.27	-0.33	-0.39
1		-0.01	-0.02	-0.06	-0.10	-0.14	-0.20	-0.26	-0.32	-0.38

However, as some regions on the upper surface of the wing have higher subsonic and supersonic Mach numbers, as seen from local Mach number contours, we need tables showing minimum underpressures in that region. Table 2 lists this data at higher subsonic Mach numbers (0.8 < M <1) and table 3 presents data at supersonic Mach numbers (1< M < 1.3).

Table 3: Cp* Associated with Shock Wave for different Mach numbers and Sweep Angles (1 < M < 1.3)

Mach No.	Cp* (No sweep)	Cp*(5-deg sweep)	Cp*(10-deg sweep)	Cp*(15-deg sweep)	Cp*(20-deg sweep)	Cp*(25-deg sweep)	Cp*(30-deg sweep)	Cp*(35-deg sweep)	Cp*(40-deg sweep)	Cp*(45-deg sweep)
1.01			-0.01	-0.04	-0.08	-0.13	-0.18	-0.24	-0.30	-0.36
1.02				-0.02	-0.06	-0.11	-0.17	-0.23	-0.29	-0.35
1.03				-0.01	-0.05	-0.10	-0.15	-0.21	-0.27	-0.33
1.04					-0.03	-0.08	-0.14	-0.20	-0.26	-0.32
1.05					-0.02	-0.07	-0.13	-0.19	-0.25	-0.31
1.06					-0.01	-0.06	-0.11	-0.17	-0.24	-0.30
1.07						-0.04	-0.10	-0.16	-0.22	-0.28
1.08						-0.03	-0.09	-0.15	-0.21	-0.27
1.09						-0.02	-0.07	-0.14	-0.20	-0.26
1.1						0.00	-0.06	-0.12	-0.19	-0.25
1.11							-0.05	-0.11	-0.18	-0.24
1.12							-0.04	-0.10	-0.17	-0.23
1.13							-0.03	-0.09	-0.16	-0.22
1.14							-0.02	-0.08	-0.14	-0.21
1.15							-0.01	-0.07	-0.13	-0.20
1.16								-0.06	-0.12	-0.19
1.17								-0.05	-0.11	-0.18
1.18								-0.04	-0.11	-0.17
1.19								-0.03	-0.10	-0.16
1.2								-0.02	-0.09	-0.15
1.21								-0.01	-0.08	-0.14
1.22								0.00	-0.07	-0.14
1.23									-0.06	-0.13
1.24									-0.05	-0.12
1.25									-0.04	-0.11
1.26									-0.04	-0.10
1.27									-0.03	-0.10
1.28									-0.02	-0.09
1.29									-0.01	-0.08
1.3										-0.07

Table 1,2 and 3 shows the minimum underpressures on the upper surface of the wing at specified sweep angles and Mach numbers that set the condition of incipient shock formation. This will help in analysing the sweep angle that is involved with Küchemann's critical pressure coefficient equation. Also, we present another table (see table 4) in which the critical pressure coefficient calculated at different Mach numbers and sweep angles corrected back to a Mach number of 0.4 following Prandtl-Glauert's correction. This will help analyse if Küchemann's equation predicts the low Mach number solution when corrected back from a high Mach number solution and the corresponding sweep angle it takes.

Table 4: Cp* Associated with Shock Wave for different Mach numbers and Sweep Angles Corrected Back to Mach Number = 0.4

MACH #	35	34.15	33.3	32.45	31.6	30.75	29.9	29.05	28.2	27.35	26.5	25.65	24.8	23.95	23.1	22.25	21.4	20.55	19.7	18.85	18
	LE	5%	10%	15%	20%	25%	30%	35%	40%	45%	50%	55%	60%	65%	70%	75%	80%	85%	90%	95%	TE
0.5	-2.41	-2.40	-2.40	-2.39	-2.38	-2.38	-2.37	-2.37	-2.36	-2.36	-2.35	-2.34	-2.34	-2.33	-2.33	-2.32	-2.32	-2.32	-2.31	-2.31	-2.30
0.6	-1.62	-1.62	-1.61	-1.61	-1.60	-1.59	-1.59	-1.58	-1.58	-1.57	-1.57	-1.56	-1.56	-1.55	-1.55	-1.55	-1.54	-1.54	-1.53	-1.53	-1.52
0.61	-1.56	-1.56	-1.55	-1.55	-1.54	-1.54	-1.53	-1.53	-1.52	-1.52	-1.51	-1.51	-1.50	-1.50	-1.49	-1.49	-1.48	-1.48	-1.47	-1.47	-1.47
0.62	-1.51	-1.50	-1.50	-1.49	-1.49	-1.48	-1.48	-1.47	-1.47	-1.46	-1.46	-1.45	-1.45	-1.44	-1.44	-1.43	-1.43	-1.42	-1.42	-1.41	-1.41
0.63	-1.46	-1.45	-1.44	-1.44	-1.43	-1.43	-1.42	-1.42	-1.41	-1.41	-1.40	-1.40	-1.39	-1.39	-1.38	-1.38	-1.37	-1.37	-1.37	-1.36	-1.36
0.64	-1.40	-1.40	-1.39	-1.39	-1.38	-1.38	-1.37	-1.37	-1.36	-1.36	-1.35	-1.35	-1.34	-1.34	-1.33	-1.33	-1.32	-1.32	-1.32	-1.31	-1.31
0.65	-1.36	-1.35	-1.34	-1.34	-1.33	-1.33	-1.32	-1.32	-1.31	-1.31	-1.30	-1.30	-1.29	-1.29	-1.28	-1.28	-1.27	-1.27	-1.27	-1.26	-1.26
0.66	-1.31	-1.30	-1.30	-1.29	-1.29	-1.28	-1.28	-1.27	-1.27	-1.26	-1.26	-1.25	-1.25	-1.24	-1.24	-1.23	-1.23	-1.22	-1.22	-1.22	-1.21
0.67	-1.26	-1.26	-1.25	-1.25	-1.24	-1.24	-1.23	-1.23	-1.22	-1.22	-1.21	-1.21	-1.20	-1.20	-1.19	-1.19	-1.18	-1.18	-1.18	-1.17	-1.17
0.68	-1.22	-1.22	-1.21	-1.21	-1.20	-1.20	-1.19	-1.18	-1.18	-1.17	-1.17	-1.16	-1.16	-1.15	-1.15	-1.15	-1.14	-1.14	-1.13	-1.13	-1.12
0.69	-1.18	-1.18	-1.17	-1.17	-1.16	-1.15	-1.15	-1.14	-1.14	-1.13	-1.13	-1.12	-1.12	-1.11	-1.11	-1.10	-1.10	-1.10	-1.09	-1.09	-1.08
0.7	-1.14	-1.14	-1.13	-1.13	-1.12	-1.12	-1.11	-1.10	-1.10	-1.09	-1.09	-1.08	-1.08	-1.07	-1.07	-1.06	-1.06	-1.06	-1.05	-1.05	-1.04
0.71	-1.10	-1.10	-1.09	-1.09	-1.08	-1.08	-1.07	-1.07	-1.06	-1.06	-1.05	-1.05	-1.04	-1.04	-1.03	-1.03	-1.02	-1.02	-1.01	-1.01	-1.01
0.72	-1.07	-1.06	-1.06	-1.05	-1.05	-1.04	-1.04	-1.03	-1.03	-1.02	-1.01	-1.01	-1.00	-1.00	-1.00	-0.99	-0.99	-0.98	-0.98	-0.97	-0.97
0.73	-1.03	-1.03	-1.02	-1.02	-1.01	-1.01	-1.00	-1.00	-0.99	-0.98	-0.98	-0.97	-0.97	-0.96	-0.96	-0.96	-0.95	-0.95	-0.94	-0.94	-0.93
0.74	-1.00	-1.00	-0.99	-0.98	-0.98	-0.97	-0.97	-0.96	-0.96	-0.95	-0.95	-0.94	-0.94	-0.93	-0.93	-0.92	-0.92	-0.91	-0.91	-0.90	-0.90
0.75	-0.97	-0.96	-0.96	-0.95	-0.95	-0.94	-0.93	-0.93	-0.92	-0.92	-0.91	-0.91	-0.90	-0.90	-0.89	-0.89	-0.88	-0.88	-0.87	-0.87	-0.87
0.76	-0.94	-0.93	-0.93	-0.92	-0.91	-0.91	-0.90	-0.90	-0.89	-0.89	-0.88	-0.88	-0.87	-0.87	-0.86	-0.86	-0.85	-0.85	-0.84	-0.84	-0.83
0.77	-0.91	-0.90	-0.90	-0.89	-0.88	-0.88	-0.87	-0.87	-0.86	-0.86	-0.85	-0.85	-0.84	-0.84	-0.83	-0.83	-0.82	-0.82	-0.81	-0.81	-0.80
0.78	-0.88	-0.87	-0.87	-0.86	-0.86	-0.85	-0.84	-0.84	-0.83	-0.83	-0.82	-0.82	-0.81	-0.81	-0.80	-0.80	-0.79	-0.79	-0.78	-0.78	-0.77
0.79	-0.85	-0.85	-0.84	-0.83	-0.83	-0.82	-0.82	-0.81	-0.80	-0.80	-0.79	-0.79	-0.78	-0.78	-0.77	-0.77	-0.76	-0.76	-0.75	-0.75	-0.74
0.8	-0.82	-0.82	-0.81	-0.81	-0.80	-0.79	-0.79	-0.78	-0.78	-0.77	-0.77	-0.76	-0.76	-0.75	-0.74	-0.74	-0.73	-0.73	-0.72	-0.72	-0.72
0.81	-0.80	-0.79	-0.79	-0.78	-0.77	-0.77	-0.76	-0.76	-0.75	-0.75	-0.74	-0.73	-0.73	-0.72	-0.72	-0.71	-0.71	-0.70	-0.70	-0.69	-0.69
0.82	-0.77	-0.77	-0.76	-0.75	-0.75	-0.74	-0.74	-0.73	-0.72	-0.72	-0.71	-0.71	-0.70	-0.70	-0.69	-0.69	-0.68	-0.68	-0.67	-0.67	-0.66
0.83	-0.75	-0.74	-0.74	-0.73	-0.72	-0.72	-0.71	-0.71	-0.70	-0.69	-0.69	-0.68	-0.68	-0.67	-0.67	-0.66	-0.65	-0.65	-0.64	-0.64	-0.63
0.84	-0.72	-0.72	-0.71	-0.71	-0.70	-0.69	-0.69	-0.68	-0.68	-0.67	-0.66	-0.66	-0.65	-0.65	-0.64	-0.64	-0.63	-0.62	-0.62	-0.61	-0.61
0.85	-0.70	-0.70	-0.69	-0.68	-0.68	-0.67	-0.66	-0.66	-0.65	-0.65	-0.64	-0.63	-0.63	-0.62	-0.62	-0.61	-0.60	-0.60	-0.59	-0.59	-0.58
0.86	-0.68	-0.67	-0.67	-0.66	-0.65	-0.65	-0.64	-0.64	-0.63	-0.62	-0.62	-0.61	-0.60	-0.60	-0.59	-0.59	-0.58	-0.58	-0.57	-0.56	-0.56
0.87	-0.66	-0.65	-0.65	-0.64	-0.63	-0.63	-0.62	-0.61	-0.61	-0.60	-0.59	-0.59	-0.58	-0.58	-0.57	-0.56	-0.56	-0.55	-0.55	-0.54	-0.54
0.88	-0.64	-0.63	-0.62	-0.62	-0.61	-0.60	-0.60	-0.59	-0.58	-0.58	-0.57	-0.57	-0.56	-0.55	-0.55	-0.54	-0.53	-0.53	-0.52	-0.52	-0.51
0.89	-0.62	-0.61	-0.60	-0.60	-0.59	-0.58	-0.58	-0.57	-0.56	-0.56	-0.55	-0.54	-0.54	-0.53	-0.52	-0.52	-0.51	-0.51	-0.50	-0.49	-0.49
0.9	-0.60	-0.59	-0.58	-0.58	-0.57	-0.56	-0.56	-0.55	-0.54	-0.54	-0.53	-0.52	-0.52	-0.51	-0.50	-0.50	-0.49	-0.48	-0.48	-0.47	-0.47
0.91	-0.58	-0.57	-0.56	-0.56	-0.55	-0.54	-0.54	-0.53	-0.52	-0.52	-0.51	-0.50	-0.49	-0.49	-0.48	-0.47	-0.47	-0.46	-0.45	-0.45	-0.44
0.92	-0.56	-0.55	-0.54	-0.54	-0.53	-0.52	-0.52	-0.51	-0.50	-0.49	-0.49	-0.48	-0.47	-0.47	-0.46	-0.45	-0.45	-0.44	-0.43	-0.43	-0.42

We first analysed the validity of Küchemann's critical pressure coefficient equation on the final design obtained in this thesis work that involves drooping applied to each airfoil (except at the root), forward camber added to the specific airfoils and modNACA0006 airfoils at the tip.

Figure 56 shows the local sweeps of isobars obtained from the line contour on the wing upper surface. The leading-edge sweep angle is ~35 degree. The other relevant local isobar sweep angles were measured using CATIA to determine the sweep angle involved in Küchemann's critical pressure coefficient. The most remarkable observation is that this equation takes the sweep of the shock to determine the critical pressure coefficient. As the shock sweep varies in the spanwise direction, Küchemann's equation predicts local C_p^* values on the upper surface of the wing based on the sweep angle of the shock. In theory, Küchemann's equation is independent of camber.

This thesis work performed simulations which showcase that even if we get a shock at and above a Mach number of 0.7 after the midspan, the shock vanishes at the tip as more and more droop was applied which evidently says that Küchemann did not consider the effect of drooping on the prediction of critical pressure coefficient. Also, the predicted design critical Mach number in VORLAX is much higher than the actual critical Mach number. Simulations have shown that the actual critical Mach number is around 0.65 for this design case.

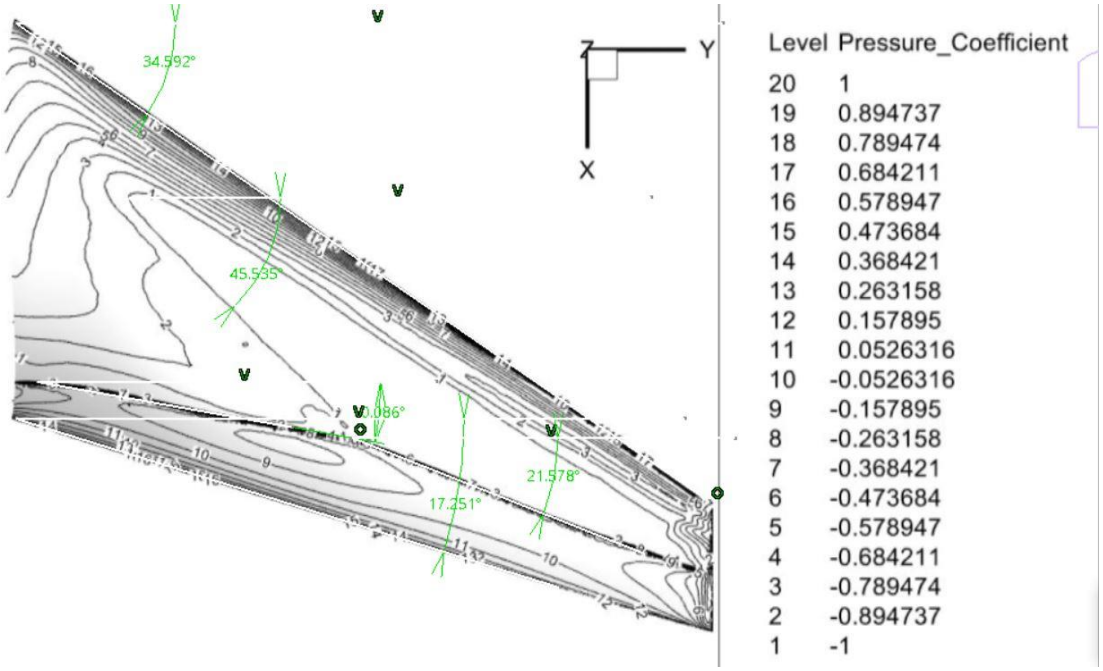

Figure 56: Upper Surface Isobar for Final Design Showing Local Isobar Sweeps and Shock Sweep @ M = 0.79, AOA = 1

The leading-edge sweep angle calculated from CATIA is ~34.6-deg which is close enough to the leading-edge sweep angle 35-deg and the trailing-edge sweep angle is ~17.25-deg which is approximately same as calculated from VORLAX (18-deg) which validate that the angles calculated from CATIA are accurate. With that, the shock sweep was calculated to be ~10-deg. From table 1, the critical pressure coefficient associated with this sweep angle at 0.79 Mach is -0.49 which agrees well with the local critical pressure coefficient of -0.474. Again, the local sweep of the shock after the midspan is ~20-deg which gives a C_p^* of -0.55 and the corresponding local pressure coefficient is ~ −0.58. These results evidently show that it is actually the sweep of the shock that is involved in the Küchemann's critical pressure coefficient equation. We suspect that the slight difference between the pressure coefficients are due to the fact that the leading-edge and trailing-edge angles does not exactly match with the design data and the approximations taken into consideration during the calculations.

Another remarkable observation was made when we corrected back the solutions at the predicted critical Mach number to a lower Mach number (M = 0.4). According to the data presented in table 2, the critical pressure coefficient on a wing with a leading-edge sweep angle of 35-degree at a Mach number = 0.79 is − 0.85 when corrected back to M = 0.4. This data surprisingly matches with the minimum C_p obtained from the simulation of the final design (see Figure 57).

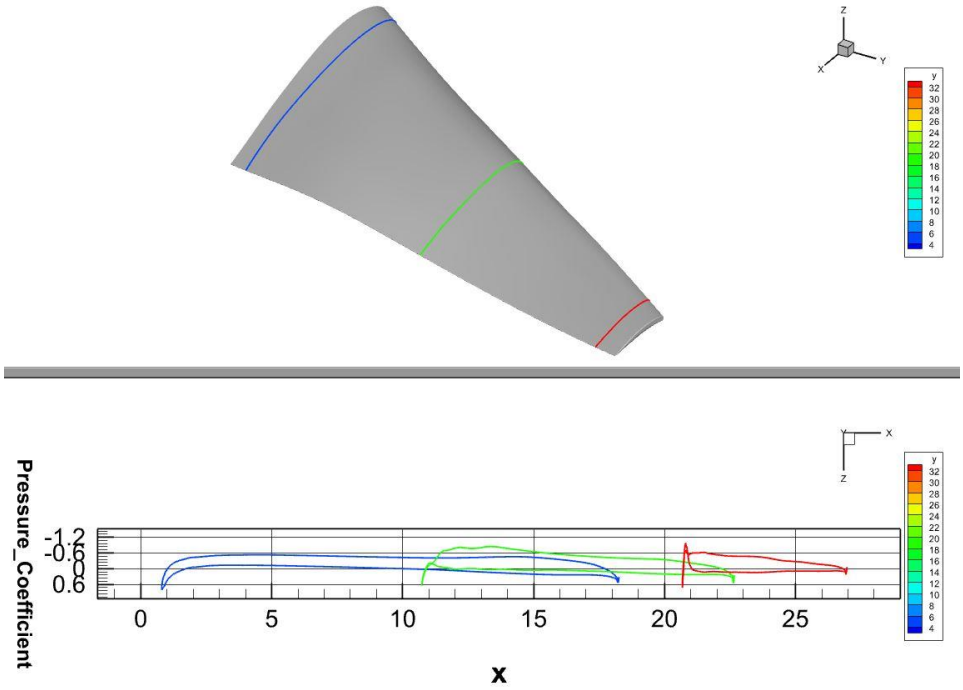

Figure 57: Cp cuts at three spanwise locations for the final design @ M = 0.4, AOA = 1

Further, to prove that this is not only the case for this design process, rather it can be applied to other designs, we extended our study to another design case with different design conditions and design critical Mach number. The design conditions undertaken are as follows:

- Design Critical Mach Number = 0.81
- Design Altitude = 40,000 ft
- Design Lift = 550,000 lbm

- Wingspan = 190 ft
- Fuselage Length = 200 ft
- Fuselage Diameter = 18 ft
- Wing-Fuselage Junction = 80 ft

And, the final design parameters in VORLAX that met these design requirements are:

- Wing Trapezoidal Planform Area (*Sref*) = 4700 ft^2
- Wing Loading (W/S_{ref}) = 117 lbf/ft^2
- Leading Edge Sweep (Λ_{LE}) = 45-deg
- Quarter Chord Sweep ($\Lambda_{c/4}$) = 42-deg
- Aspect Ratio (AR) = 7.681
- Taper Ratio (TR) = 0.25
- *t/c* at side-of-body: 16%
- *t/c* at wing-tip: 7%
- VORLAX Computed Inviscid Drag Coefficient: 0.01830
- VORLAX Computed Lift Coefficient: 0.65104
- Mach number normal to Leading-Edge: 0.5728
- Design $C_P^* = -0.7406$

The wing-fuselage junction was reproduced in CATIA and simulated in SU2 at the design critical Mach number. The upper surface isobars at the design critical Mach number are shown in Figure 58.

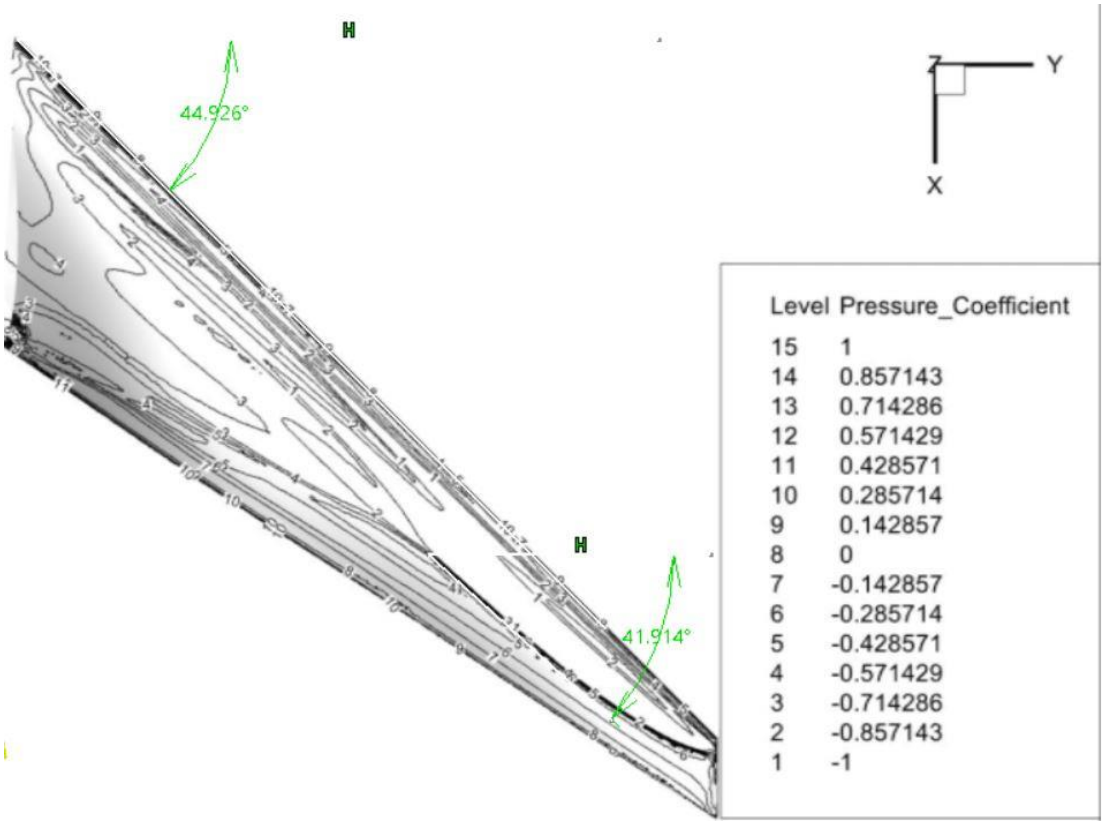

Figure 58: Upper Surface Isobars @ M= 0.81, AOA = 1

For this case, the shock sweep was found to be 41.914-deg and the leading-edge sweep angle is ~44.9-deg. The critical pressure coefficient corresponding to the leading-edge sweep is – 0.74 and that corresponding to the shock sweep is – 0.69 which closely matches with the local C_p of the shock in Figure 58. From both the design cases, we observed that it is the shock sweep that is involved in Küchemann's critical pressure coefficient equation. During the initial design in VORLAX, leading-edge sweep was considered while evaluating the C_p^* for both the design process due to which the design modifications did not produce satisfactory results. We are finally able to conclude that the accurate calculation of C_p^* plays an important role in design and dominates the design modifications.

Another remarkable observation was found when we simulated the final design at different Mach numbers. Results show that the actual critical Mach number is less

than the predicted design critical Mach number. The model was simulated on the finest mesh possible at Mach numbers 0.65, 0.68 and 0.7 to bracket the problem.

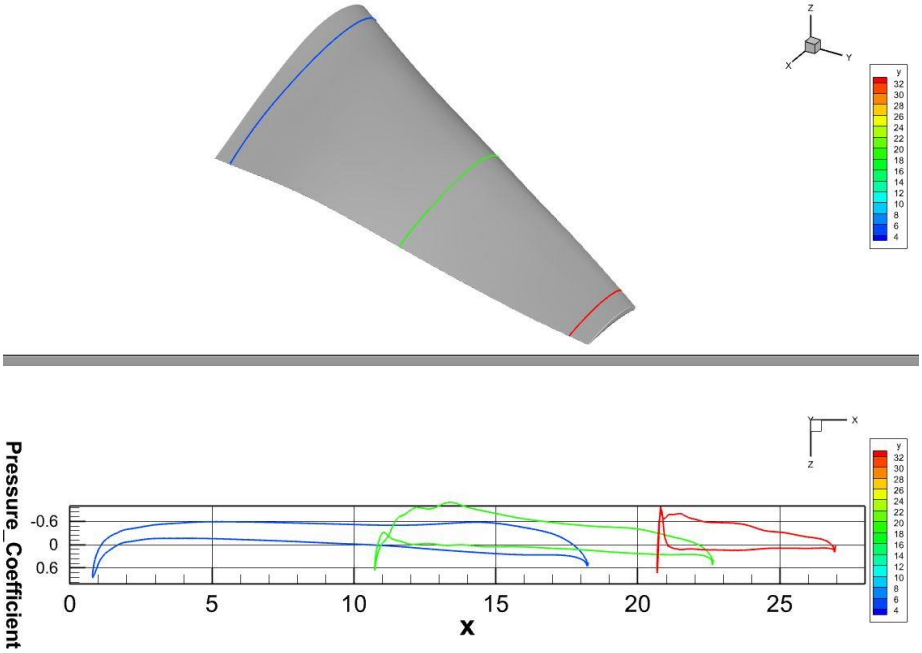

Figure 59: Cp cuts at three spanwise locations (final design) @ M = 0.65, AOA = 1

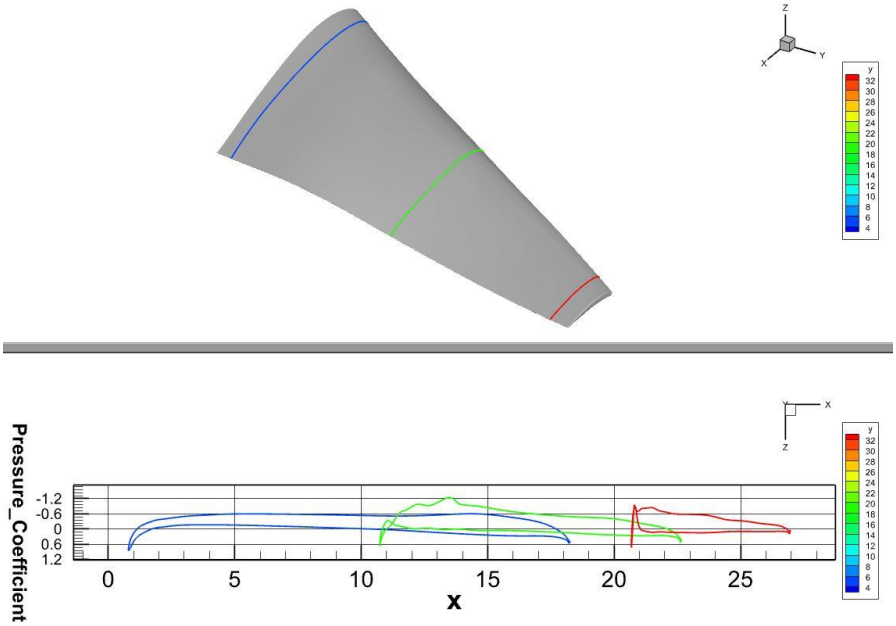

Figure 60: Cp cuts at three spanwise locations (final design) @ M = 0.68, AOA = 1

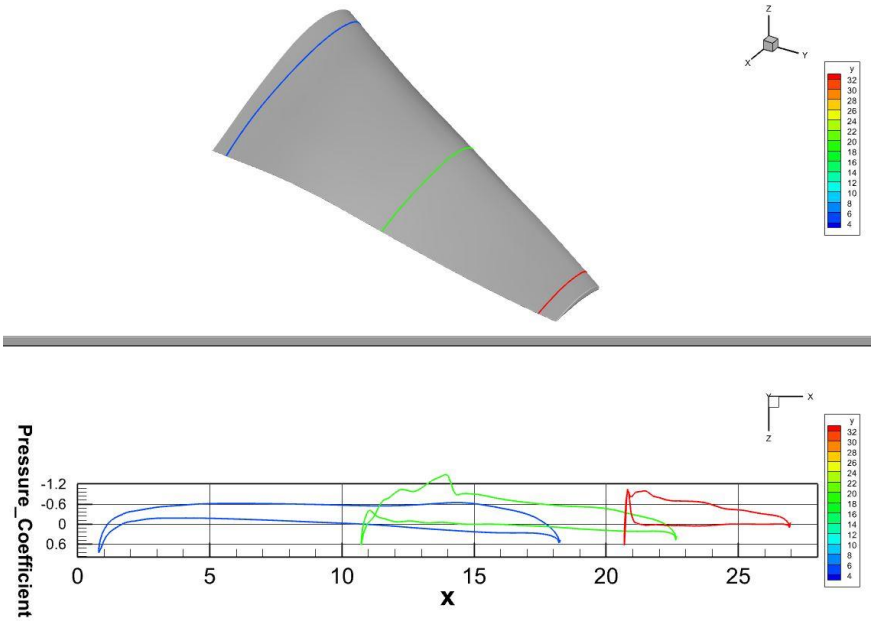

Figure 61: Cp cuts at three spanwise locations (final design) @ M = 0.7, AOA = 1

Above figures show that there is an incipient shock at the midspan of the wing at M = 0.7 and the shock vanishes at M = 0.65. The case of M = 0.68 is an intermediate case at which the shock starts to form. So, the critical Mach number for the final design lies between 0.65 and 0.68 whereas the predicted critical Mach number was 0.79. We conclude that the reduction of this critical Mach number is due to the wrong interpretation of Küchemann's critical pressure coefficient equation taken into consideration in the initial design process of the wing-fuselage combinations analysed.

CHAPTER 6

VERIFICATION OF CFD RESULTS

As the solver included Euler solver and the analysis of results were performed using computational fluid dynamics tools, verification of the results is of prime importance for the conclusion to be correct. If there is an analytical solution to the problem, then we can compare the analytical solution with the computational result to verify its

accuracy. However, that is not always the case. So, to verify the results, we used "method of manufactured solutions" and "grid density check" in this thesis work. There are two types of orders of accuracy involved in the computed results i.e., formal order of accuracy and observed order of accuracy. Formal order of accuracy is determined by Taylor series analysis for finite-difference and finite-volume methods and interpolation theory for finite-element methods. However, computed solutions do not produce formal order of accuracy due to round-off error, singularities or discontinuities in solution domain or boundaries and truncation errors. So, often "observed order of accuracy" is used to determine the actual accuracy obtained from the computed solutions.

In numerical solution error, discretization error emerges because of the mapping of PDEs to discretized equations and this can be related to the truncation error. The total discretization error is made up of two components i.e., local discretization error due to local element size and error that has been transported from nearby regions. This is what we also have incurred in our solutions as we used the discretized form of Euler equation and the mesh size was restricted due to unavailability of heavy computational tools. So, verification of the obtained computational results is necessary. The following steps were followed to verify the solution. Solution verification was performed for the final design.

Three simulations were performed on meshes that were different by a factor of 2. The two quantities of interest (lift coefficient and drag coefficient) were computed for all the three mesh sizes. The observed order of convergence was found and the corresponding GCIs (Grid Convergence Index) were calculated. Finally, a check was done to confirm asymptotic range of convergence.

Table 4: Lift and Drag Coefficients for three different meshes on final design

Mesh_Spacing (m)	Lift Coefficient (C_L)	Drag Coefficient (C_D)
0.09	0.491017	0.030215
0.18	0.490120	0.030475
0.36	0.486830	0.030951

Analysis for Lift Coefficient

$f_1 = 0.491017$

$f_2 = 0.490120$

$f_3 = 0.486830$

Observed order of convergence,

$$p = ln\left(\frac{|f_3 - f_2|}{|f_2 - f_1|}\right)/\ln(r)$$

$$p = ln\left(\frac{|0.486830 - 0.490120|}{|0.490120 - 0.491017|}\right)/\ln(2)$$

$$p = 1.87$$

Estimation of exact solution using Richardson's extrapolation:

$$f_{h=0} \approx f_1 + \frac{f_1 - f_2}{r^p - 1}$$

$$f_{h=0} \approx 0.491017 + \frac{0.491017 - 0.490120}{2^{1.87} - 1}$$

$$f_{h=0} \approx 0.491355$$

Calculation of GCIs:

$$GCI_{12} = F_{sec} \frac{\left|\frac{f_1 - f_2}{f_1}\right|}{r^p - 1}$$

$$GCI_{12} = 1.25 \frac{\left|\frac{0.491017 - 0.490120}{0.491017}\right|}{2^{1.87} - 1}$$

$$GCI_{12} = 0.00086$$

$$GCI_{23} = F_{sec} \frac{\left|\frac{f_2 - f_3}{f_2}\right|}{r^p - 1}$$

$$GCI_{23} = 1.25 \frac{\left|\frac{0.490120 - 0.486830}{0.490120}\right|}{2^{1.87} - 1}$$

$$GCI_{23} = 0.0031$$

Asymptotic Range of Convergence:

$$\frac{GCI_{12}}{GCI_{23}} r^p = \frac{0.00086}{0.0031} 2^{1.87} = 1.01$$

So, computed lift coefficient = $f_{h=0}$ + GCI_{12} in %

$$= 0.491355 \pm 0.086\%$$

Analysis for Drag Coefficient

f_1 = 0.030215

f_2 = 0.030475

f_3 = 0.030951

Observed order of convergence,

$$p = ln\left(\frac{|f_3 - f_2|}{|f_2 - f_1|}\right) / \ln(r)$$

$$p = ln\left(\frac{|0.030951 - 0.030475|}{|0.030475 - 0.030215|}\right)/\ln(2)$$

$$p = 0.87$$

Estimation of exact solution using Richardson's extrapolation:

$$f_{h=0} \approx f_1 + \frac{f_1 - f_2}{r^p - 1}$$

$$f_{h=0} \approx 0.030215 + \frac{0.030215 - 0.030475}{2^{0.87} - 1}$$

$$f_{h=0} \approx 0.02990$$

Calculation of GCIs:

$$GCI_{12} = F_{sec} \frac{\left|\frac{f_1 - f_2}{f_1}\right|}{r^p - 1}$$

$$GCI_{12} = 1.25 \frac{\left|\frac{0.030215 - 0.030475}{0.030215}\right|}{2^{0.87} - 1}$$

$$GCI_{12} = 0.0129$$

$$GCI_{23} = F_{sec} \frac{\left|\frac{f_2 - f_3}{f_2}\right|}{r^p - 1}$$

$$GCI_{23} = 1.25 \frac{\left|\frac{0.030475 - 0.030951}{0.030475}\right|}{2^{0.87} - 1}$$

$$GCI_{23} = 0.0236$$

Asymptotic Range of Convergence:

$$\frac{GCI_{12}}{GCI_{23}} r^p = \frac{0.0129}{0.0236} 2^{0.87} = 0.999$$

So, computed drag coefficient = $f_{h=0} + GCI_{12}$ in %

$$= 0.02990 \pm 1.29\%$$

From the analysis of lift and drag coefficients, it is evident that the mesh size taken into consideration is good enough to produce accurate results. Further, a grid density check was performed to study the variation of drag coefficient and lift coefficient with the mesh size (see Figures 59 and 60).

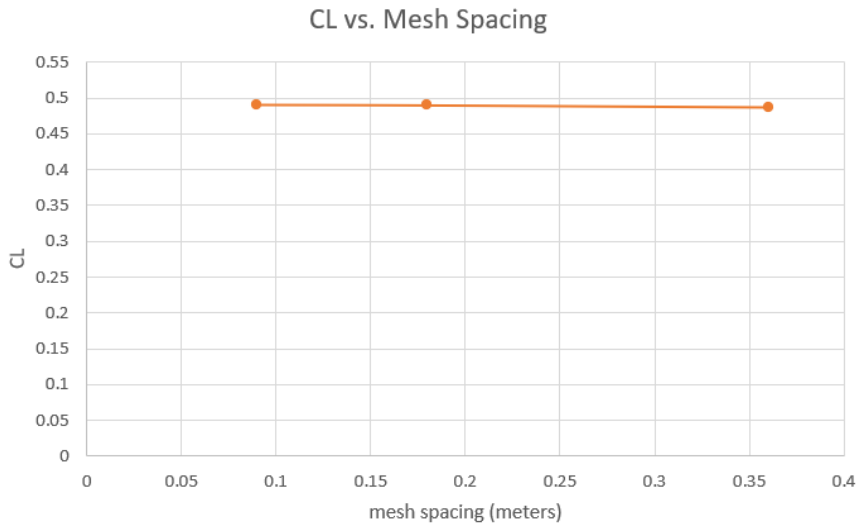

Figure 62: Variation of Lift Co Efficient with Mesh Spacing

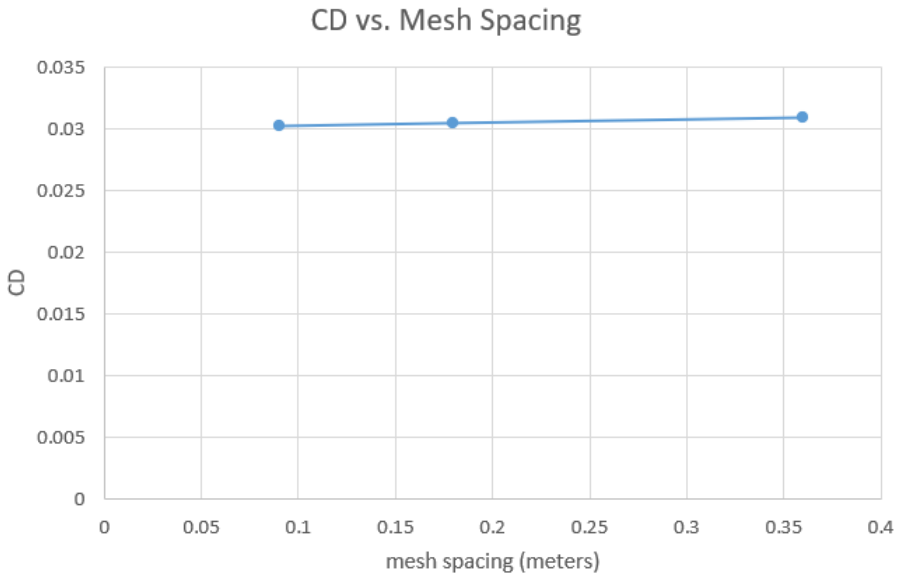

Figure 63: Variation of Drag Coefficient with Mesh Spacing

From both the figures, we conclude that the variation of lift and drag coefficient with the mesh spacing is small. So, the results that we obtained using the numerical simulations are accurate enough to for practical applications. Further, Figure 64 shows one instance in which the lift and drag coefficients do converge to a single value after a certain number of iterations.

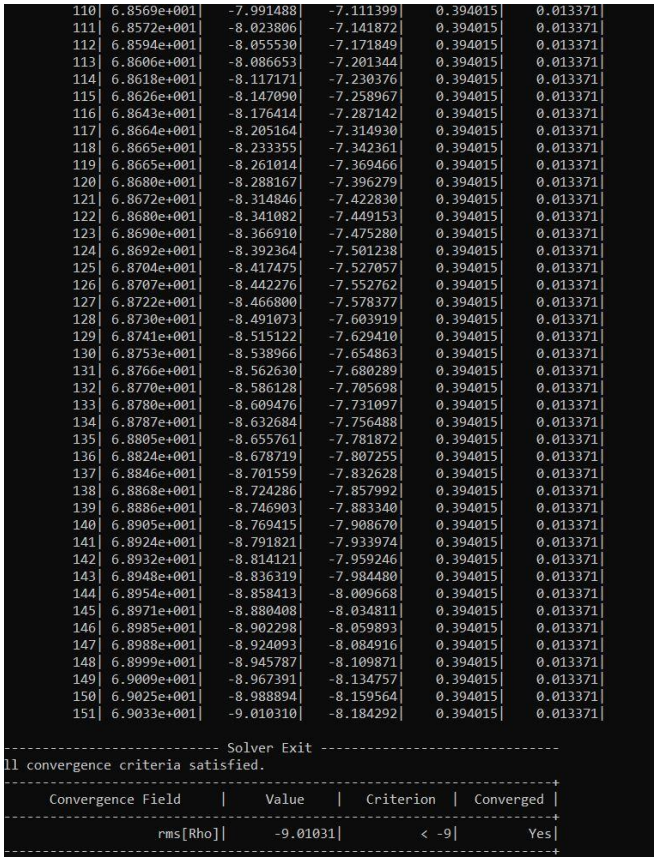

Figure 64: Convergence on the final design @ M = 0.6, AOA = 1

Further, the maximum residual was plotted against the number of iterations for both the initial and final design to prove that the solutions converged for all cases considered (see figures 65 and 66).

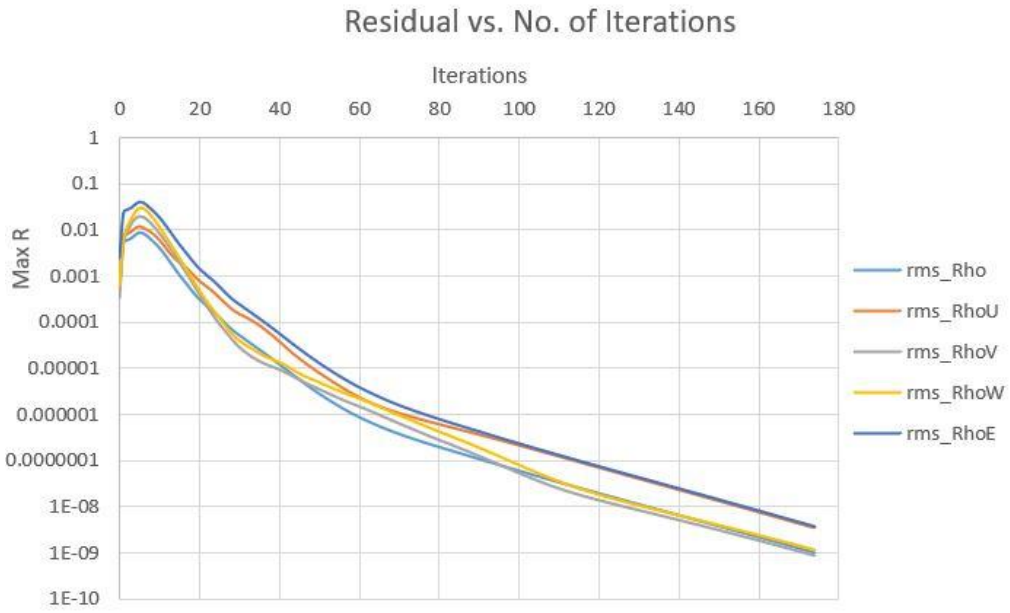

Figure 65: Convergence Plot for the Initial Design Case

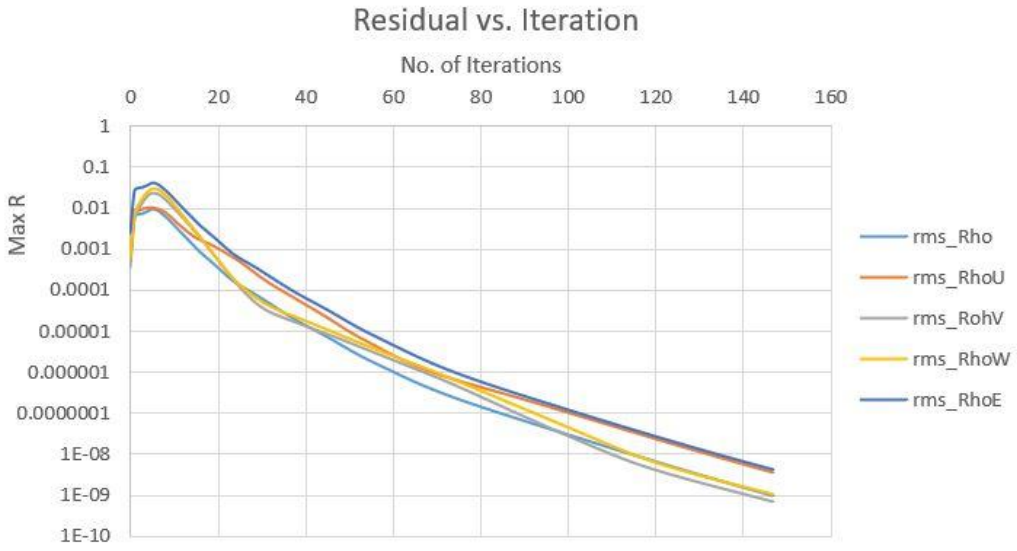

Figure 66: Convergence Plot for the Final Design Case

CHAPTER 7

ADDITIONAL CONSIDERATION

After the design analysis performed, additional considerations were made in which this thesis work extended the analysis to cases considering winglets and their effect on

the design process. Winglets were first introduced by Richard T. Whitcomb[29] as a design modification (vertical extension of wing-tip) to minimize the transonic drag and improve aerodynamic efficiency. They help in effectively increasing the aspect ratio of the wing without significant increase in the span. He also argued that winglets help reduce the intensity of wake vortices and increase efficiency by reducing vortex interference by moving the air on upper (lower pressure) and lower (higher pressure) surfaces of the wing. To study the effects of this on the design process and Küchemann's predicted critical pressure coefficient, we added a winglet at the tip of the wing as a vertical extension and the profile of the winglet was taken as the basic form of NACA0006. The winglet was created using the surface loft feature in CATIA. It was observed that addition of winglet was able to eliminate the shock at the tip effectively but it did not affect the aft shock at the root or midspan (see Figures 67 and 68). Thus, the winglet can be used as an improvement in performance if the wing is initially poorly designed (just as in this case, due to an incorrect interpretation of Küchemann's critical pressure coefficient equation).

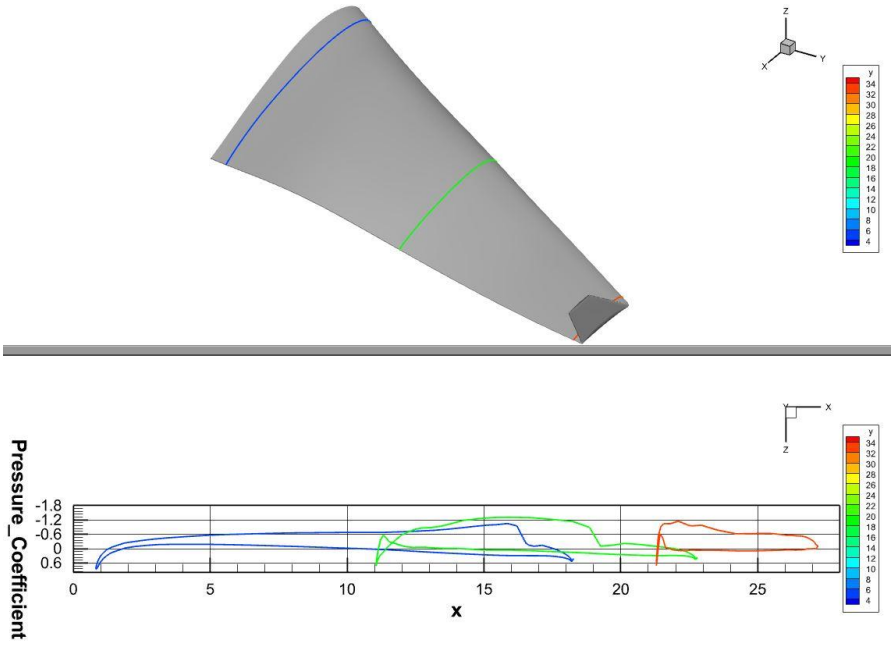

Figure 67: Cp cuts at three spanwise locations (winglet testcase) @ M = 0.79, AOA = 1

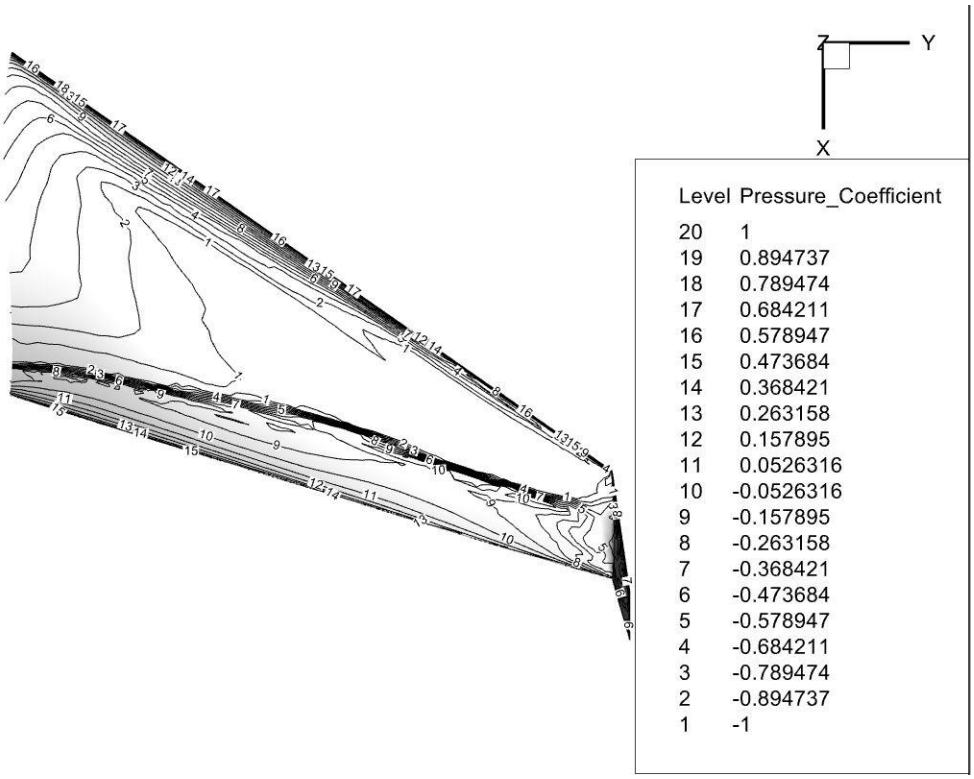

Figure 68: Upper Surface Isobars (winglet testcase) @ M = 0.79, AOA = 1

The addition of winglet to the model is independent of the amount of drooping needed to weaken/eliminate the shock. Figures 67 and 68 show the testcase where drooping has been applied twice whereas in the final design of the thesis, drooping has been applied five times/ six times depending on the airfoil profile. The final design used the shock well by placing it at the crest (maximum leading-edge suction) but was unable to get rid of the shock but an effective design of winglet helped in removing the shock from the tip.

Among other testcases, wing-fuselage combinations with no twists applied to the wing airfoil profiles were studied but they were not able to meet the design lift coefficient criterion. The negative pressure coefficients on the upper surface of the

wing were considerably reduced to less negative values as expected but it did no good in weakening/eliminating the shock. So, those cases are not included here.

CHAPTER 8

CONCLUSION

This thesis work finds that many classical explanations on the effectiveness of aerodynamic design modifications on performance of an aircraft in transonic flow conditions for swept wings are fundamentally inconsistent. The data presented in this work show that although most of the phenomena described do exist and work in certain cases, they lack documentation of conditions in which they don't perform satisfactorily and do not fully explain reality.

As a first step in documenting the effect of aerodynamic modifications, this work revisited the thickening of outboard portion of the wing. Close scrutiny of primary and secondary source literature revealed that thickness does not contribute to lift but it affects the pressure distribution over the surface of wing. Many authors have stated that thickening of outboard sections help eliminate or weaken the shock by reducing the pressure coefficients below the critical pressure coefficient. However, they did not consider the effect of wrong interpretation of critical pressure coefficient on this design modification. Through the use of VORLAX and CFD (SU2), there are evidence and data to suggest that thickening the outboard portion does not successfully work or help improve performance if the calculation of critical pressure coefficient is wrongly interpreted.

Second trade studies were performed by increasing the leading-edge radius of thin blunt airfoils that behave like sharp airfoils in the flow field. Eggers showed that a sharp airfoil with the maximum thickness clustered at its back and by employing boat-

tailing, supercritical lift characteristics compared to that of conventional profiles can be obtained. In the work of this paper, Eggers was found to handwave explanations regarding the formation of shock wave on a sharp leading-edge airfoil and its impact on the lift and drag characteristics. Moreover, results presented in this paper shows that the works of Demele & Sutton[22] did not account for cases having a high subsonic Mach number and a high Reynolds number (> 11,000,000). The increase in leading-edge radius does help introduce bluntness to the airfoils but it does not help weaken/ eliminate the shock that is generated due to tip effect/wing-fuselage junction effect. Certainly, it was observed that simple sweep theory is an oversimplification of the practical phenomena occurring in the nature. The argument made by simple sweep theory that shock on the wing stays stagnant where it is generated has been proved wrong through series of simulations performed in this thesis work. It is now evident that if a shock is generated at any location on the wing, it spreads all over the wing.

Drooped leading-edges and conical camber have been proved to be effective in delaying the flow separation to a higher lift coefficient. Literature survey has shown that conical camber is able to restore the leading-edge suction by making a thin blunt airfoil appear blunt in the flow field which would otherwise seem to be sharp. Trade studies in this thesis work prove that drooped leading-edge along with conical camber indeed help in utilizing the shock by placing it on the crest that maximizes leading-edge suction. However, the position and degree of drooping need to be optimized for better performance. Data presented in this paper proves the effectiveness of droop in delaying the appearance of forward shock to a higher Mach number but it also proves that it does not help in eliminating or weakening the aft shock.

Many authors have presented data regarding the correctness and applicability of critical pressure coefficient equations. Kirkman & Takahashi[8] has shown that Küchemann's critical pressure coefficient equation is correct and provide accurate results for a two-dimensional case. Küchemann argues that the critical pressure coefficient is dependent upon the freestream Mach number and the Mach number normal to leading-edge. Further, he does not dispute the claim that the flow normal to leading-edge must exceed the sonic condition to initiate the formation of shock, however he does argue that the sonic condition is a function of total perturbation velocity from the freestream. Hence, the importance of freestream Mach number in determining the critical pressure coefficient cannot be ignored. Although Küchemann's equation works very well for two-dimensional cases, this thesis work shows that wrong interpretation of the Küchemann's equation leads to dominate the design modifications that would help improve the performance otherwise. In his explanations, Küchemann firmly points out the importance of freestream Mach number in determining the critical pressure coefficient but handwaved explanations regarding the sweep term in the equation. This paper presents computational results to prove that the sweep involved in Küchemann's critical pressure coefficient equation is not the leading-edge sweep but the shock sweep. In many applications, designers have been misled by this phenomenon and no recent work has been carried out in this regard. Many research papers use Küchemann's equation to document and validate their design but they overlook this parameter. The reason of the misleading character of the equation is because for a well-designed wing, the surface isobars are parallel to the leading-edge, hence the shock sweep is approximately equal to the sweep of the leading-edge. So, the misleading character of this so-called "accurate" equation has not been realised in the field of design.

This paper also documents a second design case in which the leading-edge sweep is almost same as the shock sweep due to which the design does not contain a strong aft shock all the way from root to tip of the wing and it can be said that the wing is well-designed. This paper work also studied cases with no incidence applied to the airfoil profiles but they were not able to meet the design lift criterion. Additionally, cases with winglet were studied to determine its effect on the wrong interpretation of Küchemann's equation[6] (equation 1). Literature review has shown that winglets have proven to be effective by ensuring smooth airflow near the tip and reducing induced drag that arises due to tip effect. However, when the effect of winglet on performance was studied on the final design presented in this paper, it was evident that flow around the tip became smoother and the shock was indeed eliminated at the wing-tip, however no benefits were gained for shocks at other regions. So, it is now evident that shock is generated either at wing-fuselage junction or the tip and spreads all over the wing which suggests that simple sweep theory is inconsistent.

This revelation indicates that Küchemann's critical pressure coefficient rule dominates other design modifications and it must be interpreted correctly for an effective design of wing-fuselage combination and to improve the performance during secondary design process.

REFERENCES

1. Takahashi, T.T., *Aircraft Performance & Sizing, Vol. II:*, Momentum Press, New York, NY, 2016.

2. Miranda, L.R., Baker, R.D. and Elliott, W.M., “A Generalized Vortex Lattice Method for Subsonic and Supersonic Flow,” NASA CR 2875, 1977.

3. SU2 User Manual and Tutorial Guide. Retrieved May 14, 2020 (https://su2code.github.io/tutorials/home/)

4. Jensen, J. and Takahashi, T.T., "Wing Design Challenges Explained: A Study of the Finite Wing Effects of Camber, Thickness, and Twist," AIAA 2016-0718, 2016.

5. Abbott, I.H., von Doenhoff, A.E. and Stivers, L.S., “Summary of Airfoil Data,” NACA Report 824, 1945.

6. Küchemann, D., *The Aerodynamic Design of Aircraft*, AIAA, Reston, VA, 2012.

7. Anderson, J.D., *Introduction to Flight*, 5th Edition, McGraw Hill, New York, 2005.

8. Kirkman, J.J. and Takahashi, T.T., "Critical Mach Number Prediction on Swept Wings," AIAA 2017-0266, 2017.

9. Neumark, S. “Critical Mach Numbers for Thin Unswept Wings at Zero Incidence,” British ARC R&M 2821, November 1949.

10. Pearcey, H.H. “The Aerodynamic Design of Sections Shapes for Swept Wings,” Advances in Aeronautics Sciences, Vol III, 1962, p. 277.

11. Jones, R.T. “Wing Planforms for High-Speed Flight,” NACA TR-863, 1947.

12. Schlichting, H., & Truckenbrodt, E. (1979). Aerodynamics of the Airplane (H. J. Ramm, Trans.). McGraw-Hill.

13. Drela, M. (2014). 8.6 Prandtl-Glauert Analysis. In Flight Vehicle Aerodynamics (pp. 173-180). MIT Press.

14. Von Kármán, T. (1941). Compressibility Effects in Aerodynamics. *Journal of the Aeronautical Sciences*, *8*(9), 337-355.

15. Takahashi, T. T., & Kamat, S. (2015). *Revisiting Busemann: The Design Implications of Inconsistencies Found Within Simple Sweep Theory*. (American Institute of Aeronautics and Astronautics).

16. Glauert, H. (1927). *The Effect of compressibility on the Lift of an Aerofoil*. (Royal Aeronautical Society).

17. Harris, C. D. (1981). *Two-Dimensional Aerodynamic Characteristics of the NACA 0012 Airfoil in the Langley 8-foot Transonic Pressure Tunnel*. (National Aeronautics and Space Administration TM 81927).

18. Eggers A.J. (1947). Aerodynamic Characteristics at Subcritical and Supercritical Mach numbers of Two Airfoil Sections having Sharp Leading-Edges and Extreme Rearward Positions of Maximum Thickness. (Ames Aeronautical Laboratory Moffett Field, Calif.)

19. Lock R.C., M.A., Ph.D. (1962). An Equivalence Law Relating Three- and Two- Dimensional Pressure Distributions (Aeronautical Research Council Reports and Memoranda)

20. Boyd John W., Migotsky Eugene and Wetzel Benton E. (1955). A Study of Conical Camber for Triangular and Sweptback Wings. (Ames Aeronautical Laboratory Moffett Field, Calif).

21. Rogers E.W.E., Berry C.J. and Townsend J.E.G. (1962). A Study of the Effect of Leading-Edge Modifications on the Flow over a 50-deg Sweptback Wing at Transonic Speeds (Aerodynamics Division, N.P.L.)

22. Demele Fred A. and Sutton Fred B. (1951). The effects of Increasing the Leading-Edge Radius and Adding Forward Camber on the Aerodynamic Characteristics (Ames Aeronautical Laboratory Moffett Field, Calif).

23. Hunton Lynn W. (1952). Effects of Finite Span on the Section Characteristics of Two 45-deg Sweptback Wings of Aspect Ratio 6 (Ames Aeronautical Laboratory Moffett Field, Calif).

24. Pearcey H.H. and Osborne J. (1970). Some Problems and Features of Transonic Aerodynamics. (National Physical Laboratory, Teddington U.K.)

25. Takahashi Timothy T. (2012). Form Factor and Critical Mach number Estimation for Finite Wings.

26. SU2 documentation and source code. Retrieved May 14, 2020 (https://su2code.github.io/)

27. Pointwise documentation and software. Retrieved August 22, 2020 (http://www.pointwise.com/pointwise/software)

28. TECPLOT software and user manual. Retrieved Aug 25, 2020 (https://www.tecplot.com/applications/aerodynamics/)

29. Whitcomb Richard T. Documentation from NASA (https://www.nasa.gov/langley/hall-of-honor/richard-t-whitcomb)